Signal Processing Techniques for Optical Fiber Networks

by

Xingwen Yi

Submitted in total fulfilment of

the requirements for the degree of

Doctor of Philosophy

Department of Electrical and Electronic Engineering

The University of Melbourne

Australia

September, 2007

To My Parents

Abstract

Signal Processing Techniques for Optical Fiber Networks

by Xingwen Yi

At present, optical fiber transmissions are dominated by intensity modulation and direct detection, which fundamentally limit the signal processing capabilities in optical fiber networks. On the other hand, manipulation of optical phase enables advanced signal processing techniques for various applications. This thesis includes three parts and makes contributions in three research areas in optical fiber networks, by applying optical and electronic signal processing techniques.

In the first part of the thesis, optical signal processing is employed to realize a novel all-optical label swapping (AOLS) technique using synchronous phase modulation. This technique is shown to address the forwarding speed bottleneck in optical packet switched networks (OPSN). By exploiting the unique symmetry of phase-shift keying (PSK), for the first time, label erasure and insertion are performed in a single step by a phase modulator without wavelength conversion. We also propose and demonstrate a polarization insensitive phase modulator to address the polarization sensitivity of AOLS. Furthermore, we emulate multi-hop all-optical label swapping in a re-circulating loop to investigate the power penalties from the accumulated phase errors and the timing mismatch. Based on the experimental and analytical results, we show that this technique can save wavelength converters significantly if compared with conventional AOLS techniques requiring dedicate wavelength converters.

In the second part of the thesis, electronic signal processing, in particular digital phase estimation, is employed to enable coherent optical orthogonal frequency division multiplexing (CO-OFDM) transmission, which can combat chromatic dispersion and polarization mode dispersion in high-speed optical fiber transmissions. We present the detailed theoretical and experimental results of digital phase estimation, and demonstrate coherent detection of optical OFDM signals. For the first time, we experimentally apply pilot-aided phase estimation to a high-speed long-haul optical fiber transmission. We optimize the number of pilot subcarrier in

terms of bandwidth efficiency. In another experiment, we demonstrate the PMD tolerance of coherent optical OFDM. The PMD tolerance can be improved by an order-of-magnitude over conventional IM/DD systems.

In the third part of the thesis, we use two signal processing techniques to realize optical performance monitoring for optical fiber networks. Firstly, an OSNR monitor is proposed and experimentally demonstrated for consecutive packets with varying OSNR in OPSN. Secondly, a chromatic dispersion monitoring technique is demonstrated using simulation and experimental results. This technique uses the tap coefficients in an electronic dispersion equalizer, without the need for additional hardware.

This is to certify that

(i) the thesis comprises only my original work,

(ii) due acknowledgement has been made in the text to all other material used,

(iii) the thesis is less than 100,000 words in length, exclusive of table, maps, bibliographies, appendices and footnotes.

Signature_____

Date_____

Declaration

I hereby declare that this thesis comprises only my original work. No material in this thesis has been previously published and written by another person, except where due reference is made in the text of the thesis. I further declare that this thesis contains no material which has been submitted for a degree or diploma or other qualifications at any other university. Finally, I declare that the thesis is less than 100,000 words in length, exclusive of tables, figures, bibliographies, appendices and footnotes.

Acknowledgments

I would like to thank my supervisor Dr William Shieh for constant support and guidance throughout my candidature. I would also like to acknowledge Dr Fred Buchali and Dr Henning Bülow at Alcatel Research and Innovation in Germany, for giving me the opportunity to undertake an internship, and introducing me to a new research area. I am in debt to Professor Ampalavanapillai Nirmalathas and Dr Marcus Brazil, who have provided many valuable suggestions for my submission seminar.

I am grateful to the Victoria Research Laboratory, National ICT Australia, for providing financial assistance, supporting my PhD project, and sponsoring my conference and internship travels.

Many thanks go to my colleagues around me. They shared their valuable study and research experiences generously with me. They also shared many enlightening and entertaining conversations. They offered their helpful comments and suggestions kindly during the preparation of this thesis.

My special thanks to my research partners within Dr William Shieh's research group. We had many productive and insightful discussions. In particular, I appreciate the collaboration opportunity with Dr Wei Chen on several projects. She always provides constructive ideas.

My final thanks go to all the people, who have helped me over the past three years. Although I cannot mention all your names here, you all deserve my sincere gratitude.

Contents

List of Figures

x

List of Tables

Chapter 1

Introduction

1.1 Overview

Research and development of optical fiber networks has been performed for several decades. The primary motivation is to take advantage of optical fiber as an excellent transmission medium. The rapid development of optical fiber networks is highlighted by the increases of transmission speed and transmission distance of optical fiber transmission systems. The earliest commercial systems operated near 0.8 μm, at a bit rate of 45 Mb/s and allowed repeater spacing up to 10 km [1]. By the end of the 1980s, the introduction of single mode fiber shifted the operation wavelength region to 1.3 μm. During the 1990s, the invention of broadband optical amplifiers around 1.5 μm and wavelength-division multiplexing (WDM) led to rapid advances in optical fiber transmission systems. Currently various innovations still continue to break the records of transmission capacity and distance. Recent experimental demonstrations include 14-Tb/s transmission with 2 bit/s/Hz bandwidth efficiency [2] and 2000-km transmission of 10×107 Gb/s [3].

In essence, optical fiber transmission systems are band-pass systems and thus similar to wireless transmission systems. Optical signals have four dimensions in which information can be encoded: amplitude, phase, frequency, and polarization. Currently, only amplitude (intensity) is used to encode data in most commercial optical fiber networks, which is traditionally called intensity modulation/direct detection (IM/DD). The fundamental limitation of IM/DD is that photodiode only responds to optical intensity, and the remaining dimensions of optical signals can not be directly detected by photodiode. Therefore, optical phase, frequency, or polarization information must be converted into intensity information in order to be

detected by photodiode. Various conversion schemes are still under investigation for any practical applications in optical fiber networks. At present, optical fiber networks are primitive compared to the radio/wireless networks which use sophisticated signal processing techniques. For example, the optical transmitter and receiver are comparable to those used in radio communication in the 1930s [4]. The reason is that the current forms of optical transmitter and receiver do not use the phase of optical signals, namely, they are non-coherent techniques. In short, the signal processing capabilities are significantly limited in conventional IM/DD systems. The full potential of signal processing capabilities must exploit the other dimensions of optical signals, including optical phase, optical frequency, and optical polarization.

Although it is desirable to perform all signal processing in the optical domain for all-optical networks, electronic signal processing is indispensable in the foreseeable future. This is because all-optical signal processing is fairly rudimentary and does not yet have the signal processing or computing capabilities to fulfill network tasks, even after a decade of research. As a result, the present optical fiber networks rely heavily on electronics to perform the intelligent network control functions. Nevertheless, it is possible to shift some simple functions to the optical domain, such as label-swapping and forwarding [5]. Therefore optical and electronic signal processing will co-exist in optical fiber networks. For a specific function, the choice of optical or electrical approach depends on the associated performance and cost. In general, if the function involves a fair amount of sophisticated logic and processing, they are best handled in the electrical domain. If the function involves simple operation, but require a high through-output capacity, like switching, they can adopt optical approaches.

Optical and electronic signal processing can be applied to various aspects of optical fiber networks, resulting in the different research areas. In this thesis, we apply signal processing to three specific areas, as shown in Fig. 1.1. One common aim of these three areas is to transmit user data from one place to another place successfully. The three areas corresponds to three parts of this thesis:

- The first part proposes a novel technique for data routing by using all-optical label swapping (AOLS). An optical fiber network is generally shared by many
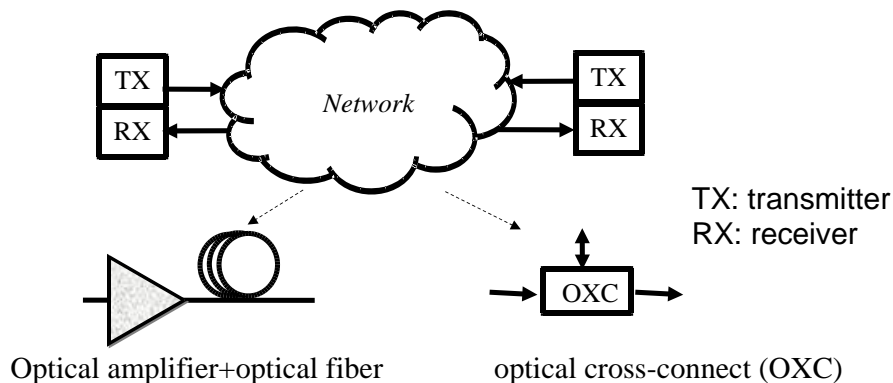
Figure 1.1: Basic functions of optical fiber networks.

users and can include optical cross-connect (OXC) as shown in Fig. 1.1. Therefore, there are many possible transmission routes. Data routing can guarantee that data are sent to the correct destination.

- The second part is electronic compensation of optical distortions using coherent optical orthogonal frequency division multiplexing (OFDM). Optical signals can experience optical distortions from optical fibers, as shown in Fig. 1.1. This technique is proposed to combat optical distortions, which arise during transmission in optical fiber networks and impose fundamental limits on transmission capacity and distance.

- The third part is optical performance monitoring using two signal processing techniques. Optical performance monitoring is of importance in terms of network management and maintenance. In another word, optical performance monitoring helps for continuous and successful data transmissions in a field network.

Although there has been a lot of research into the three areas [6, 7, 8, 9, 10, 11, 12, 13], most of the proposed techniques or solutions are impractical and costly. Innovative techniques or further improvements are required. In this thesis, we make contributions in the three areas by electronic and optical signal processing techniques. We demonstrate signal processing techniques of optical phase, which is easier to handle compared with optical polarization or frequency. Furthermore, we can take advantage of the extensive research that has been performed in wireless

communications [14].

The following three subsections briefly introduce the three parts of this thesis.

1.1.1 AOLS Using Synchronous Phase Modulation

Optical transmissions can provide enormous bandwidths such that optical transmission capacities overwhelm electronic processing speeds, which leads to the so-called electronic bottleneck, especially for data traffic. Optical packet switched networks (OPSN) are considered to be one of the most promising solutions for end-to-end delivery of high bit-rate data, video, and voice signals across optical networks of the future. AOLS processes the routing and forwarding information in the electrical domain while optical data/payload remains in the optical domain. The main benefit of AOLS is that data/payloads are transported entirely in the optical domain without unnecessary optical-electrical-optical (OEO) conversions. Therefore the information carried by the packet payload can be encoded in any format and at any bit rate, which leads to high efficiency and full transparency, in addition to increased scalability and flexibility.

There are various AOLS approaches. Most of them require wavelength converters to erase the old optical labels. However, it has been shown that it may be cost effective to share a limited number of wavelength converters, where the majority of packets pass through the switch without wavelength conversion [15], especially in multi-fiber per link networks [16]. Therefore it is highly desirable to be able to perform optical label swapping even when the packets bypass the wavelength converters. By exploiting the unique symmetry of phase-shift keying (PSK), we propose a novel AOLS using synchronous phase modulation. Optical label erasure and insertion are performed in a single step by a phase modulation without wavelength conversion. To substantiate the technique, we carry out two more experiments to investigate the polarization sensitivity of phase modulator and the multi-hop transmission performance.

1.1.2 Phase Estimation for Coherent Optical OFDM

For long-haul optical fiber networks at 10 Gb/s per channel or beyond, one main challenge is optical distortion compensation, because the requirements of accuracy, dynamic range, and adaptation speed become difficult to meet using existing compensation techniques [17, 18, 19, 20]. In such networks, optical distortions, such as chromatic dispersion (CD) and polarization mode dispersion (PMD), are the limiting factors of the physical layer. Although the optical distortions can be compensated in the optical domain, there are many advantages for compensation in the electrical domain, such as fast adaptation, cost-effectiveness and small footprint. Electronic compensation of optical distortion has become practical owing to the significant advances of microelectronics.

One approach of electronic compensation is to employ advanced modulation techniques, such as OFDM. OFDM is resilient to frequency selective fading and has been adopted in various wireless communication standards [21]. Coherent optical OFDM (CO-OFDM) has recently been proposed for optical communications [22]. If the input power into optical fiber is limited for a linear transmission, by using coherent detection, the optical fiber channel can be treated as linear. As a result, linear distortions, such as CD and PMD, can be fully compensated. Coherent detection can be fulfilled by digital phase estimation without the need for conventional phase-locked loops. We present phase estimation and compensation methods for CO-OFDM transmissions. The theories and methods are applied to two long-haul optical fiber transmission experiments. We also optimize the pilot-aided phase estimation in terms of bandwidth efficiency.

1.1.3 Optical Performance Monitoring in Optical Fiber Networks

Optical performance monitoring is of importance for optical fiber networks [23]. The realization of optical performance monitoring depends on the requirements and accessible information in different applications. In OPSN, optical packets originate from different sources and traverse different optical links. Each packet has its own

history and signal quality. We propose and demonstrate an OSNR monitor capable of monitoring consecutive optical packets with varying OSNR.

It is expected that electronic dispersion compensation (EDC) will be popular in optical fiber networks due to its fast adaptation and cost-effectiveness. In EDC receiver, optical distortions can be traced out during the compensation process. We propose a chromatic dispersion monitoring technique by analyzing the tap coefficients of tapped delay lines. We verify the technique by simulation and experiment.

1.2   Thesis Outline

The remained of this thesis is as follows:

Chapter 2: Literature Review This chapter reviews the development of optical fiber networks. Three challenges for such networks are discussed and the existing solutions are reviewed. The motivations of the thesis are presented.

Chapter 3: Signal Processing for Optical Fiber Networks This chapter provides the theoretical and mathematical background for the remained of the thesis. Generic mathematical formulations and terminologies of the optical fiber communication systems are introduced. The underlying theories, characteristics, and experimental design of optical transmitters and receivers and optical fiber channels are discussed by commonly used terms of signal processing.

Chapter 4: AOLS Using Synchronous Phase Modulation In this chapter, a novel solution to all-optical label swapping is proposed and demonstrated. By using synchronous phase modulation, label erasure and insertion are performed in a single step without wavelength conversion. The polarization sensitivity of AOLS is addressed with a polarization insensitive phase modulator. We also investigate the performance of time mismatch between the incoming label and the new label, and multi-hop transmission.

Chapter 5: Phase Estimation for Coherent Optical OFDM This chapter introduces CO-OFDM and its capabilities to combat the chromatic dispersion

and polarization mode dispersion. This chapter focuses on the phase estimation in the receiver, which is one of the enabling techniques in CO-OFDM. The theory and experimental results are presented. We also investigate the optimum number of subcarrier for pilot-aided phase estimation.

Chapter 6: Optical Performance Monitoring for Optical Fiber Networks
This chapter presents two techniques to monitor OSNR and chromatic dispersion, respectively. An OSNR monitor is proposed and experimentally demonstrated for consecutive packets with varying OSNR in OPSN. A chromatic dispersion monitoring technique is demonstrated in simulation and experiment by analyzing the tap coefficients in electronic dispersion equalizers using tapped delay lines without the need for additional hardware.

Chapter 7: Conclusions This chapter summarizes the research results of the thesis. Suggestions for future research are presented.

1.3 Contributions of the Thesis

The contributions of the thesis are listed as follows.

AOLS Using Synchronous Phase Modulation

- For the first time, optical label erasure and insertion are performed in a single step by a phase modulator without wavelength conversion. The power penalty of label swapping is found to be insignificant. [In Section 4.2]

- We address the polarization sensitivity of all-optical label swapping for the first time. The polarization insensitivity of the power penalty for label swapping is measured out for the packet label and payload, respectively. [In Section 4.3]

- We emulate cascaded all-optical label swapping in a re-circulating loop to investigate the power penalties from the accumulated phase errors. In addition, we investigate the timing mismatch between the incoming label and the new label. [In Section 4.4]

Phase Estimation for Coherent Optical OFDM

- For the first time, we discuss and apply pilot-aided phase estimation theory of OFDM to optical fiber transmissions experimentally. We find that pilot-aided phase estimation can improve the system performance in comparison with data-aided phase estimation. [In Section 5.3.3 and 5.4]

- We study the optimum number of pilot subcarriers for digital phase estimation to realize coherent detection. [In Section 5.4]

- We report the first experimental demonstration of coherent optical OFDM transmission at a norminal bit rate of 8 Gb/s over 1000 km transmission. Our work serves to substantiate the suitability of coherent optical OFDM for optical transmission without a need for optical compensation of chromatic dispersion and polarization mode dispersion. [In Section 5.4]

- We demonstrate the PMD tolerance of CO-OFDM at 10 Gb/s. The PMD tolerance can be improved by an order-of-magnitude over conventional IM/DD systems. [In Section 5.5]

Optical Performance Monitoring for Optical Fiber Networks

- We present the first experimental demonstration of an OSNR monitor for OPSN. We show the wide dynamic range and fast response of the OSNR monitor. [In Section 6.2]

- We propose a chromatic dispersion monitoring technique by analyzing the tap coefficients in electronic dispersion equalizers using tapped delay lines without the need for additional hardware. The technique is verified by simulation and experiment. [In Section 6.3]

1.4   Publications

During the my PhD study, a number of publications have been made which contribute to this thesis. The following is a list of my research papers.

Journal Papers

1. W. Shieh, R. Hui, X. Yi, and G. Pendock, "Experimental and theoretical study on the symmetries of orthogonally polarized optical signals," *IEEE Trans. Commun.*, accepted for publication.

2. W. Shieh, X. Yi, Y. Ma, and Y. Tang, "Theoretical and experimental study on PMD supported transmission using polarization diversity in coherent optical OFDM systems," *Optics Express*, vol. 15, no. 16, pp. 9936-9947, Aug. 2007.

3. X. Yi, W. Shieh, and Y. Tang, "Phase estimation for coherent optical OFDM," *IEEE Photon. Technol. Lett.*, vol. 19, no. 12, pp. 919-921, June 2007.

4. W. Chen, F. Buchali, X. Yi, W. Shieh, J. S. Evans, and R. S. Tucker, "Chromatic dispersion and PMD mitigation at 10 Gb/s using Viterbi equalization for DPSK and DQPSK modulation formats," *Optics Express*, vol. 15, no. 9, pp. 5271-5276, April 2007.

5. Y. Tang, W. Shieh, and X. Yi, "Optimum design for RF-to-optical up-converter in coherent optical OFDM systems," *IEEE Photon. Technol. Lett.*, vol. 19, no. 7, pp. 483-485, April 2007.

6. W. Shieh, X. Yi, and Y. Tang, "Transmission experiment of multi-gigabit coherent optical OFDM systems over 1000 km SSMF fibre," *Electron. Lett.*, vol. 43, no. 3, pp. 183-185, Feb. 2007.

7. X. Yi, F. Buchali, W. Chen, and W. Shieh, "Chromatic dispersion monitoring in electronic dispersion equalizers using tapped delay lines," *Optics Express*, vol. 15, no. 2, pp. 312–315, Jan. 2007.

8. W. Shieh, R. S. Tucker, W. Chen, X. Yi, and G. Pendock, "Optical performance monitoring in coherent optical OFDM systems," *Optics Express*, vol. 15, no. 2, pp. 350-356, Jan. 2007.

9. X. Yi, W. Chen, and W. Shieh, "An OSNR monitor for optical packet switched networks," *IEEE Photon. Technol. Lett.*, vol. 18, no. 13, pp. 1448–1450, July 2006.

10. X. Yi, W. Shieh, and A. V. Tran, "Cascadability study for optical label swapping using synchronous phase modulation," *IEEE Photon. Technol. Lett.*, vol. 18, no. 13, pp. 1445–1447, July 2006.

11. X. Yi and W. Shieh, "On polarization sensitivity of all-optical label swapping using synchronous phase modulation," *IEEE Photon. Technol. Lett.*, vol. 18, no. 11, pp. 1210–1212, June 2006.

12. W. Shieh, R. Hui and X. Yi, "Degree-of-polarization and eye-closure penalty associated with optical signals with orthogonal polarizations," *IEEE Photon. Technol. Lett.*, vol. 18, no. 10, pp. 1122-1124, May 2006.

13. W. Shieh, X. Yi, and A. V. Tran, "A label swapping technique using synchronous phase modulation without wavelength conversion," *Optics Communications*, vol. 264, no. 1, pp.74-77. Aug. 2006.

14. W. Chen, R. S. Tucker, X. Yi, W. Shieh, and J. S. Evans, "Optical signal-to-noise ratio monitoring using uncorrelated beat noise," *IEEE Photon. Technol. Lett.*, vol. 17, no. 11, pp. 2484-2486, Nov. 2005.

Conference Papers

1. X. Yi, W. Shieh, and Y. Ma, "Phase noise on coherent optical OFDM systems with 16-QAM and 64-QAM beyond 10 Gb/s," in *Europ. Conf. Optical Commun. (ECOC)*, Germany, Sept. 2007, accepted for publication.

2. W. Shieh, X. Yi, Y. Ma, and Y. Tang, "PMD-Supported Transmission Assisted by Polarization-diversity Detection and Coherent Optical OFDM Signal Processing," in *the 12th Optoelectronics and Communications Conference (OECC)*, PD1-7, Japan, July 2007.

3. X. Yi, W.Shieh, and Y. Tang, "Phase Estimation for Coherent Optical OFDM Transmission," in *Joint Conference on Optical Internet and Australian Conference on Optical Fiber Technology (COIN−ACOFT)*, June, 2007, paper TuA1-4.

4. W. Shieh, X. Yi, and Y. Tang, "Experimental demonstration of transmission of coherent optical OFDM systems," in *Conf. Optical Fiber Communication (OFC)*, USA, Mar. 2007, paper OMP2.

5. Y. Tang, X. Yi, W. Shieh, and R. Evans, "Optimum Design for Coherent Optical OFDM Transmitter," in *Conf. Optical Fiber Communication (OFC)*, USA, Mar. 2007, paper JThP47.

6. W. Chen, F. Buchali, X. Yi, W. Shieh, J. S. Evans, and R. S. Tucker, "Viterbi equalizer for chromatic dispersion and PMD mitigation in DPSK and DQPSK systems at 10 Gb/s," in *Europ. Conf. Optical Commun. (ECOC)*, France, Sept. 2006, paper We3.P.85.

7. W. Shieh, R. S. Tucker, W. Chen, and X. Yi, "Optical performance monitoring through channel estimation by receiver signal processing," in *Europ. Conf. Optical Commun. (ECOC)*, France, Sept. 2006, paper We3.P.104.

8. X. Yi, F. Buchali, W. Chen, and W. Shieh, "Adaptation Algorithms for Receiver Based Electronic Dispersion Equalization," in *Australian Conference on Optical Fiber Technology (ACOFT)*, July 2006, paper 140Mon.

9. W. Chen, F. Buchali, X. Yi, W. Shieh, J. S. Evans, and R. S. Tucker, "PMD Mitigation at 10 Gb/s Using Viterbi Equalizer for DPSK and DQPSK Modulation Formats," in *Australian Conference on Optical Fiber Technology (ACOFT)*, July 2006.

10. X. Yi, W. Shieh and A. V. Tran, "Multi-hop optical label swapping using synchronous phase modulation," in *Conf. Optical Fiber Communication (OFC)*, USA, Mar. 2006, paper JThB53.

11. W. Shieh, R. Hui and X. Yi, "Symmetry study for optical signals with orthogonal polarizations," in *Conf. Optical Fiber Communication (OFC)*, USA, Mar. 2006, paper OWI53.

12. X. Yi, W. Chen and W. Shieh, "Optical signal-to-noise ratio monitoring for optical packet switched networks," in *Europ. Conf. Optical Commun. (ECOC)*,

UK, Sept. 2005, vol. 3, pp. 731-732.

13. W. Chen, R. S. Tucker, X. Yi, W. Shieh, and J. S. Evans, "Uncorrelated beat noise measurement for optical signal-to-noise ratio monitoring," in *Europ. Conf. Optical Commun. (ECOC)*, UK, Sept. 2005, vol. 4, pp. 971-972.

14. X. Yi, W. Shieh, "Demonstration of polarization insensitivity for all-optical label swapping," in *The Fourth International Conference on Optical Internet (COIN)*, China, May 2005, pp. 175-177.

15. W. Shieh, X. Yi, and A. V. Tran, "Label swapping for DPSK encoded labels without wavelength conversion," in *Conf. Optical Fiber Communication (OFC)*, USA, Mar. 2005, vol. 2, pp. 43-45.

Chapter 2

Literature Review

2.1 Introduction

A communication network transmits information from one place to another place, whether they are separated by a few kilometers or by a transoceanic distance. Information is often carried by a high-speed carrier in order to be transmitted in a particular transmission medium. Radio/microwave carrier frequencies are about 1 GHz while optical carrier frequencies are typically around 200 THz. Optical fiber networks are lightwave networks that employ optical fibers as transmission media. An increase in the information capacity of optical fiber networks by a factor of up to 10,000 is expected simply because such high carrier frequencies are used [1]. Such networks have been deployed worldwide since 1980 and have indeed revolutionized the technologies behind telecommunications. Compared with the other networks, optical fiber networks are capable of operating at much higher bit rates and over much longer distances.

Currently the intelligent network functions of optical fiber networks are still performed by conventional electronic facilities, and the advantages of optical fiber technology is only appreciated as a transmission solution. As a result, *optical fiber communication system* is more frequently used than *optical fiber network*. This thesis does not distinguish them strictly since we focus on the physical layer. Optical fiber networks are more used when we describe all-optical label swapping. Optical fiber communication systems are preferred when we describe optical distortion compensation.

When the data traverse a optical fiber network, the data must travel to the right destination and can be recovered. There arise two tasks: data routing and

data recover. The first task is a network function and leads to the concept of all-optical label swapping (AOLS) for optical packet switched networks. The second task deals with transmitter and receiver in transmission systems. In particular, the thesis focuses on the design of transmitter and receiver for electronic compensation of optical distortions. Furthermore, optical performance monitoring is important for the successful data transmission in optical fiber networks. These tasks result in three research areas in which the work of the thesis is involved.

This chapter is the literature review for the available techniques in the three areas. Section 2.2 reviews the concept and structure of optical packet switched networks (OPSN) with an emphasis on all-optical label swapping (AOLS). The main existing AOLS techniques are reviewed. Section 2.3 reviews the available techniques on electronic compensation of optical distortions. The advantages and disadvantages of the techniques are also discussed. Section 2.4 reviews the existing OSNR and CD monitoring techniques. After the literature review, Section 2.5 introduces the motivations of the thesis. We introduce our alternative techniques to the existing ones.

2.2 All-optical Label Swapping in OPSN

The communication network infrastructure is based on the traffic inside the network. Circuit-switched networks are historically for telephone or voice traffic. Packet-switched networks are for bursty data traffic, such as internet protocol (IP) traffic. There is a significant change in the type of traffic that is increasingly dominating the telecommunication networks. Since the early 1990s internet traffic has been growing tremendously. IP has achieved huge success as a transmission protocol and practically all forms of end-user communications today are going to adopt the ubiquitous TCP/IP protocol [24]. Furthermore, many new services and applications being offered are also based on IP protocols, such as IP phone and IP video. It has become clear that IP will dominate the communication networks and also be a very strong candidate for the convergence of different incumbent communication networks [25].

The important signature of IP traffic is *bursty* and packet switching is much better to handle bursty traffic than circuit-switching. It is desirable to design the network infrastructure capable of packet switching. However there is a speed bottleneck from the link layer (back-bone network) to the higher layer electronic nodes, such as IP routers and asynchronous transfer mode (ATM) switches (access network). Here, the lack of optical signal processing capabilities results in optical-electrical-optical (OEO) conversion to realize network functions. Compared with optical fiber transmission development, the advances of electronics signal processing are occurring at a much slower pace. This mismatch results in the so-called electronic bottleneck.

To solve the electronic bottleneck problem, several different technologies have been developed for the transfer of packets over optical fiber networks, such as wavelength routing, optical packet switching, and optical burst switching [26]. Wavelength routing networks have already been deployed while optical packet switching and optical burst switching are still facing some technological hurdles to overcome for practical applications [27]. Optical burst switching represents a balance between circuit and packet switching. It is an intermediate solution between wavelength routing and optical packet switching and has the potential for field field applications [27]. However, optical packet switching well matches the dominant IP traffic and provides better scalability, protocol/bit-rate transparency, and service intelligence [28]. Optical packet switching also offers greater flexibility and more efficient system bandwidth management than the other technologies [27]. As a long term solution, optical packet switching is still an important research area.

2.2.1 Optical Packet Switched Network

Currently most network functions are processed by IP routers or equivalent. IP routers perform four major tasks [25, 29]:

- Routing: Routers provide up-to-date network connectivity information, which is maintained in the form of a routing table stored at each node.

- Forwarding: For each incoming packet, a router processes the packet header and defines the output port of that packet based on its routing table. The

header may also be changed depending on network functions.

- Switching: Switching is the process of switching the incoming packet to the appropriate output port defined by the forwarding process. For the conventional electronic switching, the forwarding and switching functions are usually treated as a single function.

- Buffering: One most important reason of buffering is to resolve contention by storing packets when more than one wishes to switch to the same output at the same time, due to the unscheduled nature of their arrival.
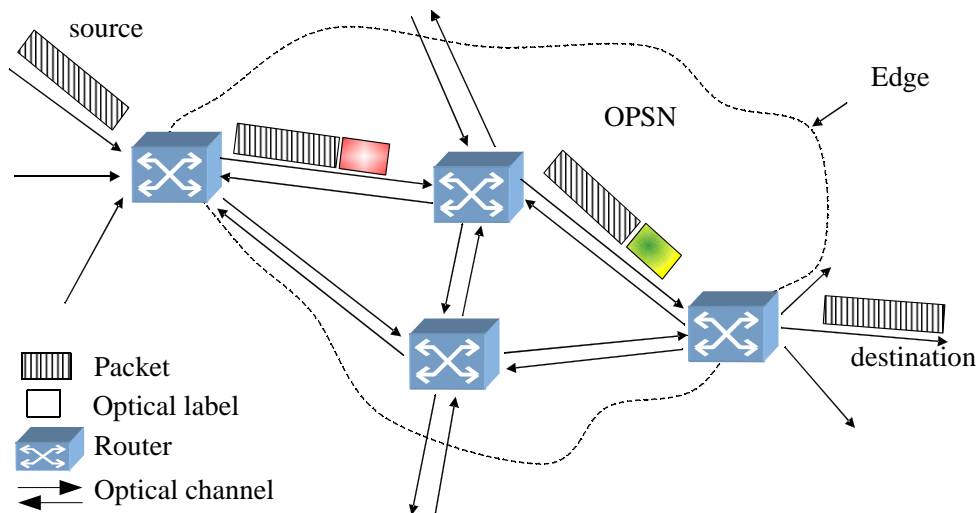
Figure 2.1: An example of optical packet switched network

Optical packet switched networks (OPSN) also need to execute these tasks. An ideal solution will shift all of them to the optical domain to obviate the electronic bottleneck. However, in ten years or more, there might be no practical and economical optical signal processing techniques to achieve this objective. So far, hybrid solutions seem more reasonable. Because packet header processing is relatively complex, routing and forwarding are carried out electronically and are independent of the optical payload/data. Transmission and switching are executed in the optical domain to maintain a higher speed. This strategy decouples the throughput and

routing/forwarding processes and permits the optical layer to support a range of networking protocols while harnessing the bandwidth of optical transmission [25].

With this strategy, an example of OPSN is illustrated in Fig. 2.1, consisting of several OPSN nodes. All the nodes can carry out the functions equivalent to conventional electronic routers. The nodes are interconnected by wavelength division multiplexing (WDM) fiber channels. IP packets are encapsulated with optical labels before entering the OPSN. Once inside the OPSN, only the optical labels are processed electronically for routing and forwarding. The IP packets (data) remain in the optical domain to avoid any optical-electronic conversion. There may have optical switching and optical wavelength conversion for the IP packet. When the IP packets exit the OPSN, the optical labels are removed and the original packets are handed back to the electronic routing hardware without any processing [30].
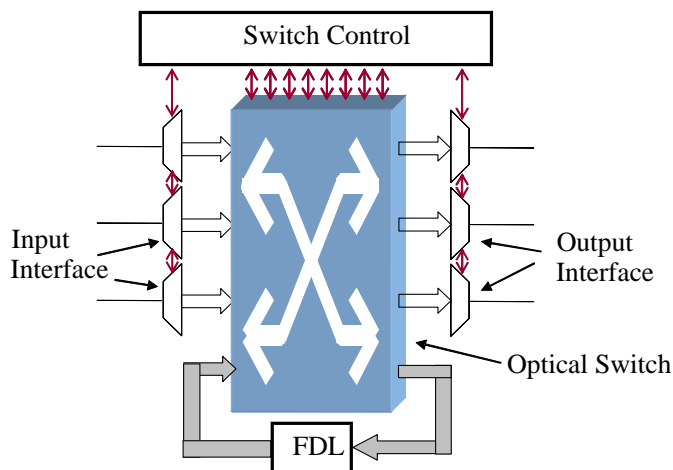
Figure 2.2: A generic OPSN node. FDL: fiber delay line.

The routers in Fig. 2.1 are the basic nodes in OPSN. A generic unidirectional OPSN node is illustrated in Fig. 2.2 [25]. There are several subblocks:

Input interface: Through the input interface, WDM channels from fiber links are space de-multiplexed by arrayed waveguide grating (AWG) or similar technologies. The input interface then extracts the label information and re-aligns the packets in different channels if needed.

Switch control: The switch control receives information from the input interface

and sends out configuration information to the optical switch (OXC) and forwarding information to the output interface.

Optical switch: The optical switch should be capable of being reconfigured for every time slot and being non-blocking, which means any input, output permutation can be configured. If the input interface re-aligns the input packets, OXC can operate internally in a slot-synchronous way.

Fiber delay line : A set of fiber delay line (FDL) emulates the cell buffering. One FDL has a delay of one time slot or integral times of time slots.

Output interface : The output interface resembles the packets and outputs them to a unique channel. Output interface also re-writes/re-generates the optical labels according to the forwarding information from the control unit. The output interface may include wavelength conversion.

The above descriptions for each subblock only include the major functions. More detailed description is given in [25, 26, 27, 28]. When a packet arrives at an OPSN node, it is first processed by the input interface. The header and data (payload) of the packet are separated, and the header is converted to the electrical domain and processed by switch control. The data remains in the optical domain and passes through the OXC. The data may be switched to FDL and go into the OXC again, which is an approach for contention resolution. After the OXC, the header is converted /generated into the optical domain and combined with the data at the output interface.

2.2.2 Optical Labeling Techniques

The generation and swapping of optical label are critical for OPSN. Several optical packet labeling techniques have been proposed to label optical packets. There are five major approaches in the literature:

Bit serial labeling: The bit serial label is encoded on the same optical carrier as the packet and is encoded as a baseband signal [31, 32]. It is basically a time division multiplexing (TDM) scheme.

Orthogonal labeling: The label and the payload data both are modulated on the same optical carrier. The modulation of the label is orthogonal to that of the payload to minimize the crosstalk between them [33, 7, 34].

Optical subcarrier multiplexed (OSCM) labeling: The baseband label is firstly modulated onto a RF subcarrier and then multiplexed with the payload data on the same optical carrier [5, 35].

WDM labeling: The label information is transmitted in a separate WDM channel. In general, multiple data channels share one label channel [6, 36].

Optical code division multiplexing (OCDM) labeling: The label information is encoded to the payload by OCDM, which scrambles the payload by a specific code [37, 38]. The label receiver decodes the label by using the code.

In WDM labeling, the label and the payload are separated and the synchronization of them poses a significant challenge. It does not well support the optical packet concept. There is a special labeling technique similar to WDM labeling, the label and the payload optical carriers come from the optical carrier suppression modulation of the same optical carrier [39]. The label is not shared by the other payload in different carriers. This technique relies on the narrow optical filter, which is difficult or expensive. The OCDM needs additional bandwidth and is quite complicated, especially the receiver. Therefore, we only discuss the rest of the three labeling techniques.

Fig. 2.3(a) shows the bit serial labeling. A fixed rate label is time division multiplexed (TDM) at the head of the payload with the label and payload separated by the guard time. The guard time facilitates label removal and re-insertion without static packet buffering and accommodates finite switching times of optical cross-connect (OXC). In general, the guard time wastes some useful bandwidth. However, the guard time may be very small in some AOLS schemes [32], depending on the synchronization performance. In the bit serial labeling, the packet and label present themselves in different time slot. There is no additional penalty for packet by labeling while the strict synchronization between packet and label should be guaranteed.
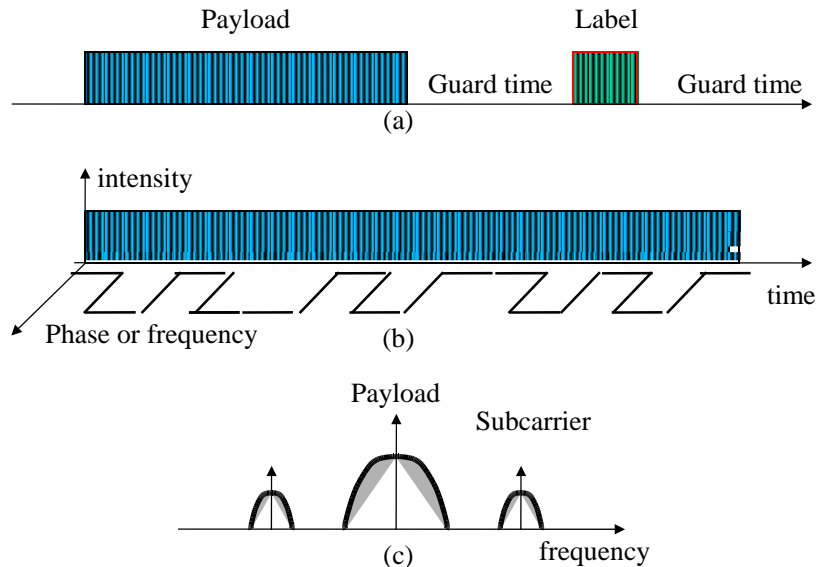
Figure 2.3: Optical labeling techniques: (a) bit serial labeling, (b) orthogonal labeling, (C) optical subcarrier multiplexed labeling.

Fig. 2.3(b) shows the orthogonal labeling. A important feature is the orthogonal modulation between the label and payload. An optical carrier has four dimensions to carry information: polarization, amplitude, frequency, and phase. Therefore there are quite a few orthogonal combinations in theory. For example, the label and the payload can be DPSK/ASK [40], ASK/DPSK [33], or ASK/DPolSK [34]. By using orthogonal labeling, the label and payload are overlapped in time domain and frequency domain. Careful design is needed to minimize the crosstalk between the label and payload. One approach is to use special coding for payload to shape its frequency spectrum, and thus minimize the frequency overlap of the label and payload [33]. As a result, however, the bandwidth efficiency is reduced because of the coding.

Fig. 2.3(c) shows the OSCM labeling in frequency domain, where the label and payload occupy the different frequency range. The baseband label is modulated onto a RF subcarrier and then multiplexed with the IP packet on the same wavelength. This multiplexing may be performed electronically or optically as described in [5, 41]. Since the subcarrier is in the higher frequency than the payload, the subcarrier modulation needs more complicated circuits even than the payload. The guard

	bit serial labeling	orthogonal labeling	OSCM labeling
bandwidth efficiency	low,variable	low when shaping spectrum	moderate, variable
synchronization	strict	not strict	not strict
transmission	no crosstalk	crosstalk	fading of subcarriers
complexity	medium	high	high

Table 2.1: Comparison of optical labeling techniques

time is not necessary for the OSCM labeling because the label is transmitted in parallel with the packet. Therefore the synchronization requirement can be relaxed. There are two approaches to detect the OSCM label: optical direct detection of a whole demultiplexed channel and converting the signal to base-band in the electrical domain; or detecting only the desired subcarrier information after the narrow optical band-pass filtering centered at the spectral location of a specific subcarrier band [42, 43]. Another disadvantage of OSCM is the fading of the subcarrier due to chromatic dispersion (CD) when transmitting in optical fiber. One solution is to use a narrow optical band-pass filter although it is challenging [43].

We summarize the major features the three optical labeling techniques in Table 2.1. More extensive comparisons can be found in [28]. Each technique has its advantages and disadvantages. Therefore, it is difficult to find the best optical labeling technique.

2.2.3 Existing All-optical Label Swapping Techniques

As discussed in Section 2.2.1, all-optical label swapping (AOLS) is one of the key technologies for OPSN and has attracted tremendous research interests. The function of AOLS is to serve the OPSN functions. The label can be dynamically altered in the intermediate nodes while the payload is kept in the optical domain. Although the ultimate goal is to keep the payload all the way from source to destination in the optical domain, some OEO generation might be adopted due to the difficulties and complexities of *all-optical*. While the label is swapped in the intermediate nodes, the

payload also needs to be switched to appropriate transmission route, which causes the contention problem when multiple payloads strive for the same transmission route at the same time. Wavelength conversion is well established as a contention resolution. Because the wavelength conversion is used for the payload, its associated label information need to be swapped onto the new wavelength. Therefore AOLS is closely related to wavelength conversion. It should be noted that wavelength conversion is not always needed in every node when the packet traverses the OPSN, which has been shown in [15].

There are various techniques demonstrated in the past decade. Their implementation can be quite different and strongly dependent on their optical labeling techniques. Therefore, we review them according to their optical labeling techniques.

Bit serial labeling

In [32], label and data are literally the same format and bit rate with bit-serial label. Delta label is generated in a new wavelength and then modify the old label through XOR logic in an integrated SOA based wavelength converter. In [31], the payload is OOK and the label is DPSK format. The label erasure takes advantage of the optical phase insensitivity of SOA and the old label is erased by SOA XPM wavelength converter. The new label is modulated to the new wavelength by a phase modulator after the wavelength conversion.

Orthogonal labeling

In [33], the label and data modulation are orthogonal, i.e., DPSK label and ASK data. A DC-balanced line code, such as 8B/10B line code, is used to minimize the crosstalk between the label and payload. For label swapping, the old label is erased in the wavelength converter, which is based on optical Kerr switching in a highly non-linear fiber. The new label is added after the wavelength conversion. In [40], the label and payload are ASK and DPSK, respectively. The advantage of this scheme is that the DPSK format has constant amplitude, which facilitates the ASK label processing. All-optical label erasure is realized by utilizing the gain saturation and non-linear birefringence evolution in the SOA. After label erasure, the new label is

added by a re-modulation. In [44], a low-speed ASK label is superimposed on top of a high-speed ASK payload, which is not orthogonal in a strict sense. However it shares the same technical challenges as the orthogonal label. 8B/10B line code is also used to minimize the crosstalk between the label and payload. For label swapping, an old ASK label is erased by modulating the combined payload and label signal with the inverse of the received ASK label. The new label is added by modulating the erased old optical signal.

OSCM labeling

In [5], old label is erased by using fiber loop mirrors, which filter out the old sub-carrier. There is always some residual subcarrier power because of the non-ideal filtering curve of the fiber loop mirrors. Therefore, the residual subcarrier is further attenuated in the wavelength converter by using the low-pass filtering function in SOA. The wavelength converter consists of two stages. First stage is to condition and convert the input optical signal into a fixed intermediate wavelength. In the second stage, the wavelength conversion is based on cross phase modulation (XPM) in SOA. The intermediate signal is converted to another wavelength and a new label is subsequently added. In [42], the label is encoded by optical single side band modulation. Consequently only one subcarrier is present in frequency domain. This is desirable when considering the conventional subcarrier fading due to CD in fiber. The label is erased simply by an optical filter. The new label is a re-modulation of the new subcarrier.

In general, most AOLS techniques require wavelength converters, and they erase the old label and generate new label separately, which involve several devices. Wave-length converters remain as expensive components and can be avoided in some applications, which is one of the motivation of the thesis as we will describe in Section 2.5.

2.3 Electronic Compensation of Optical Distortions

When a signal traverses a optical fiber network, there are many different types of impairments. In addition to the generic electrical signal impairments, the optical layers add optical impairments. In general, the optical impairments can be grouped as noise and distortion. Noise, like amplified spontaneous emission (ASE) noise from optical amplifier, is random in nature and can not be removed once added. Noise reduces signal-to-noise ratio (SNR). Distortion is a deterministic impairment resulting from CD and narrow-band filtering, etc. PMD can be treated as deterministic under certain conditions, e.g., the slowly changing first order PMD. In most times, distortion causes inter-symbol interference (ISI). Distortion can be fully compensated in theory. This thesis focuses on CD and PMD distortion.

There are many techniques on electronic compensation of optical distortions. Unfortunately, there are also many different names for this function. Before we proceed to the next sub-section, it is helpful to distinguish some terminologies. As we already mentioned, optical noise is difficult to compensate. Therefore we use optical distortion instead of optical impairment to exclude optical noise. Historically, the major targeted impairment of optical fiber networks is CD, which leads to electronic dispersion compensation (EDC). In this thesis, *compensation* means the distortion can be fully compensated in theory, *mitigation* means the distortion can not be fully compensated but partially mitigated in theory. Dispersion generally means CD only when used in *electronic dispersion mitigation*. However, the direct target of most electronic equalizers are the ISI, irrespective of the source origin. Therefore, these equalizers can mitigate the CD and PMD at the same time. Note optical distortions may originate from other sources, such as narrow bandwidth filtering, and therefore have wider meaning than dispersion.
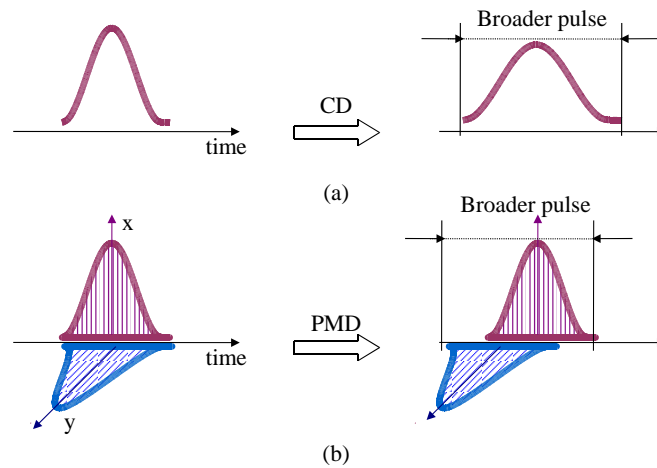
Figure 2.4: Illustration of pulse spreading due to (a) CD, (b) PMD.

2.3.1 Chromatic Dispersion and Polarization Mode Dispersion

In optical fiber networks, single-mode fibers are widely deployed. Inter-modal dispersion is absent simply because the energy of light is transported by a single mode. CD and PMD are the major impairments in single-mode fibers. They have different origins but both can cause pulse spreading in the time domain as shown in Fig. 2.4. If the pulse represents the data symbol carrying the information, when the energy of the pulse spreads to the adjacent pulses, it leads to inter-symbol interference (ISI) and reduces the symbol quality, such as extinction-ratio. This section is the qualitative introduction of CD and PMD. We will continue CD and PMD quantitatively in Section 3.4.

CD is a phenomenon when the different spectral components of a pulse travel at different velocities [1]. CD consists of material dispersion and waveguide dispersion. Material dispersion is the principle component of CD, which occurs because the refractive index of silica, the material used for optical fiber fabrication, changes with the optical frequency so that different frequency components propagate at different speeds in optical fiber. In Fig. 2.4(a), the initial pulse consists of spectral components at different optical frequency. Due to CD, the spectral components travel at different speeds and consequently cannot arrive at the destination simultaneously. As a consequence, the pulse is spreading in time domain.

In optical fiber, small departures from the perfect cylindrical symmetry lead to birefringence, which results in two different polarization modes. Each polarization mode has its own transmission constant. The two constants can be considered as equal in most low-speed applications. However, their difference can not be ignored when the transmission bit rate is high and transmission distance is long. If the input pulse excites both polarization modes, it becomes broader as the two modes disperse along the fiber because of their different transmission constants. This phenomenon is called PMD [17]. In Fig. 2.4(b), the initial pulse excites both polarization modes. Since the two pulses are aligned in time, there is no pulse spreading. Due to the PMD effect, the pulses transmit through different modes cannot arrive at the destination simultaneously. If we only consider the first order PMD, each pulse of two modes may experience no pulse spreading by itself. However, when the two pulses are added together in IM/DD systems, they cannot reproduce the initial pulse because of their time mismatch, resulting in pulse spreading in time domain.

There exist various ways to combat CD and PMD in optical fiber networks. The old and new challenge of CD and PMD compensation comes from various aspects. One driving factor is the ever-increasing transmission bit rate per channel and transmission length in optical fiber networks. In the early stage, the CD and PMD distortions were not limiting factors when the bit rate was 2.5 Gb/s and transmission distance was about a few hundred km. When the bit rate increases to 10 Gb/s, the CD and PMD tolerance for IM/DD systems both reduces by a factor of 16, square of the ratio of bit rate increment. The corresponding CD tolerance is only 80 km and the PMD tolerance is about 30 ps. As telecommunication carriers are gearing up for its 40 Gb/s backbone expansion, the CD and PMD are the limiting factors of present optical fiber networks. The CD tolerance is only 5 km and PMD tolerance is 7.5 ps. Because the tolerance is so tight, even a small change caused by the environmental changes [45, 46] are becoming troublesome. The limitation of CD and PMD will be discussed thoroughly in Section 3.4.1.

The other driving factor is the traffic inside optical fiber networks, which has been discussed in Section 2.2. The tremendous growth of the internet and the world wide web over the last decade, both in terms of numbers of users and the bandwidth

per user, makes the IP traffic dominate communication networks. Packet-switched networks are proved to be effective and efficient in transmitting the ever-increasing IP traffic. Present packet-switched networks are usually realized by using electronic switches, such IP routers or ATM switches. The conventional optical fiber networks are circuit-switched networks and the network structures are almost static. These networks provide lightpaths, which can be established and taken down in a manual way. As per the discussion in Section 2.2.1, it is desirable to perform packet switching in the optical domain. Such a concept sets a significant challenge to the optical community. In the physical layer, optical fiber transmission is complicated by one more dimension that the signal changes in a short span of one packet length, e.g., 100 ns for 1000 bits long packet at 10 Gb/s. Unlike conventional circuit-switched networks, these packets even in the same channel may come from different sources and transverse different fiber links. An example is shown in Fig. 2.5, which shows the optical power, optical noise and CD evolution of 3 packets in a dynamic optical fiber network. The 3 packets originate from 3 different sources, and the optical powers may be different when they arrive at a same node receiver. Even though the optical powers can be equalized, the noise floors are different and difficult to equalize. In the CD map, each packet has different residual CD because of the different transmission fiber and dispersion compensation modules. The shortest path does not mean smallest residual CD and best performance. It is apparent the optical packet signal changes in a wide dynamic range and on per packet basis. Therefore, CD and PMD compensation needs to cope with these fast changes.

Finally, for any practical deployment, the cost is always a concern. Conventional optical fiber networks are generally for back-bone networks, where the cost is less concerned. However, with the success of optical fiber networks, they spread to access networks or local area networks (LAN), where the cost is a primary concern. Therefore the CD compensation needs to be cost-effective.

2.3.2 Optical versus Electronic Compensation

In history, optical approaches were almost the only solution to compensate optical impairments. Then the speed of microelectronics always lagged behind the optical
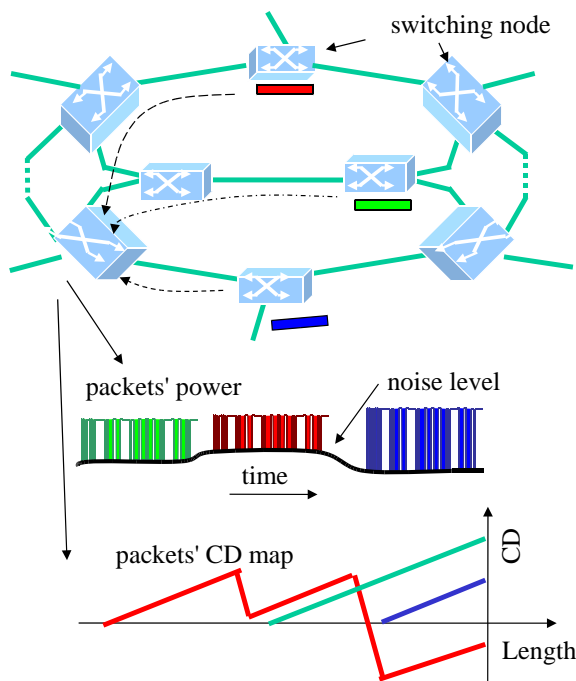
Figure 2.5: Power and CD evolution in a dynamic optical fiber network.

transmission rate. It is difficult to compensate the impairment of a high-speed signal by a low-speed circuit. There are several optical approaches for CD compensation:

Dispersion Compensation Fiber The dispersion compensation fiber (DCF) is a special kind of fiber, which is designed to have opposite dispersion parameters to that of transmission fibers. DCF provides an all-optical technique that is capable of totally compensating the CD in transmission fibers. DCF is also allowed for broadband dispersion compensation. In fact, DCF is the most mature technique in the present deployed optical fiber networks. Unfortunately DCF also has several disadvantages. DCF is a static compensation solution. The CD parameters can not be changed after the manufacture and packaging. The DCF is lossy, typically larger than 5 dB. Finally, DCF has a relatively small mode diameter, about a quarter of SSMF, which make it susceptive to non-linear effects caused by high density in optical fiber core. Another important problem in WDM systems is the dispersion slop match, or accurate CD compensation for multiple channels. Because the CD tolerance is becoming tight for high-speed transmission, it is difficult to satisfy slope match when the transmission distance is long. An example is shown in Fig. 2.6. DCF are used
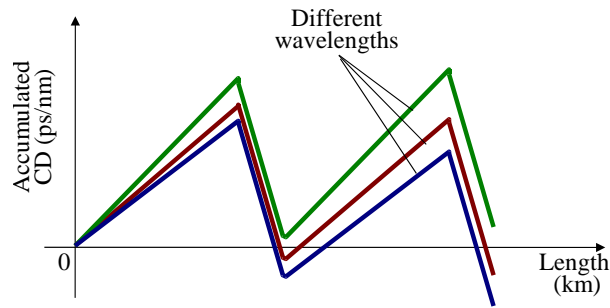
Figure 2.6: Accumulated CD map for different wavelength.

to compensate the CD of multiple channels/wavelengths. The slope mismatch means different residual CD after compensation for different channels. This difference linearly accumulates with the transmission distance. After long distance, it is impossible to compensate the residual CD within CD tolerance for multiple channels by DCF. Therefore, channel-wise CD compensation has to be used.

Fiber Grating for CD Compensation A fiber Bragg grating is a versatile device that can be used to compensate for CD. The grating can be designed to reflect different wavelengths at different points along its length, i.e., linearly chirped [17]. Effectively, the chirped FBG can introduce different delays at different wavelength and therefore compensate the CD. Several CD compensation techniques based on fiber grating (FBG) have been developed and used for system experiments [19]. The CD parameter of the FBG can be tuned by changing the grating period, e.g., by thermal change [47].

Optical Equalizer Optical Equalizer is a discrete finite impulse response (FIR) filter, trying to generate the inverse response of the channel response of CD [48, 49, 50]. The principle of optical equalizers is similar to that of electrical equalizers widely used in wireless communications [51].

There exists more CD compensators based on various techniques, such as ring resonators [52], arrayed-waveguide gratings [53], etc. They are less mature techniques and in the proof-of-concept stage.

The optical PMD compensation is basically the reverse of the PMD generation, so-called PMD emulator. Recall that PMD arises due to the fiber birefringence, which leads to a *fast* and a *slow* polarization component. The principle of PMD compensation is to split the received signal into its fast and slow polarization components, and to delay the fast component so that the DGD between the two components is compensated [17]. The challenge comes from the fact that DGD always varies as fast as *ms* [46], and therefore the PMD compensation must be carried out in real time. Because of the complexity, the PMD compensator can be classified in many different ways such as the control structure (feedback or feed-forward), the operating principle of the PMD emulator (e.g., piezo-electrical, electro-optical, thermal-optical) and the detection scheme (RF tones, degree of polarization, state of polarization, etc.) [18]. However, most PMD emulators are based on polarization maintaining fibers.

Polarization maintaining fiber (PMF) has strong birefringence and can preserve the properly oriented linear polarization of an input optical signal. A single piece of PMF can generate a fixed DGD, which can be used to compensate the PMD. The compensation condition is the proper alignment of the state of polarization (SOP) of the input signal to the PMF, which is done by a polarization controller [20].

On the other hand, electronic compensators are well known from radio and cable communications [14]. In contrast to those applications, the transmission speed of optical communication is much faster and close to the capabilities of microelectronics. Therefore, early research of electronic dispersion mitigation focused on simple structures, such as feed-forward equalizer (FFE) and decision-feedback equalizer (DFE) [54]. An example of FFE and DFE equalizer is shown in Fig. 2.7. The input signal is distorted data signals after optical-to-electrical (O/E) conversion. Within the FFE, the signal is delayed by a tapped delay line of half bit period (half-spaced). The delay line has 7 taps. The delayed data signal is tapped and weighted by the tap coefficients $C_1 \sim C_7$ and summed together. The equalization is realized by tuning the tap coefficients. The DFE comprises a decision circuit and a feedback path. The feedback signal from the decision circuit is delayed by one bit period, weighted by q coefficient, subtracted out from the input signal or the output of FFE in Fig. 2.7.
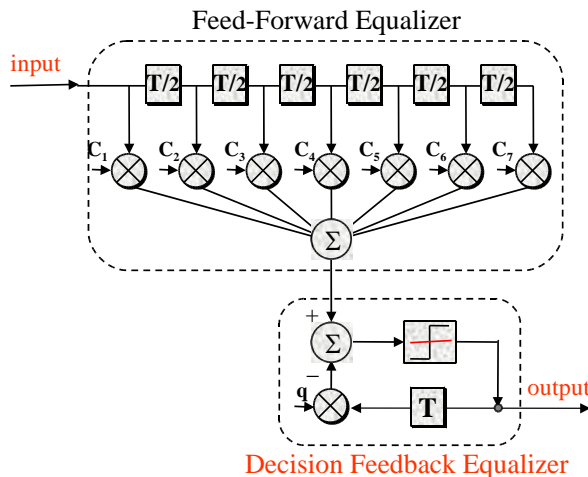
Figure 2.7: An example of FFE and DFE equalizer.

In this way, the DFE can take away post-cursors of previous decided bit. The FFE is linear filter which compensates linear distortion. The DFE is a non-linear filter which eliminates post-cursors of distorted signals. At 10 Gb/s, FFE/DFE based products have been tested for emerging telecommunication standards [55], and the sophisticated maximum likelihood sequence estimation (MLSE) receiver is already commercially available [56].

Conventionally, these equalizers are used in IM/DD systems and they belong to electronic dispersion mitigation because their simplified structure loses optical phase information. It is clear that the full optical field information must be accessed for electronic dispersion compensation. There are two approaches, transmitter based and receiver based. Transmitter based EDC distort the signal according to inverse response of optical channel [57]. If one devises the received signal carrying information only by intensity, the detection of the received signal can be a simple direct receiver. Therefore transmitter based EDC can have a simpler implementation than receiver based EDC. In general, transmitter based EDC requires a reverse feedback path. If the transmission length is 1000 km, the time delay from the feedback is about 5 ms. This means that rapid variations caused by mechanical vibration, thermal drift, optical network switching can not be compensated for. Thus transmitter based EDC is only a semi-static solution.

At receiver side EDC, it is possible to access the optical field without a local oscillator by using orthogonal band-pass filter. However it suffers from lower accuracy due to the inevitable non-linear operation and noise accumulation [58]. Another approach is using optical single sideband format at the transmitter, then the optical single sideband signal with transmitted carrier can be *self-homdyne* detected by simple direct detection and the majority of the optical phase information is converted to the electrical domain [13]. However, the inter-modulation noise cannot be avoided and impose a fundamental limit on performance. In a more conventional way, received side EDC needs a local oscillator to access the optical field of the incoming optical signal, or coherent detection. Coherent detection is a well-known technique in optical fiber communication. The next section is devoted to coherent detection.

Having reviewed optical and electronic approaches to compensate CD and PMD, we can compare them and provide some guidelines for choosing one approach for a specific application. In general, optical approaches have better performance while electronic approaches can provide competitive performance and additional advantages:

- Fast adaptation, taking advantages of the advanced integrated circuits. The fast adaptation is critical when the CD or PMD change fast. This is important for optical signals in OPSN, where every optical packet is different because it originates from different sources and traverses different optical paths [59]. A recent reported tunable optical dispersion compensator archived 1 *ms* response time [49], whereas the electrical PMD compensator showed 300 *ns* time constant [11].

- Cost-effective, which results from the mass production of integrated circuits. Though some initial electronic approaches are expensive, they can be cheaper if they are mass produced. This is appealing when optical fiber networks attack the cost-sensitive applications, such as access networks.

- Channelized solution. In a dynamic networks, like in OPSN, each channel comes from a different source and traverses a different fiber path. Consequently their impairments are different. Conventional optical approaches, like

CD compensator, target the multi-wavelength compensation, making them expensive to compensate each channel.

- Signal quality access. Since the optical signal is converted to the electrical domain, advanced signal processing technique can be adopted to estimate the signal quality without additional hardware requirements. For example, the electronic equalizers can monitor the CD [60] and estimate the optical channel characteristics [61].

- Non-linear computation. Electronic signal processing is much more sophisticated, especially digital signal processing. The non-linear computation is readily available. There are some electronic equalizers showing significant improvement by using non-linear computation [58, 62]. Even the non-linear transmission distortions in fiber can be mitigated by advanced digital signal processing [63].

From above comparisons, the electronic and optical approaches both have their pros and cons. It is expected that both approaches will co-exist in optical fiber networks.

2.3.3 Coherent Detection

Coherent detection had attracted worldwide research interests in the 1980s. Early research struggled with the noisy semiconductor laser diodes and tried to improve the receiver sensitivity [4]. Coherent local oscillator was realized by various types of optical phase-locked loops, which suffered from the noise and poor tunability of semiconductor laser diodes. On the other hand, the advent of Erbium-doped fiber amplifiers (EDFA) provided another approach to improve the receiver sensitivity. EDFA has such features as a simple configuration, high gain and low noise characteristics and excellent polarization-independent characteristics, that EDFA is quickly deployed in optical fiber networks. The receiver sensitivity of the IM-DD system has come to be comparable to the sensitivity of a coherent receiver because of the utilization of an optical pre-amplifier. The development of coherent detection had come to a standstill with the appearance of the EDFA. After almost 10 years, the

research interest of coherent detection re-appears as the high spectral efficiency and optical distortion compensation are important. Coherent detection has an inherent feature that can not be provided by IM-DD systems. It can achieve high spectral efficiency by taking advantage of the sharp cut-off characteristics of the electrical filters to demultiplex adjacent channels in a WDM systems.

Up to date, the practical optical phase-locked loop (OPLL) is yet available [64]. The re-advent of coherent detection takes advantages of advanced microelectronics and uses digital signal processing (DSP) to estimate and compensate the phase noise of local laser [65, 66]. Thus coherent detection is realized without conventional OPLL. Compared with the situation a decade earlier, the distributed feedback (DFB) laser linewidth is reasonably narrow as 100 kHz to 10 MHz and the data rate per channel is typically 10 Gb/s and beyond. These two facts support the coherent detection by DSP:

- The phase change of the laser is much more slower than the data rate. Therefore it is possible to obtain an accurate phase estimation by extracting the phase information over many data bits.

- The ratio between the laser linewidth and data rate is from 10^{-5} to 10^{-3} for coherent detection. Note when the ratio is 5×10^{-4}, at 10 Gb/s, even the most stringent PSK homedyne scheme can be realized with 1 dB power penalty at a BER of 10^{-9} [67]. Therefore the transmission performance can be guaranteed especially when considering the wide usage of feed-forward error correction (FEC) in optical fiber networks.

After laser phase compensation, conventional FFE or DFE filter can be used to remove the optical impairments since all the optical field information is known [68, 12, 65]. High spectral efficiency and ultra long-haul transmission with phase estimation [66] have also been demonstrated. All these experimental demonstrations show that coherent detection by phase estimation is feasible.

2.4 Optical Performance Monitoring in Optical Fiber Networks

To determine the health of optical signals in optical fiber networks, it is necessary to monitor many parameters in the physical layer such as optical power [69, 70], OSNR [71, 72], CD [73, 74, 75], Q-factor [76, 77], PMD [78, 79]. Due to the wide deployment of optical amplifiers, optical transmission systems can transmit over a long distance, e.g., 1000 km. In this scenario, OSNR and CD are two of the most important parameters to monitor because they can be limiting factors. In the following two subsections, we separately review the existing techniques for OSNR and CD monitoring.

2.4.1 OSNR Monitoring

The optical signal power and optical noise power within the interested frequency band need to be measured out for OSNR calculation. Unlike the optical power, it is challenging to measure the optical noise power due to two reasons below:

- The interested frequency band of optical noise is generally overlapped with that of the optical signal. Due to the presence of the optical signal, it is difficult to separate the optical noise.

- The optical noise power is generally much smaller than the optical signal power. For example, the optical noise power is only 1% of the optical signal power when the OSNR is 20 dB. Therefore, it is more difficult to measure the optical noise accurately.

There exist a number of OSNR monitoring techniques. All of these techniques focus on the measurement of the optical noise power directly or indirectly. They can be grouped as out-of-band monitoring and in-band monitoring.

Out-of-band Monitoring

In out-of-band monitoring technique, the ASE noise is measured out of optical signal frequency band. The measured ASE noise is then used to derive the ASE noise power

within optical signal frequency band. Therefore it is important for this kind of monitoring technique that the out-of-band ASE noise has a known relationship with the in-band ASE noise. This condition can be met when the ASE noise has much wider frequency range than optical signals. This condition can also be compromised when the optical signal with optical noise is filtered by a narrow filter, where the out-of-band ASE noise is not an accurate estimation of the true ASE noise power within the optical signal. As a result, the accuracy of out-of-band monitoring is conditional.

The conventional optical spectrum analyzer (OSA) is based on out-of-band monitoring. The working principle of OSA is detailed in [80]. Due to delicate optical components and precise mechanical movement, the OSA is an expensive solution for OSNR monitoring. Many alternative approaches try to use low-cost components but in a similar principle to OSA. For example, the optical spectrum scanning can be realized by a tunable optical filter [81] or using dispersive optical element such as arrayed waveguide grating together with an array of photodiodes [82]. Both techniques may achieve cost-effectiveness but they cannot avoid the inherent demerit of out-of-band measurement.

In-band Monitoring

To overcome the disadvantage of out-of-band monitoring, various in-band monitoring techniques have been proposed and demonstrated. These techniques try to discriminate the optical noise power from the optical signal power either in the optical domain or electrical domain and then measure the optical noise power directly. Inherently, in-band monitoring is more accurate than out-of-band monitoring.

In the optical domain, the optical noise and optical signal have different optical properties. For example, the optical signal is highly polarized whereas the optical noise is highly depolarized. Based on this difference, quite a few techniques using polarization nulling are demonstrated [83, 84, 71]. The basic principle is to device a destructive interference for the optical signal and therefore the optical signal can be suppressed lower than the optical noise power. From the principle, it is expected that the technique may be limited by the imperfect polarization states and interference

[84]. Subsequently, an improved technique by addition of off-center narrowband filtering is reported to be PMD-insensitive in [85].

In the electrical domain, the optical noise power can be analyzed from the RF spectrum resulting from the beating between the optical signal and optical noise. For example, by using a pair of offsetted narrow optical filters and a pair of balanced receivers, the optical signal can be subtracted out whereas the uncorrelated signal-to-ASE beating noise remains and can be measured out by using RF power meter [72]. This technique relies on the narrow optical filter and balanced receivers, and consequently may need more calibrations for accurate monitoring.

2.4.2 Chromatic Dispersion Monitoring

As optical fiber transmission systems evolve to high bit-rates and long reach transmissions, CD becomes one of the major limiting impairments. Moreover, CD is no longer a static parameter with the introduction of dynamic reconfigurable optical networks, such OPSN. As a result, CD monitoring has become not only a beneficial, but also essential function for optical fiber networks.

CD introduces different time delays among different frequency components. If we modulate the optical signal with a sinusoidal RF signal, or RF tone, the optical signal is introduced two discrete frequency lines/components. Due to CD, two frequency components travel at different speeds and have varying phase relationship between them. When a square-law photodiode is used, two frequency components may have constructive or destructive interference depending on their phase relationship caused by CD, which will be further discussed in Section 3.4.2. The detected RF power of the RF tone has a periodic fading characteristic with increasing amounts of CD [86]. Therefore, CD can be monitored by measuring the RF power of the RF tones. There may have monitoring ambiguity owing to the periodic fading characteristic. A simple solution is to add more RF tones. Combining the monitoring information from multiple RF tones, it has been demonstrated for an extended monitoring range [74].

Adding RF tones for monitoring requires to modify the transmitter structure. It is desirable to perform CD monitoring without modifying the transmitter. One

technique is to analyze the clock frequency components since most digital modulation formates have the residual clock. To avoid the beating between the clock frequency components in the conventional direct detection, coherent detection can be used [87]. In RF domain, the two clock components can be processed and narrowly filtered out. CD can be extracted out by measuring the time delay between the two clock frequency components. This technique also suffers from the monitoring ambiguity when the phase/time difference of the two clock is beyond π radian.

2.5 Motivations of the Thesis

Having reviewed the existing techniques for the research areas of this thesis, we introduce our motivations as follows.

2.5.1 AOLS Using Synchronous Phase Modulation

AOLS is one of the enabling techniques in OPSN and closely related to wavelength conversion. However the primary purpose of wavelength conversion is contention resolution instead of AOLS. Furthermore, wavelength converters are still expensive and it is cost effective to minimize the usage of them. In the OPSN node structure as shown in Fig. 2.1, each input interface or output interface should be equipped with a wavelength converter since the contention can happen at every interface. It is shown in [15] that only a small part of tunable wavelength converters is simultaneously utilized, which is due to two main reasons:

- each channel can not always have full 100% load. Therefore some channels contain no packet at a given instant.

- when two packets contending for the same output line, they do not need wavelength conversion if they are already carried by different wavelengths.

Wavelength converters can be further reduced in multi-fiber OPSN because each output have multiple fiber links and contention resolution can be done in one more dimension of different fiber link [16]. It is clear every input interface or output interface does not need a wavelength converter. As a result, it is cost effective to

share a limited number of wavelength converters where the majority of packets pass through the switch without wavelength conversion, especially in multi-fiber per link networks. However the AOLS is still needed for routing and forwarding purposes. Therefore it is highly desirable to be able to perform optical label swapping even when the packets bypass the wavelength converters. Although the approach using superimposed subcarrier label over ASK payload is able to meet this criterion [88], it requires additional DC-balanced-line-coding for the payload, resulting in lower effective bandwidth.

At the same time, DPSK format has attracted increasing research interests [89]. It shows better non-linearity tolerance in long-haul transmission [90]. Therefore many recent long-haul WDM transmission records at rates of 10 and 40 Gb/s per channel are now held by systems based on DPSK [91, 92, 93]. DPSK is becoming a mature technique. DPSK/PSK format has unique symbol symmetry, by which one symbol can be swapped to anther by a phase shift. For example, the symbol $'0'$ and $'\pi'$ are interchangeable by a phase shift of π. This symmetry is unique to PSK. For OOK, the $'0'$ symbol has no optical power, and there is no simple way to swap it to $'1'$ symbol. Base on the unique symmetry of DPSK, we propose AOLS using synchronous phase modulation, where old label is synchronously modified to a new symbol and no wavelength conversion is needed [94]. Considering network application, it is also of interest to investigate the technique in a multi-hop transmission.

2.5.2 Phase Estimation for Coherent Optical OFDM

Electronic compensation of optical distortion can resort to advanced modulation formats, such as OFDM. OFDM is a special form of frequency division multiplexing, which transmits a high-speed data stream over a number of low-speed subcarriers. OFDM has been attracted tremendous research interests in wireless community because it is resilient to frequency selective fading in transmission channels. In optical fiber communications, OFDM has been demonstrated for multi-mode fiber transmission [95]. Standard OFDM requires a high bias to convert bipolar electrical to unipolar optical signals, which degrades receiver sensitivity by more than 5 dB. One main difficulty to employ OFDM in optical communications is the square law detec-

tion of the photodiode, which loses the optical phase information. Recently, optical single sideband (OSSB) has been proposed because it can map optical phase distortion to the electrical domain [96]. However, such a scheme requires a frequency guard band of at least the width of data spectrum and the residual carrier suffers from transmission noise.

It is advantageous to combine coherent detection and OFDM, which has been recently proposed and shown for the enormous tolerance of CD and PMD distortion [22, 97]. Intuitively, the resilience of CD and PMD distortion of OFDM is a natural result from the much lower bit rate of each subcarrier. By using coherent detection, if the optical power into optical fiber is limited to linear range, the optical fiber transmission becomes a linear channel for the electrical signals and the linear distortion can be fully compensated. For coherent detection, it is advantageous using phase estimation instead of conventional OPLL based on our review in Section 2.3.3. Therefore, phase estimation is one of the important technique in coherent optical OFDM. In conventional modulation format, data are encoded to one optical carrier in time domain. In OFDM, however, data are encoded to multiple optical carriers in frequency domain. Although phase estimation has been done in wireless communications [21], it is important to investigate and demonstrate it in optical communications.

2.5.3 Optical Performance Monitoring in Optical Fiber Networks

There exist various OSNR and CD monitoring techniques. Each technique has its advantages and disadvantages depending on the applications. In this thesis, our researches fall into OPSN and electronic compensation of optical distortions.

In a node of OPSN, the incoming optical packets may originate from different sources and traverse different optical links. Consequently, each optical packet has its own history and signal quality. In particular, the signal quality may change in a short time duration, such as 100 ns for a 1000-bit long 10 Gb/s optical packet. To address this challenge, we propose an OSNR monitor capable of measuring the

varying OSNRs of consecutive optical packets. Each optical packet only lasts about 102.4 ns.

It is expected that electronic compensation of optical distortions will spread into optical fiber networks as adaptive and cost-effective compensation is needed. An inherent nature of electronic compensation is that optical distortions are , fully or partly, down-converted to the electrical domain. When the electronic compensation receiver compensates the optical distortion, it also reflects the strength of optical distortion. For example, the tap coefficients of FFE receiver are strongly decided by the optical distortion. Thus it is possible to monitor the optical distortion by analyzing the tap coefficients [60]. The advantage of this technique is that there is no additional hardware requirement in addition to electronic compensation receiver. The optical distortion monitoring is carried out by further signal processing in generic digital signal processors.

2.6 Conclusion

Two primary tasks for optical fiber networks are data routing and data transmission. Centered around the two tasks, the work of this thesis fall into three areas. In this chapter, we have explored the literature pertinent to the three research areas of this thesis.

In Section 2.2, we have reviewed the available AOLS techniques, which are essential to route IP packets in OPSN. By using AOLS, optical label information is swapped at each node in the electrical domain, while optical data/payload remains in the optical domain to avoid the unwanted OEO conversion. Several optical labeling techniques have been discussed and compared. The AOLS techniques are strongly determined by optical labeling techniques, and consequently they are reviewed according to the different optical labeling techniques.

In Section 2.3, we have reviewed the available techniques on electronic compensation of optical distortions. The advantages and disadvantages of the techniques are also discussed. Electronic compensation of optical distortions has become feasible due to the fast advances of microelectronics. On the other hand, the evolution of

optical fiber networks requires adaptive and cost-effective compensation solutions. Electronic approaches are promising to satisfy the requirements. The structure and performance of electronic compensator vary vastly. It depends on the application to choose an appropriate electronic compensator.

Optical performance monitoring is increasingly important for optical fiber networks. The new applications, such as OPSN, create many new challenges to the existing monitoring techniques. Section 2.4 has reviewed the existing OSNR and CD monitoring techniques.

From the literature review in this chapter, innovative techniques or further improved techniques are required in the three research areas. We have then discussed our motivations for each of our proposed new techniques in Section 2.5.

Chapter 3

Signal Processing for Optical Fiber Networks

3.1 Introduction

Fig. 3.1(a) shows a generic block diagram of optical communication systems. The objective of the communication is to transmit data through the networks from one place to another place. The fundamental difference of optical fiber networks is that data are carried on optical carriers. Therefore, transmitters, receivers, and transmission links are designed to the needs of optical signals. The network can be in various forms, from simple to sophisticated. Fig. 3.1(b) is a simple one, consisting of optical fiber cables. Even though optical fiber is a superb transmission medium, it still has attenuation and dispersion, which is troublesome for the higher bit rate and longer distance transmission. Attenuation is generally compensated by optical amplifier, which introduces optical noise unfortunately. Optical noise can not be compensated and therefore imposes a fundamental limit for long-haul transmission. In this thesis, we only deal with single mode fibers, and therefore dispersion includes chromatic dispersion (CD) and polarization mode dispersion (PMD). Dispersion is much more difficult than attenuation to compensate. Dispersion compensation is a major target of this thesis. Furthermore, the optical channel is a pipeline, which is aggregated from small traffic. It is natural to add and drop some traffic from the optical channel since not all the traffic go to the same destination. Fig. 3.1(c) is a conventional optical-electrical-optical (OEO) switch. The function of the switch is to drop and add part of traffic from the optical signal. This approach is based on mature techniques but is considered costly and inefficient because all the traffic including the passing through traffic are converted to the electrical domain and then converted back to the optical domain again. Since the optical signal speed

43
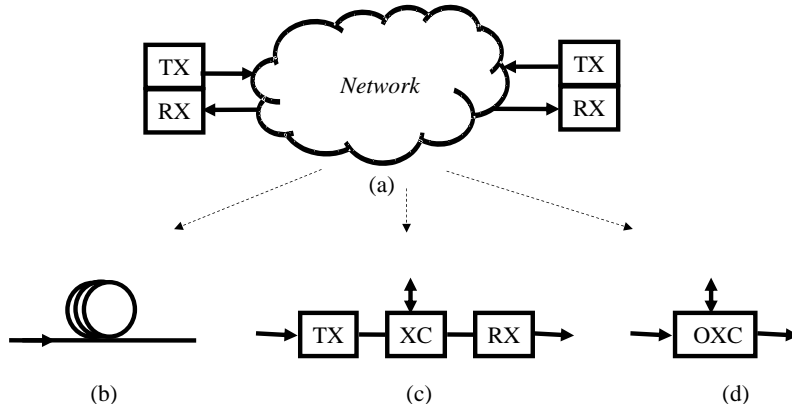
Figure 3.1: (a) A generic diagram of optical communication systems, (b) optical fiber channel, (c) OEO electrical switch, (d) optical switch. Tx: Transmitter. Rx: Receiver.

is generally very high, this OEO conversion is demanding for the electrical-speed, which causes so-called electronic bottleneck. Fig. 3.1(d) is an optical cross-connect (OXC) and envisioned as a critical element of the future optical networks. While the actual realization of the optical switch is quite diverse, the purpose is to keep the signal in the optical domain as much as possible to avoid OEO conversion. There are numerous challenge to realize the optical switch and many of them are still open problems [28].

In this chapter, we present the equivalent low-pass system to describe the optical transmission system in Section 3.2. Section 3.3 details the building blocks of transmitter and receiver from the perspective of signal processing. Section 3.4 introduces optical impairments in optical fiber links. The limits from the major impairments are mathematically described. We also introduce optical re-circulating loop, which is an experimental platform for long-haul optical transmissions. The purpose of this chapter is to provide the technical background and define the pertinent terminologies for the ensuing chapters.

3.2 Equivalent Low-pass Signal and System

For a monochromatic light,the electric field vector $\vec{E}$ as a function of time t can be written as [1]:

$$\vec{E}(t) = \vec{r}|E(t)|\,cos[2\pi f_c t + \theta(t)] \tag{3.1}$$

where $\vec{r}$ is a two-dimensional vector denoting the coordinate in the direction perpendicular to the propagation direction,$|E|$ is amplitude, f_c is the light frequency, and θ is the phase. The vector $\vec{r}$ also means the polarization of the light. Fundamentally, there are four dimensions of a light to carry information, i.e., polarization, amplitude, frequency, and phase. In the context of digital modulation, they correspond to polarization-shift keying (PolSK) [98], amplitude-shift keying (ASK), frequency-shift keying (FSK), and phase-shift keying (PSK). However, the available receiver or photodiode in optical fiber communications only responds to the optical power/intensity. Therefore, only intensity/amplitude modulation can be directly detected by optical receivers. Optical polarization, phase, and frequency have to be converted to optical intensity information by additional components and devices, which consequently increases the implementation complexity. Therefore the simplest technique is to change the optical power between zero and one, which is often called on-off keying (OOK) to reflect the on-off nature of the resulting optical signal.

This thesis focuses on optical amplitude and phase. Since polarization is generally constant or slowly varying, it is more convenient to use a scalar expression to replace (3.1):

$$E(t) = |E(t)|\,cos[2\pi f_c t + \theta(t)] \tag{3.2}$$

It is clear that $E(t)$ in (3.2) is a band-pass signal, which is conventionally expressed as:

$$s(t) = a(t)cos[2\pi f_c t + \theta(t)] \tag{3.3}$$

where $a(t)$ is the signal amplitude.

Throughout this thesis, equations (3.1) and (3.3) both are used to represent the optical signal. Equation (3.1) emphasizes the optical characteristics whereas equation (3.3) is for the general signal processing.

In optical communication systems, information-bearing signals are transmitted by modulating optical carriers. Since optical signals and channels are limited in certain bandwidth, they are characterized as band-pass signals and channels. Without loss of generality and for mathematical convenience, it is desirable to express all band-pass signals and channels to equivalent low-pass signals and channels. In fact, optical communications are quite similar with wireless communications, the major difference is that the frequency of optical carriers are higher than 100 THz, compared with GHz of RF carriers.

Rigorous derivation of equivalent low-pass signals of (3.3) can be found in [99]. Equivalent low-pass signals can also be derived by mathematical manipulation of (3.3) as below:

$$
\begin{aligned}
s(t) =& a(t)cos[2\pi f_c t + \theta(t)] = \Re\{a(t)e^{j[2\pi f_c t + \theta(t)]}\} \\
=& \Re\{a(t)e^{j\theta(t)}e^{j2\pi f_c t}\} = \Re\{s_l(t)e^{j2\pi f_c t}\}
\end{aligned}
\tag{3.4}
$$

where j is complex unit throughout this thesis, $j = \sqrt{-1}$. $s_l(t)$ is the equivalent low-pass signal of the real signal $s(t)$ and is generally a complex number as shown below:

$$
\begin{aligned}
s_l(t) =& a(t)e^{j\theta(t)} = x(t) + jy(t) \tag{3.5} \\
a(t) =& \sqrt{x^2(t) + y^2(t)} \tag{3.6} \\
\theta(t) =& tan^{-1}\frac{y(t)}{x(t)} \tag{3.7}
\end{aligned}
$$

$x(t)$ and $y(t)$ are called the in-phase and quadrature components of the band-pass signal $s(t)$. To see this, (3.3) is re-written with trigonometry as:

$$
\begin{aligned}
s(t) =& a(t)cos[2\pi f_c t + \theta(t)] \\
=& a(t)cos[\theta(t)]cos(2\pi f_c t) - a(t)sin[\theta(t)]sin(2\pi f_c t) \\
=& x(t)cos(2\pi f_c t) - y(t)sin(2\pi f_c t)
\end{aligned}
\tag{3.8}
$$

(3.8) is the basis to understand quadrature signal processing.

The input and output of optical systems are both band-pass signals. If optical signals can be represented by equivalent low-pass signals, optical channel can also be represented by equivalent low-pass channel. Thus, we shall deal only with the transmission of equivalent low-pass signals through equivalent low-pass channels, which is not only for mathematical convenience but also for computer simulation efficiency. To simulate optical communications in computers, the continuous-time signal are sampled and converted to discrete time versions. According to the Nyquist's criterion, a signal of bandwidth B can be reconstructed from samples taken at the $2B$ samples/s. The typical light frequency in optical fiber communications is about 100 THz, which is very demanding to simulate this absolute bandwidth. However, the data bandwidth modulating the light is generally about GHz, which can be easily simulated using equivalent low-pass signal and channel.

Through out this thesis, the equivalent low-pass signal and channel description are used. The band-pass signal can be obtained by using (3.4).

There are three digital modulation format used in this thesis. As an example, the equivalent low-pass of BPSK and QPSK can be expressed as:

$$s_l(t) = e^{j2\pi \frac{x_n}{M}}, \tag{3.9}$$

$$x_n = \begin{cases} 0, 1; & M = 2; \\ 0, 1, 2, 3; & M = 4; \end{cases} \tag{3.10}$$

The base-band signal is encoded to optical carrier by in-phase quadrature (IQ) modulation. In signal processing, the encoding is obtained by multiplying a complex carrier $e^{j2\pi f_c t}$ to the base band signal as below:

$$s(t) = s_l(t)e^{j2\pi f_c t} = e^{j2\pi(f_c t + \frac{x_n}{M})} \tag{3.11}$$

The real signal is simply the real part of the complex signal. When the signal is sampled to digital domain, the variable t is replaced by nT for a digital sequence.

3.3   Transmitter and Receiver

The main role of optical transmitter and optical receiver is to convert the data signal between the electrical and optical domain. This corresponds to modulation and demodulation in terms of signal processing. The standard modulation/demodulation scheme being employed in the present commercial optical fiber communications is called IM/DD scheme. The term IM means that the light intensity (not the amplitude) is modulated linearly with respect to the input signal voltage and basically no attention is paid to the phase of the carrier. The term DD stems from that the signal is detected directly at the optical stage of the receiver; neither the frequency conversion (heterodyne or homodyne scheme) nor sophisticated signal processing at lower frequency is performed. However, it is advantageous to know optical phase, which requires more complex transmitter and receiver. One way is coherent detection, which is generally achieved by using a local oscillator to beat with the incoming signal. DPSK can be viewed as a special case to make use of optical phase, where the preceded signal is used to beat with current signal.

3.3.1   Laser Source

Optical fiber communication systems use semiconductor lasers due to their several advantages, such as compact size, high efficiency, good reliability, and right wavelength range [1]. Most lasers used in optical fiber communication systems are distributed-feedback (DFB) lasers. As its name suggests that the feedback is not localized at the facets but achieved through an internal built-in grating that leads to a mode selection. DFB lasers have advanced significantly and are commercially available. As a fact, DFB lasers are used routinely for WDM systems.

An ideal laser source can be described as (3.1), which has a single spectral line in frequency domain. However, the practical laser source always has amplitude and phase noise, which contribute a finite spectral linewidth. The phase noise and the non-zero linewidth of semiconductor lasers come from spontaneous emission in laser materials. In computer simulation, the laser phase noise can be simulated by white Gaussian frequency noise [100]. In IM-DD systems, a narrow laser linewidth

is essential for high-speed transmission when CD takes effects. Fortunately, the linewidth requirement can be easily met by the commercial DFB lasers. The present narrowest DFB laser is about 100 kHz [101]. In coherent system, the linewidth characterizes the strength of the phase noise, which sets one of the fundamental limits. The variance of phase noise of finite laser linewidth is:

$$\sigma^2 = 2\pi \Delta f T \tag{3.12}$$

where T is the observation time of the laser phase change, Δf is the full width at half-maximum of the laser freqency spectrum. From (3.12), if the laser linewidth is wider, the phase noise is stronger. When the phase noise is too strong, the useful phase information is corrupted and can not be recovered any more. Therefore, optical phase modulation format generally requires narrow linewidth lasers. In laboratory, the external cavity lasers are also used when the narrower linewidth, i.e., low phase noise is desirable.

3.3.2 External Modulator

Optical modulator using electro-optic or electro-absorption effect plays an important role in high-speed optical communication systems. The main stream of external modulator is based on lithium niobate crystal.

Fig. 3.2 shows the principle of a phase modulator. As shown in Fig. 3.2(a), the main structure of phase modulator comprises optical waveguide and RF electrode. When voltage is applied to the RF electrode, due to the electro-optic effect of LN substrate, refractive index is changed by the electrical field, and the phase of the optical signal in one arm is advanced, i.e., phase shift. Fig. 3.2(b) is an example of π phase shift and the corresponding RF voltage is denoted as V_π. One disadvantage of the LN waveguide is polarization sensitivity. Therefore the polarization stage of the input light needs to be aligned appropriately. Polarization misalignment can cause polarization dependent loss (PDL), or the output optical power varies with the input polarization state. The polarization misalignment can also change the phase shift value even when a constant voltage is applied to the RF electrode. In all the
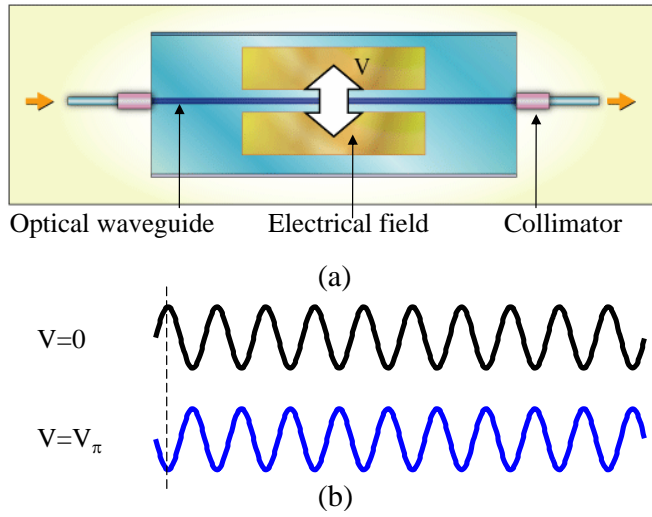
Figure 3.2: (a) Structure of phase modulator, (b) Phase shift by phase modulation.

experiments of this thesis, the optical modulators are all equipped with polarization controllers before the input port even there is no mention in experimental setup figures and descriptions, which is for the sake of simplicity.
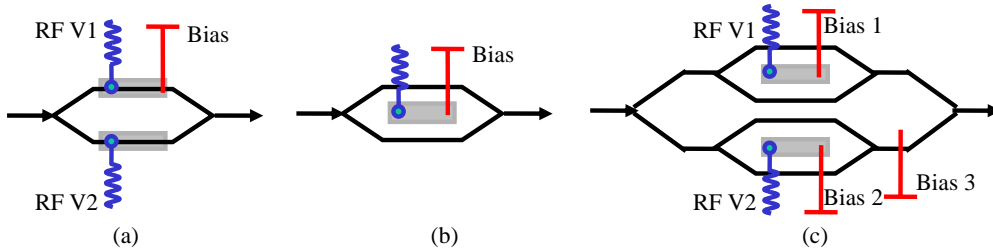
Figure 3.3: Typical structure of MZ modulators.

For amplitude/intensity modulation, the modulator is generally configured as a Mach-Zehnder (MZ) interferometer [17]. Two waveguides form the two arms of the MZ interferometer. When the optical fields in the two arms experience the identical phase shifts, the output optical signal is maximal, which is called constructive inter-ference. When the phase difference between two arms is π, the output optical signal is minimal, which is called destructive interference. There are also different ways to arrange the electrode for the waveguide. Fig. 3.3 (a) shows a dual-electrode MZ modulator, where two RF signals can be applied to. The output of a dual-electrode

is:

$$E_o = \frac{E_i}{2}(e^{j\pi\frac{V_1}{2V_\pi}} + e^{j\pi\frac{V_2}{2V_\pi}}) \tag{3.13}$$

where V_1 and V_2 are the RF signals. If we let $V_1 = -V_2$, this configuration is called push-pull mode. If we want to generate a π phase shift between two arms in a dual-electrode MZ modulator, each arm only needs to produce $\frac{\pi}{2}$ phase shift, one negative, one positive. Therefore, a factor of 2 is included in MZ transfer function. The output of the modulator can be simplified as:

$$E_o = E_i cos(\pi\frac{V_1}{2V_\pi}) \tag{3.14}$$
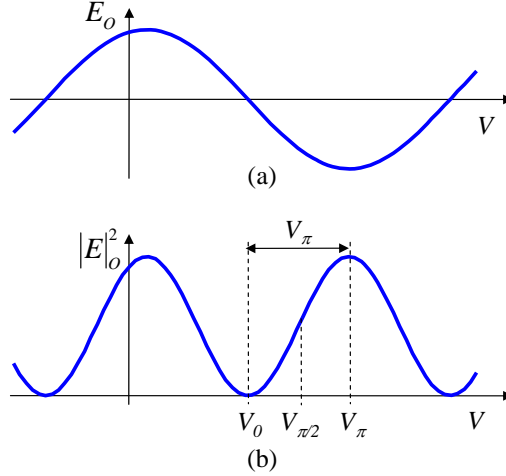
Figure 3.4: Amplitude and intensity transfer curves of an MZ modulator.

Since IM-DD system is prevalent, it is popular to express the output of the modulator in terms of intensity as:

$$|E_o|^2 = |E_i|^2 cos^2(\pi\frac{V_1}{2V_\pi}) \tag{3.15}$$

In reality, V_1 is generally an AC only signal, which is added with a DC voltage signal, or DC bias V_B. The procedure is called to bias the modulator. Equation (3.15) is extended to include the DC bias as below:

$$|E_o|^2 = |E_i|^2 cos^2(\pi\frac{V_1 + V_B}{2V_\pi}) \tag{3.16}$$

Fig. 3.4 shows the typical amplitude transfer and intensity transfer curves. Note, because of the manufacturing process, when no DC bias, the transfer curve can shift left or right for different modulators. When $V_1 = 0$, i.e., no RF signal input, the DC bias voltage controls the output optical power. The DC bias voltage corresponding to minimum output, in theory $|E_o|^2 = 0$, is defined as V_0, or biased at null point. In a similar way, the voltage corresponding to maximum output is defined as V_π. For IM-DD binary systems, the bias point is generally set at the 50% transfer curve, or quadrature point.

The push-pull mode modulator can be further simplified to a single electrode. By changing the RF voltage, the output optical signal power can be switched between two levels, one of which is set to zero. This modulation format is generally called OOK to reflect the on-off nature of the resultant optical signal, which is described below:

$$Eo^2 = \begin{cases} 0; & V_1 = V_\pi \\ E_i^2; & V_1 = 0 \end{cases} \quad OOK\,modulation \tag{3.17}$$

This modulator can also generate binary phase-shift keying (BPSK) when biased at the null point. If we compare the amplitude and intensity transfer curve in Fig. 3.4, V_π is defined according to the intensity transfer curve, which is actually the equivalent $V_{\pi/2}$ point for amplitude transfer curve. It can be seen as below that the output is only intensity modulated and there is no any phase modulation. Hence in this push-pull mode, the modulator is called chirp free.

$$Eo = \begin{cases} -E_i; & V_1 = -V_\pi \\ E_i; & V_1 = V_\pi \end{cases} \quad BPSK\,modulation \tag{3.18}$$

Recently, the dual-parallel MZ modulator is very attractive for arbitrary optical field modulation [102]. Each of the two inner zero-chirp MZ modulators acts independently and the outer MZ structure is biased with a $\frac{\pi}{4}$ phase shift. The transfer function is:

$$E_o = \frac{E_i}{2}[cos(\pi\frac{V_1 + V_{B1}}{2V_\pi}) + e^{j\pi\frac{V_{B3}}{V_\pi}}cos(\pi\frac{V_2 + V_{B2}}{2V_\pi})] \tag{3.19}$$

If we set $V_{B3} = -\frac{V_\pi}{2}$, $E_i = e^{j2\pi f_c t}$, and define $I \triangleq cos(\pi\frac{V_1+V_{B1}}{2V_\pi})$, $Q \triangleq cos(\pi\frac{V_2+V_{B2}}{2V_\pi})$, the output real signal is:

$$s(t) = \Re\{E_o\} = Icos(2\pi f_c t) - Qsin(2\pi f_c t) \tag{3.20}$$

Compare with (3.8),the modulator approximates an ideal Cartesian EO converter, which can modulate optical intensity and optical phase in an arbitrary way.

3.3.3 Direct Detection Receiver

The function of photodiode can be described as a square-law detector as below:

$$i(t) = r\,|E_i(t)|^2 \tag{3.21}$$

where $i(t)$ is the output current, and r is the responsivity of the photodiode. One important result from this direct detection is that the phase information of the optical carrier is totally lost. Consequently, the optical field can not be accessed.

The major complications in the photodiode are the additional noises. The shot noise and thermal noise are the two fundamental noise mechanisms responsible for current fluctuations in all optical receivers even when the incident optical signal power is constant. Shot noise is a manifestation of the fact that an electric current consists of a stream of electrons that are generated at random times. The thermal noise current is from the random motion of electrons that is always present at any finite temperature. In most practical direct detection receivers, the thermal noise is much stronger than the shot noise [17]. In addition to the imperfection of photodiode, the imperfection of the optical signal converts to the electrical current noise after the photodiode. The optical signal source always has phase noise and intensity noise as mentioned in Section 3.3.1. Furthermore, the optical amplifier always adds amplified spontaneous noise (ASE). Both optical noises or optical power fluctuations are converted into current fluctuations in photodiode. In optically amplified optical fiber communication systems, ASE is generally the dominant noise, which is further elaborated in Section 3.4.1 .

Receiver has a decision circuit to identify bits, which can be compared with the transmitted bits to calculate bit-error rate (BER). BER is frequently used to characterize the performance of digital systems. An important parameter for any receiver is the receiver power sensitivity. It is usually defined as the minimum average optical power required to realize a specific BER level, e.g., 10^{-3} or 10^{-9}. In an optically amplified system, optical receivers always has enough optical power and the BER performance is dominant by amplifier noise, where optical signal-to-noise ratio (OSNR) is used to evaluate the noise strength. In such systems, OSNR sensitivity is often used to evaluate the minimum OSNR required for a particular BER while the optical power is kept adequate to optimize the receiver performance.

Noise and other impairments degrade the signal quality. Therefore received optical power is generally increased to satisfy the same BER of the receiver without those noise and impairments. The increase of the optical power is referred to as the optical power penalty. In a similar way, OSNR penalty is used to evaluate the strength of the noise and impairments.

3.3.4 Differential Receiver

In a differential receiver, the received signal in any given signaling interval is compared with the phase of the received signal from the preceding signaling interval. Therefore differential receivers do not require a local oscillator and are often considered to be non-coherent receivers.

In optical fiber communications, the differential demodulator can be realized by an MZ interferometer, which is also called optical demodulator. MZ interferometers can access optical phase difference of a fixed time interval. In this method, optical phase estimation and recovery are not required, which is often considered to be a non-coherent communication technique. This method is much simpler than coherent detection and consequently find wide applications in differential detection optical systems. An MZ interferometer is illustrated in Fig. 3.5(a), consisting of two optical couplers, and a delay line. The principle is to interfere a signal with its delayed version.

Following the description in Section 3.2, the equivalent low-pass of a binary PSK
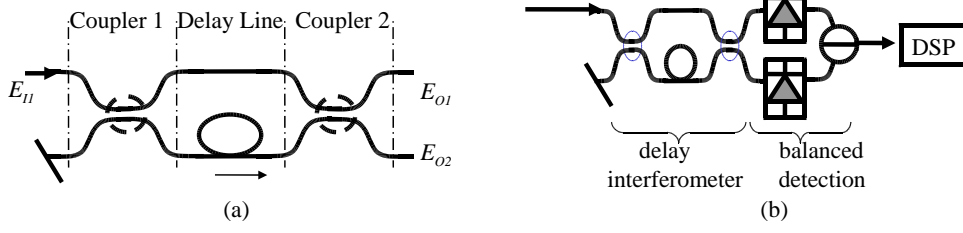
Figure 3.5: (a) Interferometer structure, (b) Balanced differential detection

modulated signal waveforms may be expressed as:

$$E(nT) = e^{j\pi x(nT)\pi}, \qquad x(nT) = 0 \ or \ 1, n = 0, 1, 2, \cdots \tag{3.22}$$

The outputs of the MZ interferometer with a time delay of one bit period T are:

$$\begin{cases} E(nT) + E(nT - T) * e^{j\phi}, & constructive \ interference \\ E(nT) - E(nT - T) * e^{j\phi}, & destructive \ interference \end{cases} \tag{3.23}$$

where ϕ is the phase change caused by the delay line. If we choose a MZ interferometer as an optical demodulator of DPSK, we will adjust time delay to the bit period T and phase delay so that $\phi = 2n\pi$, $n = 0, 1, 2, \cdots$. Since a square-law photodiode is used to detect optical powers, the output powers of MZ interferometer are calculated as:

$$\begin{cases} P_{O1} = & |E(nT) + E(nT - T)|^2 \\ P_{O2} = & |E(nT) - E(nT - T)|^2 \end{cases} \tag{3.24}$$

where P_{O1} is from constructive interference port and P_{O2} is from destructive interference port.

The truth table of the optical demodulator is shown in Table 3.1. It is clear P_{O1} is the XOR logic output of $E(nT)$ and $E(nT - T)$ and P_{O1} is the XNOR logic output of $E(nT)$ and $E(nT - T)$. If we use a balanced receiver as shown in Fig. 3.5(b), the detected power is $P_{O1} - P_{O2}$, which is also listed in Table 3.1. The $'0'$ and $'1'$ signal spacing is doubled from $[0 \quad 4|E|^2]$ to $[-4|E|^2 \quad 4|E|^2]$, which explains the almost 3 dB advantage of balanced detection [89].

$\phi(nT)$	$\phi(nT-T)$	P_{O1}	P_{O2}	$P_{O1} - P_{O2}$
0	0	$4\,\lvert E\rvert^2$	0	$4\,\lvert E\rvert^2$
0	π	0	$4\,\lvert E\rvert^2$	$-4\,\lvert E\rvert^2$
π	0	0	$4\,\lvert E\rvert^2$	$-4\,\lvert E\rvert^2$
π	π	$4\,\lvert E\rvert^2$	0	$4\,\lvert E\rvert^2$

Table 3.1: Truth table of optical demodulator

3.3.5 Coherent Receiver

In a coherent receiver, a local oscillator laser is incorporated with an optical receiver. Depending on the frequency difference between the local oscillator and incoming optical carrier, coherent detection can be classified as heterodyne or homodyne detection. In a coherent heterodyne detection scheme, the optical frequency of the signal is about several gigahertz different from that of the local oscillator light. The modulated signal is down converted into an electrical intermediate frequency (IF) signal by the square-law characteristics of a photo diode, the following electronic demodulator demodulates the IF signal into the transmitted signal. In a coherent homodyne detection scheme, the optical frequencies and phases of the signal and the local oscillator are completely matched, so that the modulated optical signal can be directly demodulated into the baseband signal.
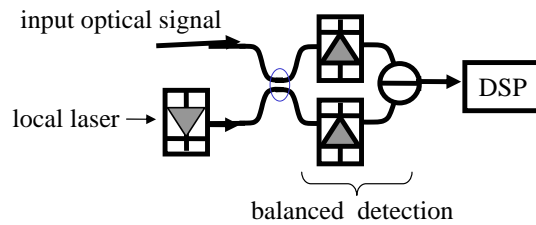
Figure 3.6: Coherent receiver.

A simple coherent receiver is shown in Fig. 3.6. The incoming light is mixed with a local oscillator signal via an optical coupler and sent to the photodiode. For the interference purpose, the polarization states of the two waves need to be aligned. Hence, there is always a polarization controller before the optical coupler in the coherent detection experiments of this thesis. The incoming signal is: $E_s = a(t)e^{j2\pi f_c t + j\theta_c(t)}$, where $a(t)e^{j\theta_c(t)}$ carries the useful information and the lo-

cal oscillator with unit amplitude is: $E_l = e^{j2\pi f_l t + j\theta_l(t)}$. After photo detection, the electrical currents of the two arms are:

$$i(t) \propto |E_s(t) + E_l(t)|^2 = E_s(t)E_s^*(t) + E_l(t)E_l^*(t) + \Re\{E_s E_l^*\} \tag{3.25}$$

$$i(t) \propto |E_s(t) - E_l(t)|^2 = E_s(t)E_s^*(t) + E_l(t)E_l^*(t) - \Re\{E_s E_l^*\} \tag{3.26}$$

where $|\cdot|^2$ is modulus square operation; $\cdot^*$ is conjugate operation and $\Re\{\cdot\}$ represents the real part. In general, a balanced detection is used by subtraction of the two electrical currents, which is:

$$i(t) \propto |E_s(t) + E_l(t)|^2 - |E_s(t) - E_l(t)|^2 = 2\Re\{E_s E_l^*\} \tag{3.27}$$

$$=2a(t)cos[2\pi(f_c - f_l)t + (\theta_c - \theta_l)] \tag{3.28}$$

The advantage of balanced detection is the disappearance of $E_s(t)E_s^*(t) + E_l(t)E_l^*(t)$ in (3.28), which means much less noise.

From (3.28), if we want to recover the useful information, two conditions below need to be satisfied:

$$f_c - f_l = 0 \tag{3.29}$$

$$\theta_c - \theta_l = constant \tag{3.30}$$

The first condition is called frequency locking, which can be done in one step in homodyne or two steps in heterodyne. The second condition is called phase locking. Traditionally, phase locking is carried out by optical phase-locked loop. However, as mentioned in Section 2.3.3, another promising approach is to employ digital signal processing, which is equivalent of OPLL in digital domain. The carrier phase is estimated and compensated in digital signal processor. In [103], the carrier phase estimation for a QPSK encoded signal is discussed in detail. The principle is to raise the data sequence to the fourth power. As a result, the phase modulation of data is canceled but the residual phase is 4 times of the optical carrier phase. It is an example of Mth-power law method and we will continue to discuss it in

Section 5.3.3. Because the estimation is corrupted by Gaussian noise, it is necessary to average the the carrier phase over many symbol intervals to obtain an accurate phase estimation. In short, coherent detection by phase estimation can achieve the same performance by conventional OPLL.

As discussed in Section 3.3.3, thermal noise or ASE noise is prevalent in IM-DD systems. However, we can increase the local laser power sufficiently higher than the incoming signal light. In this condition, the shot noise from the local laser is dominant, which is called shot noise limited condition. In general, shot noise is smaller than thermal noise, which explains the better sensitivity by coherent detection.

3.4   Optical Fiber Channel

When an optical signal is transmitted in a optical fiber channel, optical impairments degrade its quality. Optical impairments can be grouped as noise and distortion. Noise mostly comes from optical amplifiers and degrades the signal-to-noise ratio. Noise can not be mitigated once it is added to optical signal because of its random nature. Distortion generally causes inter-symbol interference. The distortion considered in this thesis include CD and PMD, which can be fully compensated in theory. Another distortion source is non-linearity in fiber, which is not discussed in this thesis because we focus our work on linear transmission domain by controlling the optical power into optical fiber.

3.4.1   Optical Amplifier

In an optical communication system, the optical signals from the transmitter are attenuated as they propagate through the optical fiber. Many optical components, such as couplers and optical switches, also attenuate the optical signal. Prior to the advent of optical amplifier, the only option was to regenerate the signal, that is, to receive the signal and retransmit it. Optical amplifier has become an essential component in optical networks to compensate the transmission losses. The most common optical amplifier today is the erbium-doped fiber amplifier (EDFA). The

development of EDFAs in the late 1980s and early 1990s enables the optical long-haul transmission and the applications of WDM. In addition to providing optical gain, EDFAs also add undesired noise onto the amplified signal, which is called amplified spontaneous emission (ASE) noise.

The total ASE noise power in an optical bandwidth B_o is given as [104]:

$$P_{ASE} = 2n_{sp}hf(G-1)B_o \qquad (3.31)$$

where n_{sp} is the spontaneous emission noise factor, hf is the photon energy, and G is the gain of the optical amplifier. The factor of 2 captures the ASE noise in all polarization since the ASE noise is typically unpolarized. n_{sp} is used to approximate the noise figure (NF) of the optical amplifier:

$$NF \approx 2n_{sp} \qquad (3.32)$$

An optical fiber link may include several optical amplifiers. The ASE noise accumulates over the amplifiers and degrades the OSNR. When all the amplifiers are evenly spaced and have the same gain , which is the case in many laboratory experiments using optical re-circulating loops, the accumulated ASE power at the receiver is [104]:

$$P_{ASE} = NFhf(G-1)B_oN \qquad (3.33)$$

where N is the number of amplifiers or the spans of systems. (3.33) is frequently used to estimate the OSNR performance in optical re-circulating loop experiments. For engineering convenience, (3.33) is converted to logarithm scale with the assumptions: $G-1 \approx G$ and $B_o = 0.1 \ nm$.

$$P_{ASE}^{dB} = -58 + NF^{dB} + G^{dB} + 10log_{10}N \qquad (3.34)$$

In an IM/DD system, ASE noise is generally the dominant noise. ASE noise in the optical domain can be simulated as additive complex white Gaussian noise. Therefore ASE adds the intensity and phase fluctuations to the optical signals. In

photo diode, ASE noise beat with optical signal and convert to the electrical domain, the resultant electrical current $i(t)$ is:

$$i(t) \propto |E_s(t) + E_{ASE}(t)|^2 = E_s(t)E_s^*(t) + E_{ASE}(t)E_{ASE}^*(t) + \Re\{E_s(t)E_{ASE}^*(t)\}$$

(3.35)

where $|\cdot|^2$ is modulus square operation; $\{\cdot\}^*$ is conjugate operation and $\Re\{\cdot\}$ represents the real part. The first term in the right hand side of (3.35) is signal intensity. The second term is spontaneous-spontaneous beat noise. The third term is the product of signal and ASE noise, which is called signal-spontaneous beat noise.

In addition, because of optical amplifiers, the optical fiber communications systems can have high power signals or high count signals. This causes the non-linearity easily in optical fiber. This thesis focus on linear optical transmission systems by controlling the optical power.

3.4.2   Chromatic Dispersion

In optical communication systems, single-mode fibers are widely deployed. Intermodal dispersion is absent simply because the energy of light is transported by a single mode. However, CD is dominant in single-mode fibers. CD is a phenomenon by which different spectral components of a pulse travel at different velocities [1]. CD consists of material dispersion and waveguide dispersion. Material dispersion is the principle component of CD, which occurs because the refractive index of silica, the material used for optical fiber fabrication, changes with the optical frequency so that different frequency components propagate at different speeds in optical fiber.

For a monochromatic light propagating along the fiber, or the z direction, it can be expressed as:

$$E(t, z) = |E| \cdot cos(\omega_c t - \beta z) = \Re\{E e^{j(\omega_c t - \beta z)}\}$$

(3.36)

where ω_c is the angle frequency of the carrier, β is the propagation constant in the fiber. Because of CD, β is a function of angle frequency ω_c. If we encode the carrier with a frequency $\Delta\omega$, the complex fiber transfer function of a distance from $z = 0$

to $z = z$ is :

$$H(z, \Delta\omega) \triangleq \frac{Ee^{j(\omega_c+\Delta\omega)t - j\beta_{(\omega_c+\Delta\omega)}z}}{Ee^{j(\omega_c+\Delta\omega)t}} = e^{-j\beta_{(\omega_c+\Delta\omega)}z} \tag{3.37}$$

where the attenuation of the fiber is ignored for simplicity. In general, $\Delta\omega << \omega_c$, the propagation constant $\beta_{(\omega_c+\Delta\omega)}$ is described by Taylor expansion up to the second order at angle frequency ω_c:

$$\beta_{(\omega_c+\Delta\omega)} = \beta(\omega_c) + \beta_1\Delta\omega + \frac{1}{2}\beta_2\Delta\omega^2 \tag{3.38}$$

where β_2 is the group velocity delay parameter and related to CD parameter. CD is usually characterized by the CD parameter $D = -\frac{2\pi c}{\lambda^2}\beta_2$, where c is the speed of light, λ is the wavelength and β_2 is the group velocity dispersion (GVD) parameter [1]. The units of CD are $ps/nm/km$, which express the temporal spread (ps) per unit propagation distance (km) per unit pulse spectral width (nm). Standard single-mode fiber (SSMF) has $D = 17ps/nm/km$ at 1550 nm.

The first two terms in (3.38) describe the linear part and cause no distortion, which simply means a time delay $[\beta(\omega_c) + \beta_1\Delta\omega]z$ of the signal after transmission. Therefore we keep the second order term, the fiber transfer function can be re-written as:

$$H(z, \Delta\omega) = e^{j\frac{1}{2}\beta_2\Delta\omega^2 z} = e^{-j\pi Dcz\frac{\Delta\omega^2}{\omega^2}} \tag{3.39}$$

Inherently, CD is a linear effect in the optical domain, or independent of optical power. As a result, it can be fully compensated, e.g., by CD compensation module.

For conventional intensity modulation and direct detection (IM-DD), the two side bands $\omega \pm \Delta\omega$ beat together in photodiode. The transfer function after photodiode is:

$$\begin{aligned} H^2(z, \Delta\omega) &= [e^{j\pi Dcz\frac{\Delta\omega^2}{\omega^2}} + e^{-j\pi Dcz\frac{\Delta\omega^2}{\omega^2}}]^2 \\ &= cos^2(\pi Dcz\frac{\Delta\omega^2}{\omega^2}) \end{aligned} \tag{3.40}$$

If we insert some typical values into the transfer function, ω=193.55 THz, D=17
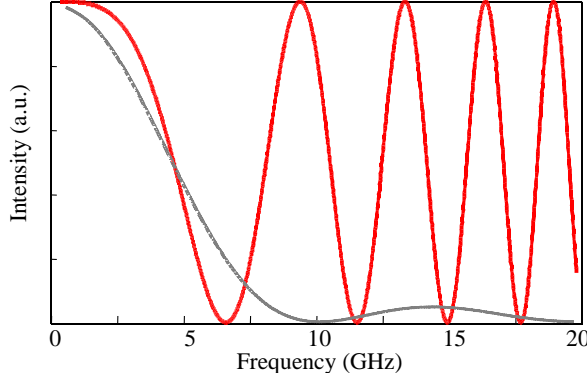
Figure 3.7: Intensity transfer curve of 80 km SSMF versus frequency $\Delta\omega$. The gray curve is the power spectrum density of a 10 Gb NRZ signal.

ps/nm/km, z= 80 km, we can plot the transfer curve as in Fig. 3.7. The transfer curve has a null point at 6.75 GHz , which means some spectral components are lost, so-called frequency selective fading. With the transfer curve in Fig. 3.7, 10 Gb/s signals can transmit in 80 km SSMF fiber with acceptable performance degradation, but 40 Gb/s signals fail because of in-band spectral components are lost.

In the time domain, pulse broadening is the main impact caused by CD. The extent of pulse broadening for a pulse occupied $\Delta\lambda$ bandwidth after a fiber of length L is given by:

$$\Delta T = DL\Delta\lambda \tag{3.41}$$

Therefore, shorter time pulse, wider frequency spread and longer fiber length all cause pulse broadening linearly. In general, the pulse broadening should be smaller than one bit period, or the reciprocal of bit rate B. This condition can be approximated by the criterion $B\Delta T < 1$, which provides an order-of-magnitude estimate. The (3.41) shows the importance of using nearly monochromatic laser source, otherwise the pulse broadening of CD effects will limit the achievable transmission length. In present optical communication systems, distributed-feedback lasers without modulation can output light with very narrow spectrum. Therefore the bandwidth is determined by the modulation of bit rate B. After modulation, the spectral width is approximated as:

$$\Delta\lambda = -\frac{\lambda^2}{2\pi c}\Delta\omega \approx -\frac{\lambda^2}{2\pi c}2\pi B = -\frac{\lambda^2}{c}B \tag{3.42}$$
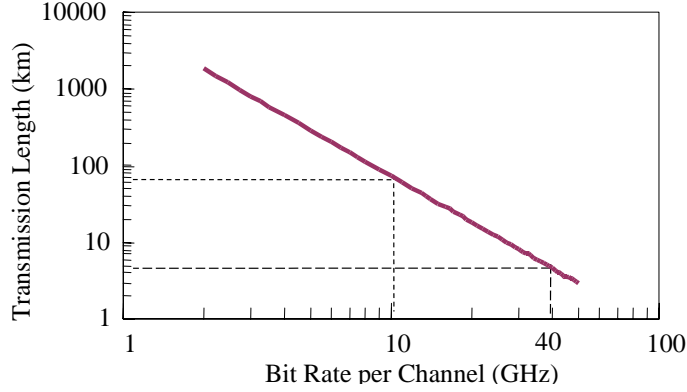
Figure 3.8: CD limit on bit rate and transmission length.

Insert (3.41) and (3.42) into the criterion expression, the length limited by the bit rate is:

$$B^2 L < -\frac{c}{\lambda^2 D} \tag{3.43}$$

It can be seen from (3.43), the maximum transmission length decreases as the square of bit rate. For example, we plot the data rate B as a function of fiber length L in Fig. 3.8. In the 1550 nm transmission window, the maximum transmission distance for 10 Gb/s is about 80 km of standard single-mode fiber. If we increase the bit rate to 40 Gb/s, the maximum transmission distance is only about 5 km. Therefore, CD is a major limiting factor for the optical signal of 10 Gb/s, 40 Gb/s, and beyond.

3.4.3 Polarization Mode Dispersion

In optical fiber, small departures from the perfect cylindrical symmetry lead to birefringence, which results in two different polarization modes. Each polarization has its own transmission constant corresponding to fast mode β_f and slow mode β_s. Equation (3.1) represents a special condition when $\beta_f = \beta_s$, which is acceptable for most applications. However, the difference between β_f and β_s can not be ignored when the transmission bit rate is high and the transmission distance is long. If the input pulse excites both polarization modes, it becomes broader as the two modes disperse along the fiber because of their different transmission constants, illustrated in Fig. 2.4. This phenomenon is called the polarization mode dispersion

(PMD). PMD is considered as a limiting factor in high-speed long-haul optical fiber communication systems and therefore has been extensively studied.

The pulses transmitting in different polarization modes have different transmission speeds. Therefore the pulses have a time delay after a distance of L, which is defined as DGD:

$$DGD = |\beta_f - \beta_s| \, L \tag{3.44}$$

which is only effective in short fiber. In long-distance optical fiber, there are random mode-coupling effects because power of one polarization mode leaks into the other mode. Such mode-coupling makes temporal response of a long fiber no longer deterministic but can only be estimated based on stochastic parameters. Mode-coupling process is phase sensitive and therefore the temporal response of a long fiber becomes sensitive to the fiber environment because high-coherence sources such as DFB lasers are used [105]. Therefore the DGD is random variable with its mean value defined as PMD:

$$PMD = < DGD > \tag{3.45}$$

Although many people use PMD and DGD terminology interchangeably, their difference is clear that PMD is the average of DGD probability distribution, which can be approximated by Maxwellian distribution [17]. Unlike DGD, the PMD of long fiber is proportional to the square root of the fiber length.

Since the instantaneous DGD in a fiber link varies randomly with time, the power penalty caused by DGD also changes randomly. Numerical simulation shows that DGD of about 30% of the bit period, so-called DGD_{MAX}, causes 1 dB power penalty. In most system design, the PMD of the fiber link must be below DGD_{MAX} and their difference is referred as safety factor. Intuitively, even when PMD is much smaller than DGD_{MAX}, the instantaneous DGD and associated power penalty can be very large though the probability is small. ITU Recommendations provide reference table for the safety factor [106]. For example, if the probability of the DGD of a fiber link exceeding the DGD_{MAX} is wanted to be less than 4.2×10^{-5}, then the PMD of the link must be smaller than $\frac{1}{3}$ of DGD_{MAX}, almost $\frac{1}{10}$ of one bit period as a mnemonic rule. PMD is a linear and scalable distortion in the optical domain [11]. For example,

if the transmission distance limited by PMD distortion in a long-distance fiber is 1000 km for 10 Gb/s, then a 40 Gb/s signal can only transmit 62.5 km.

In computer simulations of PMD effects, we use frequency domain Jones Matrix approach, which is based on the principle states polarization (PSP) model. It was shown that *in any linear optical transmission media that has no polarization-dependent loss there exist orthogonal input states of polarization for which the corresponding output states of polarization are orthogonal and show no dependence on wavelength to first order* [107]. Therefore PMD can always be simulated by two principle states. Following (3.1), we can rewrite the optical signal as:

$$\vec{E}_i = \begin{pmatrix} E_x \\ E_y \end{pmatrix} \tag{3.46}$$

where E_x and E_y are scaler as (3.2) and they corresponds the two PSP of the input. The PMD effect of the optical link can be lumped as a transfer matrix. In frequency domain, the output is:

$$\vec{E}_o = M\vec{E}_i \tag{3.47}$$

where

$$M = M_R R_- M_{DGD} R_+, \tag{3.48}$$

M_{DGD} is the DGD between two PSPs, R_- and R_+ are polarization direction rotation, and M_R is the phase delay between two PSPs. For a long fiber with random coupling, the total transfer matrix is the product of multiple (3.48). However, we only discuss deterministic DGD effects in this thesis and therefore (3.48) is applicable.

3.4.4 Optical Re-circulating Loop

It is important to investigate the performance of long haul optical links. For a longer optical link, more optical fibers, optical CD compensators and optical amplifiers are required. It is not always practical and economical to construct such a linear link.

One alternative way is to use optical re-circulating loop, where the optical signals re-circulate through an optical loop consisting of shorter transmission link [108]. Re-circulating loop plays an important role in the development of long-haul transmission systems by providing a flexible and economical platform for transmission measurements.
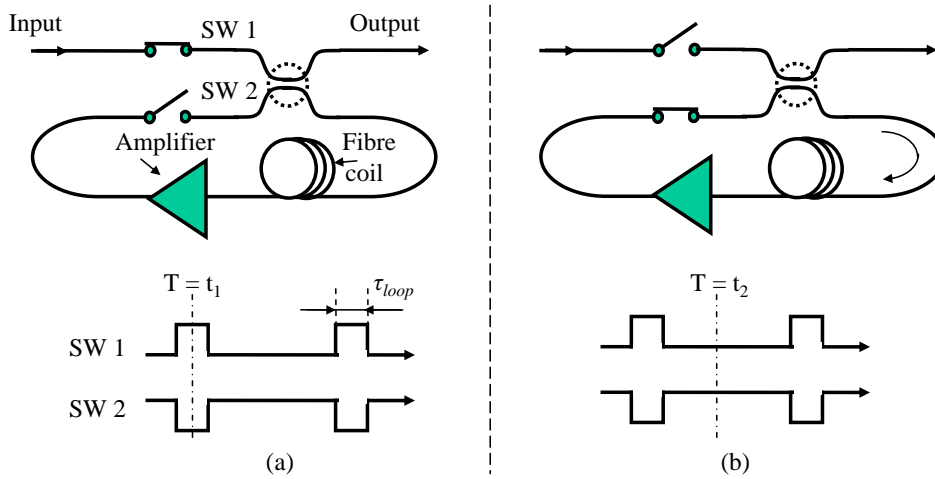
Figure 3.9: Main states of a re-circulating loop, (a)load state; (b)loop state.

Fig. (3.9) shows the structure of one type of a re-circulating loop and its main states. The loop consists of two optical switches (SW), an optical coupler, a fiber link, and an optical amplifier. The principle of re-circulating loop can be explained as two states as in Fig. 3.9:

- Load state: SW1 is close and SW2 is open. Therefore, the input optical signal will fill the loop. The two switches are held in this load state long enough to fill the loop with the optical data signal.

- Loop state: SW1 is open and SW2 is close. The optical signal is then allowed to re-circulate around the loop for some specified number of revolutions.

Hence, by precisely controlling the two SWs, the optical signal is loaded into the loop, re-circulated for some distance, and sent out for detection. The loop will repeat the load state and loop state continuously. The basic time unit for the experiment is

the round trip time of the closed loop τ_{loop}, which is calculated based on 4.89 μs/km of fiber [108].

Among different re-circulating loop structures, the one in Fig. 3.9 has two features:

- There is no state to empty the loop. Therefore there are always optical signals in the loop after start. This will facilitate the optical amplifier inside the loop because it amplifies an almost continuous optical signal.

- Whenever the optical signals arrive at the optical coupler, one part of signal will travel back to the loop while the other part will couple out of the loop. Therefore, there are always optical signals at the output.

Because of the second feature, the measurement instruments at the output need to be synchronized to the timing of the loop operation. The instruments should also be capable of being triggered by a gate signal to detect a burst optical signal. It is convenient to measure the signal from different loops by changing the delay of the gate signal, and therefore realize the emulation of different length transmissions.

3.5 Conclusions

In this chapter, we have presented the technical background for this thesis. optical fiber communication systems are band-pass transmission systems, similar to cable/wireless systems. Therefore it is convenient to inherent the research experience in the other band-pass system and adopt the equivalent low-pass signal and channel for optical fiber communication systems.

We have discussed some important aspects in optical transmitters and receivers. We consider the laser sources, external modulators in optical transmitters. The direct detection photodiode, differential receivers and coherent receivers are covered in optical receivers. The difference among various options in optical transmitters and receivers are high-lighted, which helps to make a choice for a specific application.

In optical channels, CD and PMD are most notorious impairments for high-speed and long-haul optical fiber transmissions. Some theoretic aspects of CD and PMD

have been presented with the emphasis of the system performance limits. Based on their characteristics, the CD and PMD impairments can be fully compensated if the full optical field information can be accessed. Optical amplifiers is ubiquitous in the present optical fiber communication systems. Unfortunately optical amplifiers always add noise to the amplified signal. The noise accumulation over multiple optical amplifiers are presented. Optical re-circulating loop serves as an important platform to investigate the long-haul optical fiber transmission. We have briefly introduced its structure and working principle.

From the next chapter onwards, we will focus on our own contributions to the three research areas we have introduced in Chapter 1.

Chapter 4

AOLS Using Synchronous Phase Modulation

4.1   Introduction

In Section 2.2, we have reviewed optical packet switched networks (OPSN). In such networks, routing and forwarding are carried out electronically with a lower speed label whereas optical payloads remain in the optical domain throughout [5]. Recently, different modulation schemes for packet payload/label have been proposed, such as amplitude-shift keying/frequency-shift keying (ASK/FSK) [109] and amplitude-shift keying/differential phase-shift keying (ASK/DPSK) [33]. They both require a dedicated wavelength converter for the label erasure of each packet. However, it has been shown that it may be cost effective to share a limited number of wavelength converters where the majority of packets pass through the switch without wavelength conversion [15], especially in multi-fiber per link networks [16]. Therefore it is highly desirable to be able to perform optical label swapping even when the packets bypass the wavelength converters. Although the approach using superimposed subcarrier label over ASK payload is able to meet this criterion [88], it requires additional DC-balanced-line-coding for the payload resulting in lower effective bandwidth.

In this chapter, we describe a novel all-optical label swapping (AOLS) using synchronous phase modulation in section 4.2. In our experimental demonstration, label erasure and insertion are performed in a single step without wavelength conversion. The phase modulator plays an important role in this technique. Unfortunately, it has strong polarization sensitivity. In section 4.3, we then propose a polarization insensitive phase modulator to realize polarization insensitive label swapping [110]. In Section 4.4, we consider the practical application in OPSN, where optical packets will pass through multiple core nodes with the label swapped in each node, and

consequently it is essential to investigate the cascadability of optical label swapping [44, 39, 109, 111]. We derive an analytical expression for the accumulated phase errors. To emulate a multi-hop transmission network, we use a re-circulating loop to investigate the performance degradation after multiple label swapping [112]. Finally we compare the simulation and experimental results of timing mismatch effects.

4.2 AOLS Using Synchronous Phase Modulation

4.2.1 Operation Principle

Phase-shift keying (PSK) format encodes the information in the optical phase domain. The optical power is maintained constant in each bit slot with binary data encoded as either a $'0'$ or $'\pi'$ radian. With DPSK, the data demodulation is obtained by comparing the phase of the current bit with that of the previous bit, avoiding the requirement of an absolute phase reference for coherent receivers. Fig. 4.1 shows the constellation diagram for PSK/DPSK [89]. We can observe a symbol-swapping symmetry in a sense that when a phase change of π radian is applied to either symbol, it will be swapped to the other symbol. For instance, a phase change of π radian changes symbol $'\pi'$ to $'2\pi'$ or $'0'$, observing that $'0'$ is identical to $'2\pi'$ for DPSK encoding. This symmetry is unique to phase encoding including DPSK/PSK, but does not apply to other label encoding such as ASK or FSK.
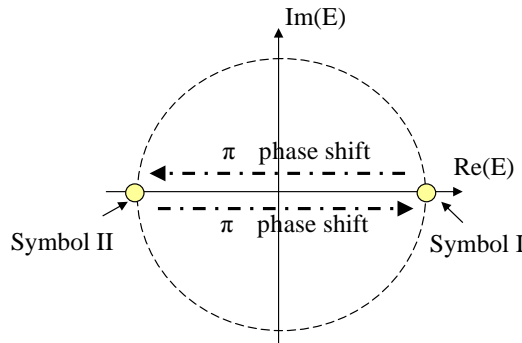
Figure 4.1: PSK/DPSK constellation.
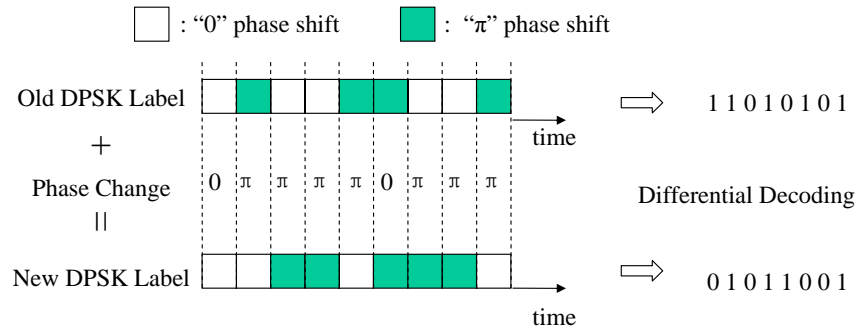
Figure 4.2: Synchronous phase modulation

Fig. 4.2 shows an example of DPSK label swapping using synchronous phase modulation. DPSK encoding uses symbols of $'0'$ and $'\pi'$, which can be interchanged by applying a phase change of π radian. As shown in Fig. 4.2, if we want to change a bit in the old label, we apply $'\pi'$ phase change synchronously with a phase modulator (PM). Otherwise we apply $'0'$ phase change, or no phase change.

Fig. 4.3 shows the conceptual diagram of an all-optical label swapping unit exploiting the unique symmetry of DPSK coding. We use an optical packet format where a DPSK label precedes an ASK payload. The advantage of this serial label and payload is to enable maximum modulation efficiency for both label and payload without suffering crosstalk penalty between them. The incoming packet is detected with a DPSK receiver, including a DPSK demodulator and a photodiode, and fed into a switch controller. The switch controller processes the incoming label and computes a new label containing routing information for the next node. A delta label is generated by performing bit-wise Exclusive Or (XOR) operation of the old label and new label. The corresponding phase modulation of the delta label with DPSK pre-coding is encoded onto the optical packet with a phase modulator. *Synchronous* refers to the timing alignment between the delta label and the incoming old label. A fixed delay is used to achieve timing alignment between the delta label and the old label in each optical packet. Fig. 4.2 shows an example. Assuming that one-byte incoming label of $'11010101'$ is differentially coded with a phase pattern of $'0\pi00\pi\pi00\pi'$, if a new label of $'01011001'$ is called for, a delta label of $'10001100'$ will be applied to the optical packet with a corresponding phase modulation of
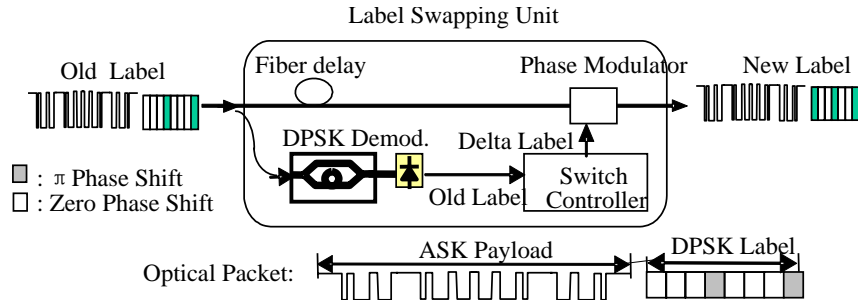
Figure 4.3: Conceptual diagram of label swapping unit.

$'0\pi\pi\pi0\pi\pi'$. Thus a new label is generated by modifying the old label.

4.2.2 Experimental Setup

The optical packet coding technique we choose is bit-serial label, which has been reviewed in Section 2.2.2. We define a packet length of 2^{10} bits at 10 Gb/s or 102.4 ns for demonstration. We start from a 2^{10} PRBS pattern and set all the beginning 128 bits to $'1'$ to allow for DPSK labelling. The label is 16 DPSK bits at 2.5 Gb/s. The guard time between the label and payload and neighboring packets are 2.8 ns and 3.2 ns, respectively.
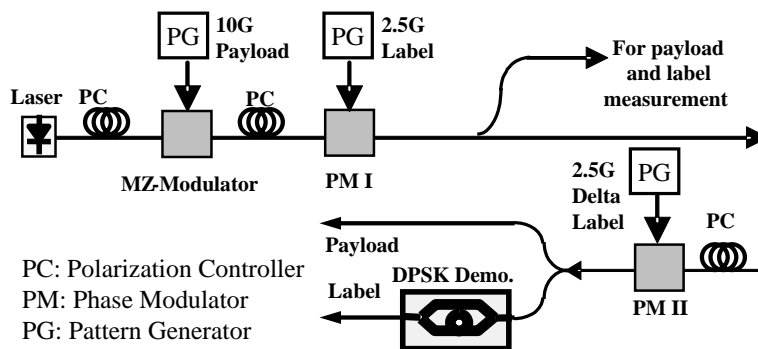
Figure 4.4: Experimental setup for label swapping.

Fig. 4.4 shows the experimental setup for demonstrating the label swapping. The sequences of optical packets are repetition of two consecutive packets with different labels. The payload data for the packet is generated by a pattern generator at

10 Gb/s. Two different 16-bit labels (label 1 and label 2) are generated by a pattern generator at 2.5 Gb/s. Following an external cavity laser, an MZ modulator is used for payload encoding and a phase modulator is used for DPSK label encoding. The optical packet is fed into another phase modulator which is driven by a delta-label generated by a second 2.5 Gb/s pattern generator. Polarization controllers are used to optimize the polarizations for the intensity modulator and two phase modulators. The three pattern generators are synchronized with each other. The delta label is aligned with the incoming packet by adjusting the delay electrically. The driving voltages for both phase modulators are adjusted to ensure π radian phase encoding between two symbols. The DPSK demodulator is a one bit delay interferometer. We only use a single detector following one port of the DPSK demodulator instead of balanced detection. Such a label receiver seems to be an economical choice, since there is a sufficient power margin for the low speed label as we will show in the following measurements. The Bit-Error-Ratio (BER) performance, packet bit patterns and eye diagrams of the label and payload are measured before and after the label swapping. The BER for the label and payload is obtained with an optically pre-amplified 2.5-Gb/s receiver and a pre-amplified 10-Gb/s receiver, respectively.

PG @ 2.5Gb/s Label

PG @ 10Gb/S

PG @ 2.5Gb/s Delta Label

2.5 GHz clock
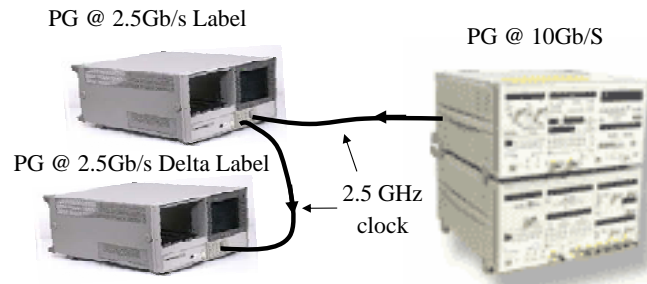
Figure 4.5: Clock connections to synchronize the 3 BERTs.

The timing of the 3 BERT is critical to realize the synchronous phase modulation in this experiment. Because the signal rate is in GHz range, conventional 10-MHz clock reference can not provide bit by bit synchronization of 2.5-GHz and 10-GHz data signals. We elect to use the high-speed clocks of the BERTS as the synchronization signal. Fig. 4.5 shows the clock connection of 3 BERTs. The 10 Gb/s

PG can output a quarter clock at 2.5 Gb/s, which is used to trigger the 2.5-Gb/s PG. The delta label PG follow the clock of the label PG at the transmitter. In this clock connection, bit by bit timing synchronization is achieved because the clock is 2.5 GHz as high as the bit rate.

4.2.3 Measurement Results

Fig. 4.6 shows the two packets after DPSK detection. There is a residual modulation from the payload after DPSK demodulation since only a single receiver is used instead of a balanced receiver. Because a packet label is usually differentiated by a unique flag pattern at the start [113], this residual modulation would be simply ignored by the switch controller due to lack of this flag pattern. The inset shows the bit patterns for 'label 1' before and after swapping. We construct a special delta label with a value of all ones, imposing an alternate phase reversal to the old label. The complete inversion of bit patterns of the old label to those of the new label in the inset shows successful swapping for this special case.
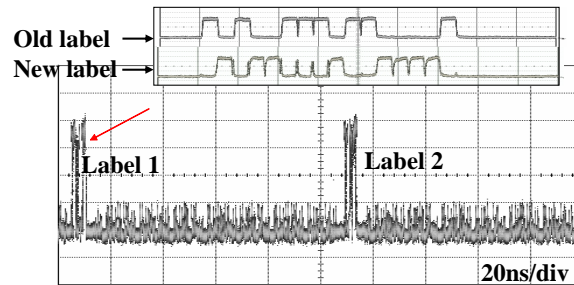
Figure 4.6: Packets after DPSK demodulation.

Fig. 4.7 (a), (b), and (c) show the measured bit patterns for the old label, new label and delta label for 'label 2', respectively. The delta label in Fig. 4.7(c) is obtained by measuring the new label while turning off the DPSK phase encoding for the incoming label. We can see that the sequences of these labels satisfy the equation of $c = a \oplus b$ in bit-wise logic operation as predicted by the theory. In the new label of Fig. 4.7(b), there is a spike between two consecutive $'0's$, which is a unique signature of DPSK demodulation. It causes no eye-closure to the new label

because it always takes place in the eye-crossing away from the center of the eye diagram.
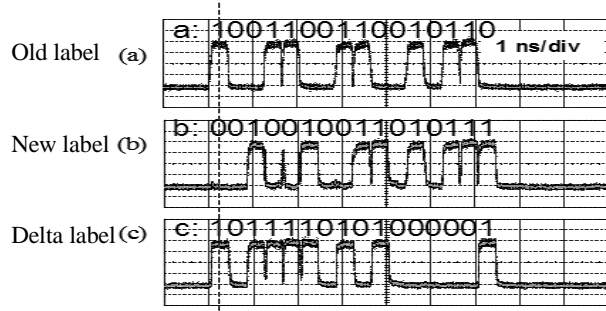
Figure 4.7: Bit patterns for (a) the old label, (b) the new label, and (c) the delta label.

We perform receiver sensitivity measurements before and after label swapping as shown in Fig. 4.8. For the payload, there is no observable power penalty because label swapping has no impact on the OOK payload at different time slot. For the label, the power penalty is less than 0.2 dB from 10^{-9} to 10^{-5} BER. The inset shows the eye diagrams for the label before and after the label swapping.
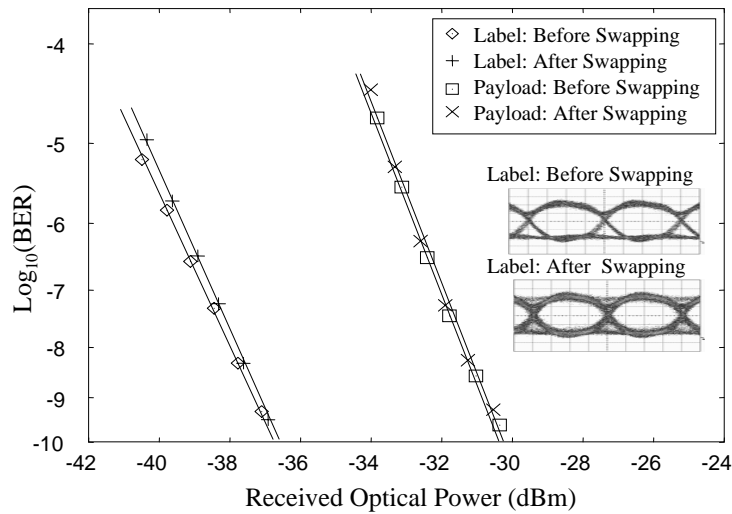
Figure 4.8: System performance of label swapping for the label and payload.

4.2.4 Experimental Results of Timing Mismatch

Synchronization is critical in our proposed technique. It is of importance to investigate the power penalty of timing mismatch, which is carried out by intentionally tuning the electrical delay of delta label so that it is misaligned with the incoming optical packet. Fig. 4.9 shows the receiver penalty as a function of the timing mismatch, which is normalized to one bit period. We can see that receiver power penalty will be limited to 1 dB as long as the timing mismatch between the new label and optical signal is kept from -18% to 18%. The inset is the eye diagram for the -18% timing mismatch. Given that the jitter generation of clock recovery modules can be much smaller than 18% [114], this result shows that the penalty from timing mismatch and clock recovery can be maintained below 1 dB.
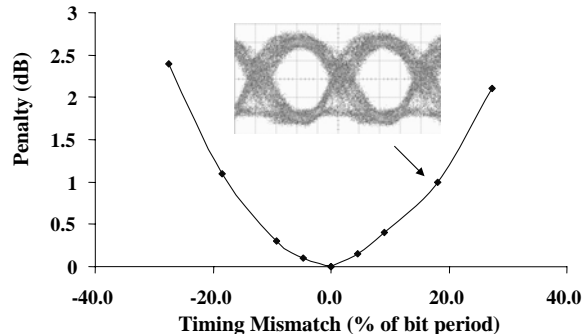
Figure 4.9: Receiver penalty as a function of the timing mismatch between the delta label and the incoming optical packet.

4.3 Polarization Insensitive AOLS

To achieve polarization insensitivity for optical devices is a perennial research for optical signal processing such as soliton phase modulation [115], wavelength conversion [116], and wavelength de-multiplexing [117]. In our AOLS technique, the phase modulator is the key device but it is very polarization sensitive, such as a polarization dependent loss (PDL) of 20 dB. This polarization sensitivity potentially presents a significant problem to the label swapping as the incoming packet polarization is randomly varying. The polarization sensitivity can be addressed during the

design and manufacturing of optical modulators [118]. However, such approaches need more improvements for practical implementations. In this section, we propose a polarization insensitive phase modulator based on polarization diversity [119]. We demonstrate its effectiveness to realize polarization insensitive AOLS.

4.3.1 Operation Principle and Setup

Fig. 4.10 shows the schematics of polarization insensitive phase modulator (PIPM) where the incoming light is polarization split into two orthogonal polarizations, each passing through a phase modulator (PM I or PM II) and recombined with a polarization combiner. The polarization beam splitter divides the input light to vertical and horizontal polarization, which is equal to the combination of a vertical polarizer and a horizontal polarizer.
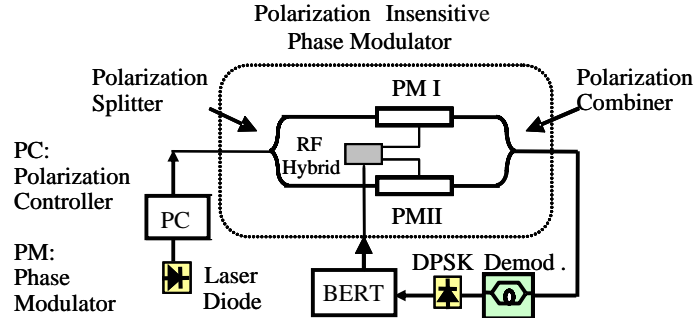
Figure 4.10: Configuration of the polarization insensitive phase modulator and associated characterization setup.

We use Jones calculus to describe the principle of PIPM. The Jones matrices of an ideal linear vertical polarizer and an ideal linear horizontal polarizer are:

$$J_{VP} = \begin{pmatrix} 1 & 0 \\ 0 & 0 \end{pmatrix} \qquad J_{HP} = \begin{pmatrix} 0 & 0 \\ 0 & 1 \end{pmatrix} \qquad (4.1)$$

Rotation matrix is:

$$J_R(\theta) = \begin{pmatrix} cos\theta & sin\theta \\ -sin\theta & \cos\theta \end{pmatrix} \qquad (4.2)$$

The output of two ports of polarization splitter is:

$$\vec{E}_{O1} = J_R(-\theta) \cdot J_{VP} \cdot J_R(\theta) \cdot \vec{E}_I \tag{4.3}$$

$$\vec{E}_{O2} = J_R(-\theta) \cdot J_{HP} \cdot J_R(\theta) \cdot \vec{E}_I \tag{4.4}$$

After the polarization beam combiner, the output is:

$$\vec{E}_O = \vec{E}_{O1} + \vec{E}_{O2} \tag{4.5}$$

Note $J_{VP} + J_{HP} = I$, $J_R(\theta) \cdot J_R(-\theta) = I$, it is easy to show by explicating above equation:

$$\begin{aligned}
\vec{E}_O &= J_R(-\theta) \cdot J_{VP} \cdot J_R(\theta) \cdot \vec{E}_I + J_R(-\theta) \cdot J_{HP} \cdot J_R(\theta) \cdot \vec{E}_I \\
&= J_R(-\theta) \cdot (J_{VP} + J_{HP}) \cdot J_R(\theta) \cdot \vec{E}_I \\
&= I \cdot \vec{E}_I \\
&= \vec{E}_I
\end{aligned}$$

Since we have $\vec{E}_O = \vec{E}_I$ for arbitrary $\vec{E}_I$, we conclude that the PIPM is polarization insensitive.

Such a configuration can be implemented in a single package, for instance, with thin-film polarization splitter/combiner and two LiNbO$_3$ integrated phase modulators. Similar configuration has been proposed for soliton phase modulation [115]. In this paper, we apply the same technique to all-optical label swapping with an emphasis on the precise $'\pi'$ radian phase encoding for an optical packet. To demonstrate the concept, we use commercial components to construct the PIPM. The two branches use polarization maintaining fibers to guarantee the optimal inputs of the phase modulators. The physical delay of the two polarization arms (or DGD of the PIPM) is matched to be about 10 ps and the PDL of the PIPM is measured to be less than 0.2 dB. We expect the DGD of the PIPM to be reduced to sub-ps by integration. The two polarization beam splitters together have additional 1.4 dB insertion loss. The electrical signal is split with an RF hybrid and applied to the

two phase modulators. Regardless of the polarization state of the input signal, the signal will be phase modulated by either one of the modulators or both modulators, and therefore the polarization insensitivity is achieved.

4.3.2 Experimental Setup

Fig. 4.11 shows the experimental setup for demonstrating the polarization insensitivity of label swapping. The configuration in Fig. 4.11 is similar to that in Fig. 4.4 except that the PM II and the PC before it are replaced with the PIPM and a polarization scrambler (PS). The PS is used to emulate the polarization fluctuations in long fiber links.
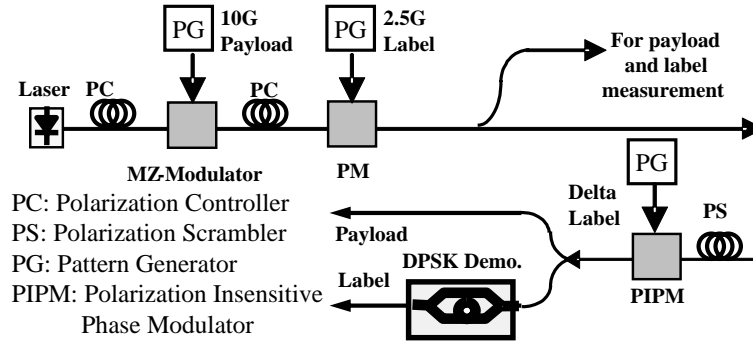
Figure 4.11: Experimental setup for all-optical polarization-insensitive label swapping.

4.3.3 Measurement Results

The polarization insensitivity of PIPM is firstly demonstrated as a DPSK phase encoder as shown in Fig. 4.10. An external cavity laser is followed by a polarization controller (PC), which generates different input polarizations for the following PIPM for phase encoding. The modulated signal is passed to a DPSK demodulator with a single detector and the BER performance is measured for various polarizations. Fig. 4.12 shows the measurement results for three input polarizations: TE, TM and even split of TE and TM, where TE/TM is defined as one of the polarization branch inside the PIPM. It shows that the PIPM achieves polarization insensitivity with

negligible 0.2 dB power penalty. There is an additional penalty of 0.2 dB compared with the baseline performance where a single phase modulator is used under optimal input polarization. This small penalty and polarization sensitivity are caused by the mismatch of the drive voltages to the phase modulators, residual DGD of the PIPM, and RF distortion due to the RF splitting.
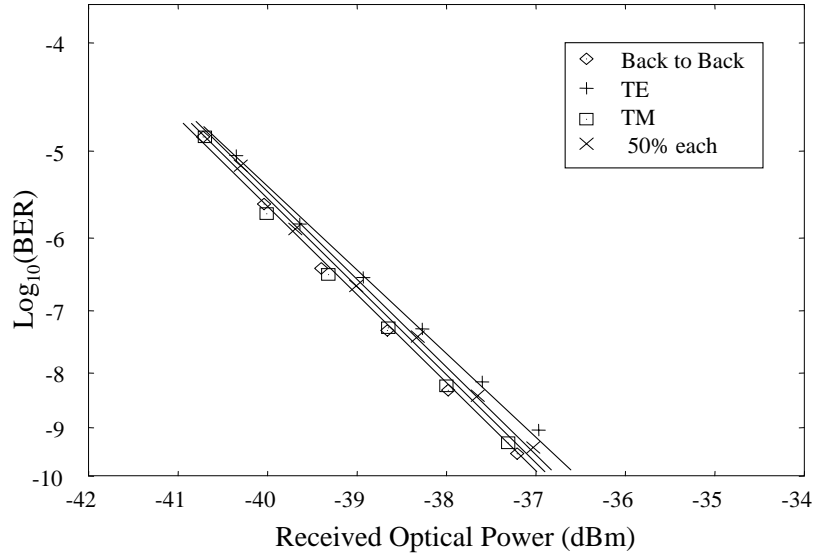
Figure 4.12: BER curves of various launch polarizations for the proposed phase modulator.
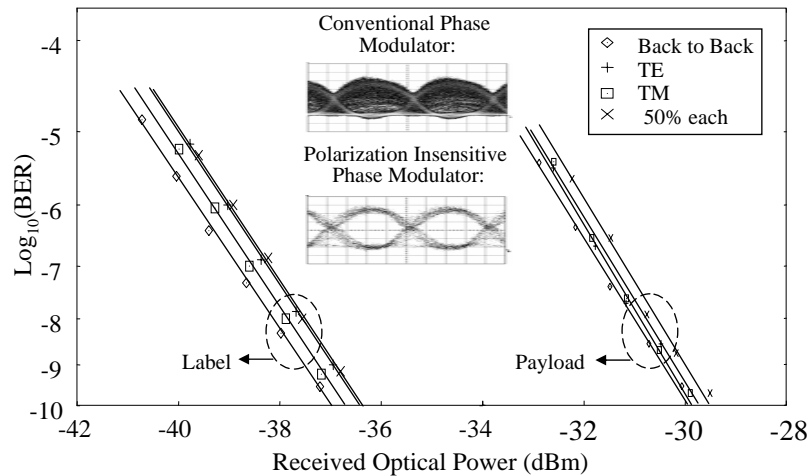
Figure 4.13: BER curves with various polarizations before and after label swapping for the label and the payload.

Having verified the performance for the polarization insensitive phase modulator (PIPM), we apply this PIPM to all-optical label swapping using the experimental

setup in Fig. 4.11. We measure the polarization sensitivity for label swapping by varying the input polarization. For the label, Fig. 4.13 shows that the polarization sensitivity of the optical label after swapping is less than 0.5 dB from 10^{-9} to 10^{-5} BER. The inset shows a completely closed eye-diagram for the swapped label if a conventional phase modulator is used while the input polarization is scrambled, but an open eye-diagram if the PIPM is used when the input polarization is scrambled. Although the eye-closure is due to large PDL of 20 dB for the conventional phase modulator, the severe polarization dependence of phase shift will also cause eye-closure if the input polarization is scrambled. For the payload, Fig. 4.13 shows a polarization sensitivity of less than 0.5 dB after label swapping. The main cause for this sensitivity is the ~ 10 ps DGD in the PIPM, which can be resolved by better packaging.

4.4 Multi-hop Transmission

In OPSN, optical signals traverse many switch nodes toward their destination. At a switch node, the low speed label is extracted, processed and replaced for the transmission to the next node. In contrast to the conventional all-optical label swapping techniques [33, 31], our proposed technique modifies the old labels to realize the label swapping. The phase errors from the old labels and phase modulation will accumulate because there is no regeneration for label swapping. In order to achieve a larger number of all-optical label swapping stages using synchronous phase modulation, two conditions in Fig. 4.3 need to be optimized: (i) the phase modulator applies a precise π radian phase modulation on the old label, as well as the label encoder (phase modulator) in the transmitter; (ii) the old label and new label are time aligned. In the following experiment, we will investigate the cascadability of all-optical label swapping using synchronous phase modulation limited by the accumulation of phase errors and timing mismatch of the old label and new label [120].

4.4.1   Experimental Setup

Fig. 4.14 shows the experimental setup. A pattern generator (or BER tester) at 10 Gb/s and a pattern generator at 2.5 Gb/s generate the payload and the label, respectively. Another pattern generator at 2.5 Gb/s outputs label changes (delta label) for optical label swapping and also functions as a switch control. At the transmitter side, a tunable laser is followed by an MZ intensity modulator for payload encoding and a phase modulator for label encoding. An EDFA is then used to boost the power of the modulated optical signal. Two acoustic-optical switches and a 2×2 3-dB coupler are used to couple optical signals into and out of the re-circulating loop. Inside the re-circulating loop, the chromatic dispersion of 100-km SSMF is fully compensated by a dispersion compensation module (DCM). The transmission loss of the loop is balanced by two EDFAs before and after the DCM. A second phase modulator is used to perform the optical label swapping. The old label and the delta label are time-aligned by setting the electrical delay of the pattern generators. An optical delay line is used to time-align the delta label and the old label after transmission of the first loop. At the receiver side, the optical power is monitored after an optical attenuator. The optical signal coupled out of the loop is pre-amplified and filtered by a 1-nm bandpass filter (BPF). The signal is split for separate label and payload detection. The label receiver includes a one bit delay interferometer as an optical demodulator and an integrated module with APD photodiode, clock and data recovery (CDR) module. The payload is received and detected by a 10-Gb/s receiver, a limiting RF amplifier, and a CDR module. The received optical signal-to-noise ratio (OSNR) with 0.1 nm noise bandwidth is above 20 dB after 7 loops. Therefore the power penalty from the ASE noise is negligible.

Polarization controllers, not shown in Fig. 4.14, are used to optimize the input polarizations for both the intensity modulator and two phase modulators. The drive voltages for both phase modulators are adjusted to ensure π radian phase encoding between two symbols. The pattern generators for the label and data are synchronized with each other and trigged by a loop controller. Another 2.5-Gb/s pattern generator for the delta label uses the recovered clock from the label receiver to avoid the
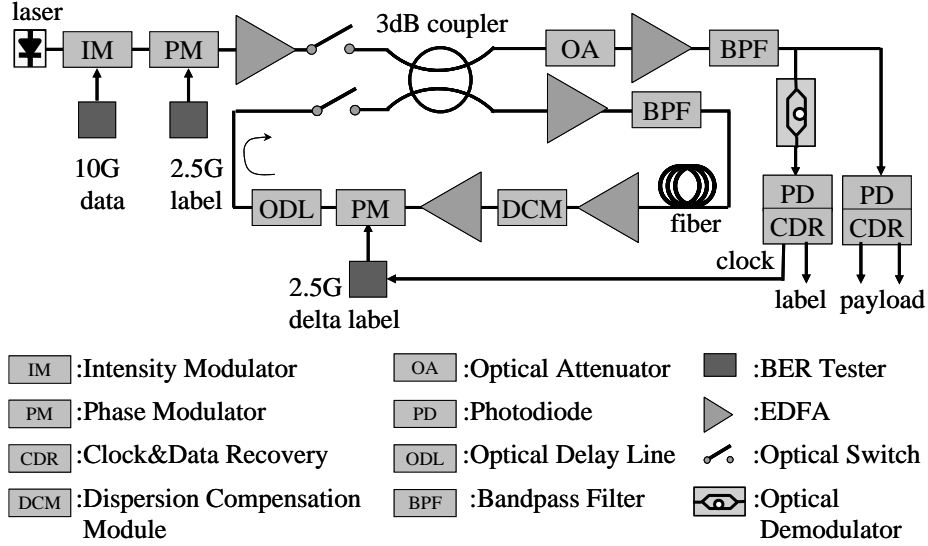
Figure 4.14: Experimental setup for cascadability of all-optical label swapping.

time jitter of long haul transmission. The original label is firstly generated in the transmitter. Each time the signal arrives at the phase modulator inside the loop, the delta label is applied to the phase modulator to modify the old label into a new label. This optical label swapping process is equivalent to the packet going through one hop in an all-optical network.

The experiment involves quite a few components and instruments, which are adjusted to co-operate properly. Two important aspects are the re-circulating loop and polarization alignment of every loop.

The loop is controlled by two signal generators, which have 4 output channels in total. 2 channels control the two optical switches. Channel 1 outputs a gate signal for the measurement instruments, such as optical spectrum analyzer and BERT. As described in Section 3.4.4, the loop loads the optical signal and then re-circulates the optical signals. Fig. 4.15 shows the timing signal of the loop. The upper trace is the control signal of switch 1. The control signal of switch 2 is the complementary signal of switch 1 and is not shown in Fig. 4.15. The width of the gating signal depends on the 1 loop transmission delay of the optical signals, or τ_{loop}, which includes the propagation time in the 100-km fiber and a chromatic dispersion compensator. τ_{loop} is 660 μs in this experiment. The loop repeat the load and re-circulating procedures. The repeating time is decided by the longest distance distance we want to transmit,
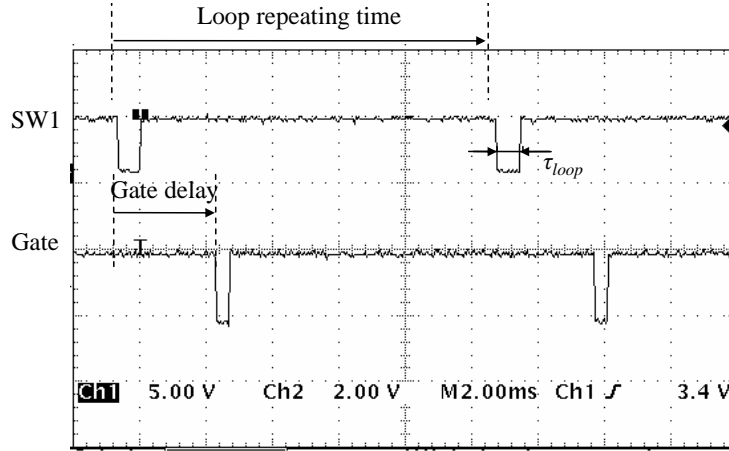
Figure 4.15: Loop control signals

Loop	1	2	3	4	5	6	7	8
Gate Delay(μs)	660	1220	1780	2340	2900	3460	4020	4580
Distance (km)	100	200	300	400	500	600	700	800

Table 4.1: Time delay configuration of the loop switches

which is 10 loops. The bottom trace in Fig. 4.15 is the trigger signal for the instruments. By setting different delay of the gate signal, we can test the signal from various re-circulating times. The width of gate signal is generally smaller the transmission delay time of one loop. The delay of the gate signal is an integral times of τ_{loop}, which is listed in Table 4.1 for different loops. Both conditions can guarantee the instrument receiving the correct signal of interest.

As described in Section 4.3, phase modulator is polarization sensitive device. Because of the shortage of the optical components, we only use one conventional phase modulator inside the loop to realize the AOLS. The polarization controller need to adjust more carefully than without loop, because the polarization controller needs to guarantee the polarization of optical signal simultaneously for every loop. Fig. 4.16 shows a comparison of different configuration of the polarization controller. In the left oscilloscope trace, we can the see the optical signal of 1st loop is decreased because of the improper polarization state. It is interesting to note the polarization state is better after the 1st loop as the output optical signal is stronger. The right

84
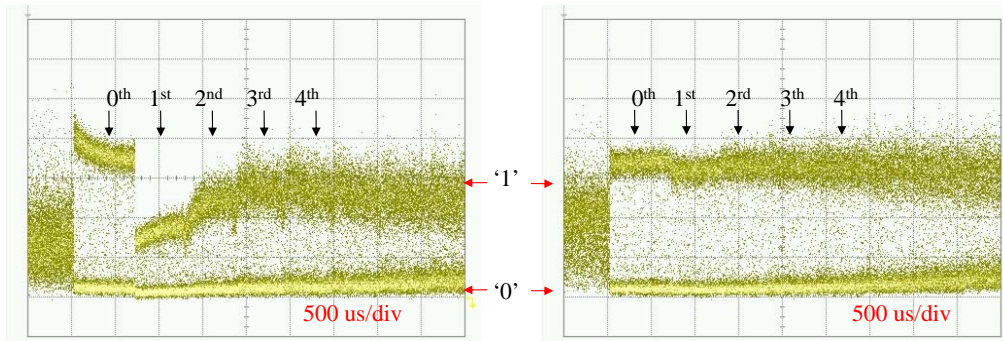
Figure 4.16: Output power of the loop with different polarization control.

oscilloscope trace is with the appropriate polarization state. The output of every loop is almost constant. Therefore, the power penalty from the polarization misalignment is negligible.

4.4.2 Measurement Results of Multi-Hop Transmission

We first collect some exemplary eye-diagrams after different times of label swapping as shown in Fig. 4.17. It is clear the eye-diagram is degraded after label swapping. Two impairments can be seen from the eye-diagram. The first one is the eye-closure caused by imperfect π phase modulation of the delta label. The second one is the spike at the edge of the eye diagram, which is caused by the imperfect timing of the delta label. These impairments accumulate over loops and limit the maximum times of AOLS. We evaluate the system performance of multi-hop transmission in this section. In the next two section, we will discuss the performance degradation from the two impairments separately.

We measure the BER for the label and payload respectively at 0 loops as the baseline, and then repeat the measurement after every loop. Fig. 4.18(a) shows the BER curves of the label through multiple hops. For the label BER measurement, a 2^{15} PRBS pattern is used while the payload encoding is disabled. The advantage of using a long PRBS is that the resultant BER is more meaningful than that with a particular pattern, such as a repeated 16 bits pattern. We find no error floor when we increase the received optical power. The power sensitivity is relatively low
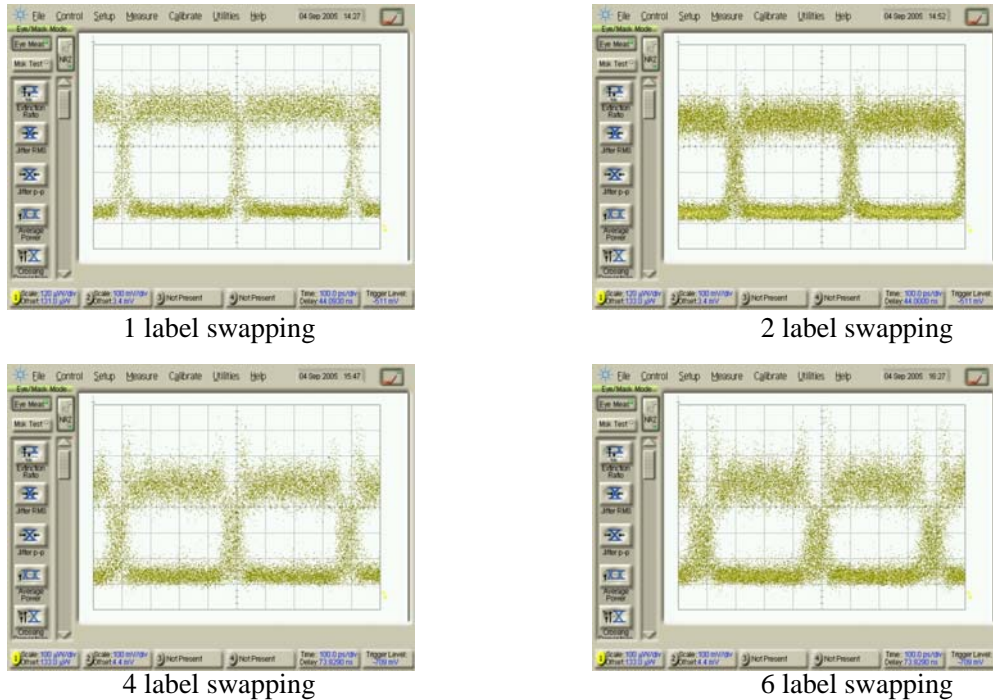
Figure 4.17: Eye diagrams after label swapping.

because we use an APD photodiode. Fig. 4.18(a) also shows the power penalty is less than 1 dB at 10^{-7} BER after 5 hops, or 5 swaps of the optical label. The power penalty quickly increases to 2.2 dB after 6 hops and 4 dB after 7 hops. The non-ideal RF driving signal shape and driving amplitude of phase modulators reduce the eye-opening and cause the power penalty. Fig. 4.18(b) shows the BER performance of the payload transmission, which is tested while the label modulation is on. The power penalty is well below 1 dB at 10^{-7} BER after 700 km transmission. In theory, the power penalty should be even smaller considering our bit-serial configuration of the label and payload. One possible reason is because we test the BER for the optical packet frame with a non-burst mode receiver, and the long '1' bits for label encoding at the beginning of the optical packets may degrade the performance of the payload.

The implication of finite cascadability of the proposed label swapping technique is that label regeneration is necessary after 5 hops, for instance, using a wavelength converter for regeneration [31]. We believe this configuration only modestly in-
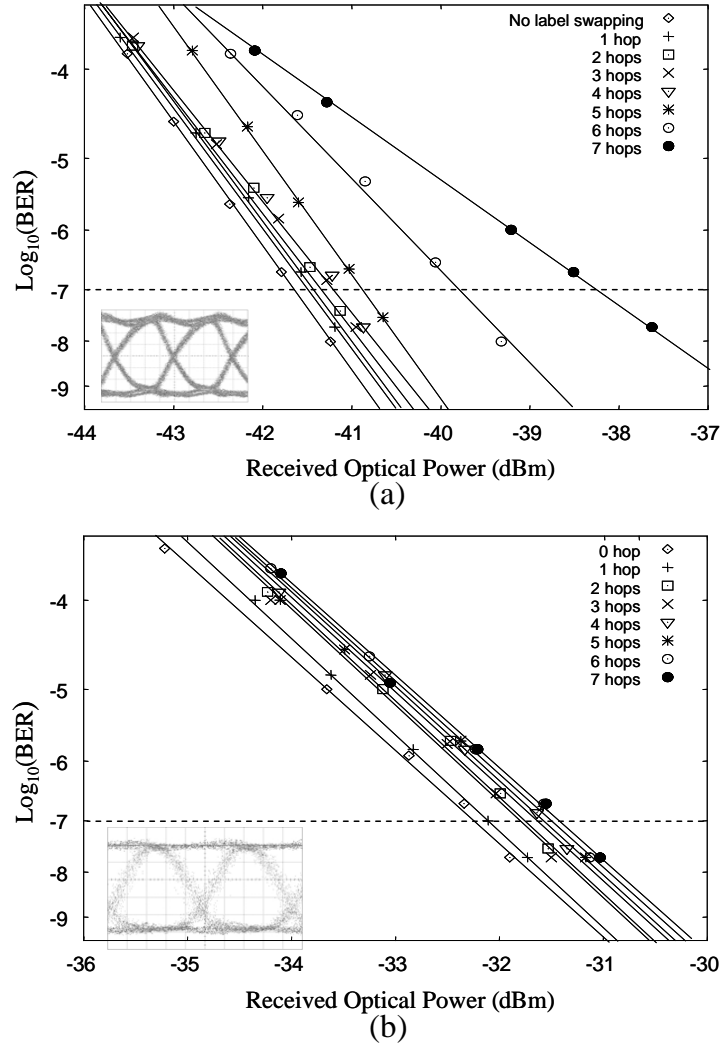
Figure 4.18: BER curves of multi-hop label swapping for (a) the label, (b) the payload. The insets are error free eye-diagrams measured after 5 hops transmission.

creases the system complexity because the wavelength converter would be needed for packet contention resolution in optical label switches with shared wavelength converters [15, 16]. Our proposed label swapping technique even with the moderate cascadability of 5 hops may save up to 80% of wavelength converters in optical packet switched networks, in comparison with some techniques that use dedicated wavelength converters for label swapping.

4.4.3 Theoretical Analysis of Accumulated Phase Errors

As described in Section 4.2, the phase difference between two symbols in DPSK should be π radian. In reality, there always has deviation around the ideal value. When we use synchronous phase modulation for all-optical swapping, the deviation results from the imperfect phase modification of the old labels and accumulates after every label swapping. This accumulation degrades the eye-opening in the receiver. Therefore we can analyze the cascadability of the label swapping using the power penalty of phase deviation. We can express equivalent low-pass PSK signal as below:

$$E = |E| e^{j(\pi x_n + \delta)}; \qquad x_n = 0, 1 \tag{4.6}$$

where δ is the phase deviation to the ideal value and θ has $'0'$ and $'\pi'$ two values to carry the binary information.

After the optical demodulator, the phase modulation information is converted to the intensity modulation information, which is described in Section 3.3.4. Assume the worst case, the constructive and destructive interference results are:

$$\begin{cases} \pm |E| \cos(\delta); \\ \pm |E| \sin(\delta); \end{cases} \tag{4.7}$$

After the power and envelope detection of photodiode, the corresponding binary values are:

$$\begin{cases} |E|^2 \cos^2(\delta); \\ |E|^2 \sin^2(\delta); \end{cases} \tag{4.8}$$

The extinction ratio r can be written as:

$$r \triangleq \frac{|E|^2 \cos^2(\delta)}{|E|^2 \sin^2(\delta)} = \cot^2(\delta); \tag{4.9}$$

The extinction ratio is degraded by the δ phase deviation. The signal is assumed with high OSNR, hence the power penalty P from extinction ratio degradation is [121]:

$$P = 10 \log_{10} \frac{1+r}{1-r}; \tag{4.10}$$

Substituting the (4.9) into (4.10), we write the power penalty P of the phase deviation δ as:

$$P = 10 \log_{10} \frac{1 + \cot^2(\delta)}{1 - \cot^2(\delta)}; \tag{4.11}$$

In order to compare (4.11) with the experimental result in Fig. 4.18(a), we need to estimate the phase error increase after every label swapping, which is slightly bigger than 5 degree after we minimize the mean square errors between the experimental and analytical data. In Fig. 4.19, as the label swapping times increase, the phase error accumulates the bigger phase deviation and the power penalty increases accordingly. The experimental data generally agree with the analysis curve. But there is bigger difference between them after 4 times of label swapping. The major reason is the analytical model above is simple and some assumptions during the derivation of (4.7), (4.9), and (4.10) will be void for a practical system.
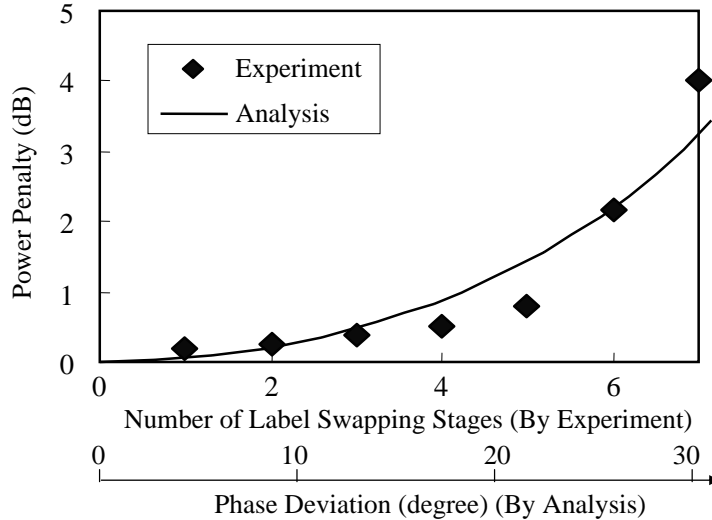
Figure 4.19: Power penalties of label swapping by experiment and analysis.

4.4.4 Experimental and Simulation Results of Timing Mismatch

Timing synchronization between the old label and delta label is a critical issue for optical label swapping using synchronous phase modulation technique. Timing mis-

bit rate	2.5 Gb/s
center frequency	193.3 THz
optical power	-10 dBm
pulse rise time	0.1/bit rate
receiver bandwidth	0.7*bit rate
sample rate	640 GHz
PRBS type	FixedMarkNumber
time window	1.28 ns

Table 4.2: Major simulation parameters in VPI.

match will produce distortion at the bit transition. Timing mismatch is defined as the phase difference between the old label and delta label, and is measured as a percentage of one bit period in this paper. We use the same experimental setup of Fig. 4.14 to investigate this issue and compare the experimental results with numerical simulation results using commercial software, $VPItransmissionMaker^{TM}$. The major parameter settings are in Table 4.2. To isolate the timing mismatch, the phase modulator and optical demodulator are ideal and no fiber transmission is included. The original simulation outputs the Q penalty, which is multiplied by a factor of 0.6 for OSNR penalty [122].

The timing mismatch is generated by setting different electrical delays provided by the pattern generator inside the loop. In the re-circulating loop, the timing mismatch of each loop accumulates linearly instead of statistically, therefore the test simulates the worst case of timing jitter accumulation of the CDR modules in a multi-hop network. For instance, if we add a timing mismatch of 2.5% of one bit period on the delta label in the first loop, there will be 12.5% timing mismatch between the old label and the delta label after 5 hops.

The timing mismatch impact on the label receiver sensitivity is measured after 5 hops. Fig. 4.20 shows the power penalty at 10^{-7} BER due to timing mismatch. The experimental power penalty is below 1 dB within 20% timing mismatch, which corresponds to 4% timing mismatch per hop. Given that the jitter generation of clock recovery modules can be much smaller than 4% [114], this result shows that the penalty from timing mismatch can be maintained below 1 dB on the optical label swapping using our technique. In addition, the timing mismatch/jitter accumulates statistically in real networks and subsequently grows much more slowly than the
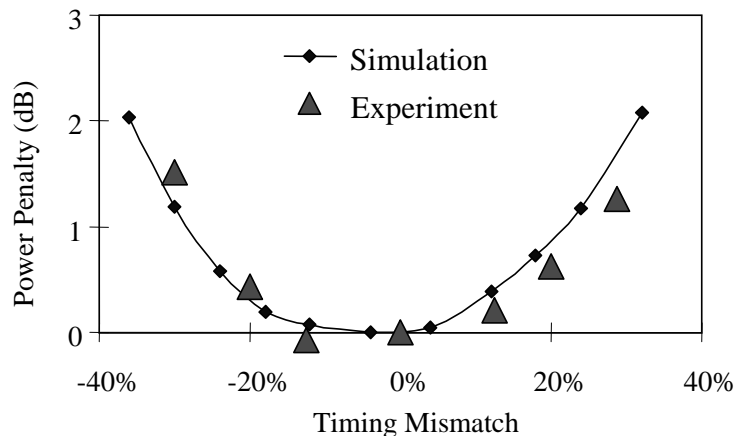
Figure 4.20: Power penalty as a function of timing mismatch. The unit of timing mismatch is a percentage of one bit period.

linear accumulation in our experiment. In Fig. 4.20, the experimental data agree with the simulation curve with 0.6 dB maximum deviation.

4.5 Conclusions

In this chapter, we have proposed and demonstrated a novel AOLS technique. We exploit the unique symbol swapping symmetry in the phase domain of DPSK labels, by observing that one symbol can be swapped to the other symbol with a phase change of π radian. We have performed label swapping of DPSK labels using an approach of synchronous phase modulation by a phase modulator without the need for wavelength conversion. For the first time that label erasure and insertion are performed in a single step.

In real field optical networks, the polarization state of optical signals is not maintained. On the other hand, the phase modulator used in this technique can be very polarization dependent, which potentially presents a significant problem to the label swapping because the incoming packet polarization is randomly varying. We have then proposed a polarization insensitive phase modulator for label swapping. We have carried out the first experimental investigation on the polarization sensitivity of AOLS. Using this device, the polarization insensitivity of power penalty for the label swapping is found to be less than 0.3 dB and 0.5 dB for the packet label and

payload respectively. The performance of the device may be further enhanced by integration.

In OPSN, optical packets transmit through multiple core nodes with the label swapped in each node, and consequently it is essential to investigate the performance of multi-hop optical label swapping. As the proposed label swapping technique relies on a synchronous π phase shift to achieve label swapping, any non-ideal drive voltage and timing mismatch on the phase modulator incur phase errors to the new label, and the accumulation of such phase errors limits the cascadability of such a technique. To address these problems, we have emulated cascaded all-optical label swapping in a re-circulating loop to investigate the power penalties from the accumulated phase errors and the timing mismatch [112]. The power penalty from the phase errors is less than 1 dB at 10^{-7} BER after 5 hops. This power penalty also conforms to the analytical expression we have derived. The experimental power penalty is below 1 dB for a timing mismatch within 20% of one bit period. We have found that it is possible to save up to 80% wavelength converters in optical packet switched networks by using our technique, compared with alternative label swapping techniques requiring dedicated wavelength converters.

Chapter 5

Phase Estimation for Coherent Optical OFDM

5.1 Introduction

As described in Section 2.3, optical signals are degraded by optical distortions when they traverse optical fiber networks. Optical distortions can be compensated in electrical domain. One approach to electronic compensation of optical distortions is to employ advanced modulation format, such as orthogonal frequency division multiplexing (OFDM). OFDM is a special form of multi-carrier transmission and is resilient to frequency selective fading. It has been rapidly and widely adopted in wireless communication systems, such as IEEE 802.11g [123]. Recently, coherent optical OFDM (CO-OFDM) has been proposed for optical fiber communications to combat chromatic dispersion (CD) [22]. CO-OFDM has also been shown to be insensitive to polarization mode dispersion (PMD) in transmission fibers [97]. Conventional coherent detection requires optical phase-locked loop (OPLL), which has only been demonstrated in research labs despite more than 10 years research. Recently, coherent detection by digital phase estimation has been proposed and demonstrated for optical communications [64, 103]. This technique does not require OPLL and can achieve similar performance of OPLL. Therefore, we employ digital phase estimation to achieve coherent detection for CO-OFDM. Because of the coherent detection used in CO-OFDM receivers, it is important to investigate the optical phase noise impact on system performance and explore the optimal approach to estimate phase evolution of OFDM signals. In contrast to conventional single carrier optical transmission systems, OFDM systems transmit a data stream over a number of lower rate subcarriers simultaneously. This opens an opportunity to employ advanced phase estimation techniques, such as pilot-aided phase estimation. Although

such an advanced phase estimation technique has been proposed and employed in wireless communications [21], it is the first time that pilot-aided phase estimation is analyzed and experimentally demonstrated in optical communications.

In this chapter, we introduce the theory of OFDM in the context of optical fiber transmission in Section 5.2. The conditions to eliminate the CD and PMD distortion are presented. Phase estimation and compensation is one of the enabling functionalities in the CO-OFDM receiver. We then present the theory of digital phase estimation with pilot subcarriers for CO-OFDM transmission in Section 5.3 [124]. In our first experimental demonstration in Section 5.4, we show as few as 5 subcarriers are sufficient for pilot-aided phase estimation. The transmission performance is measured for CO-OFDM systems with a nominal data rate of 8 Gb/s after 1000 km transmission over standard single mode fiber (SSMF) [125]. The second experiment in Section 5.5 includes a PMD emulator of 340 ps differential group delay (DGD) at the transmitter side. The second experiment proves that the phase estimation theory is applicable in the presence of strong PMD.

5.2   Orthogonal Frequency Division Multiplexing

Conventional single carrier systems use one frequency to carry all the data as shown in Fig. 5.1(a). An alternative approach is to use frequency multiplexing techniques when using single carrier is not desirable for performance or economics. Fig. 5.1(b) shows an example of frequency division multiplexing (FDM) technique. The data information in single carrier can be demultiplexed to four different frequency carriers. As a result, each carrier carries much lower bit rate data. Because different carriers share the same transmission media, attention must be paid to avoid any crosstalk among different carriers. Conventional FDM has to use frequency spacing to minimize the interference. As shown in Fig. 5.1(c), OFDM is a special form of FDM. It is an optimum version of FDM if we note the carrier spacing is minimized by using orthogonal carriers. Fig. 5.1 also illustrates that the multi-carrier techniques are resilient to channel fading. The dashed line is an example of frequency selective fading, in which there is big attenuation at some frequency ranges. In such a channel,

the single carrier technique occupies a wide frequency range and all the data suffer distortion. In the multi-carrier scheme, each subcarrier only needs a much narrower frequency range. Although the channel response is not flat globally, for most subcarriers the channel response is flat because they only occupy narrow frequency bands. Therefore those carriers can transmit successfully in such a channel.
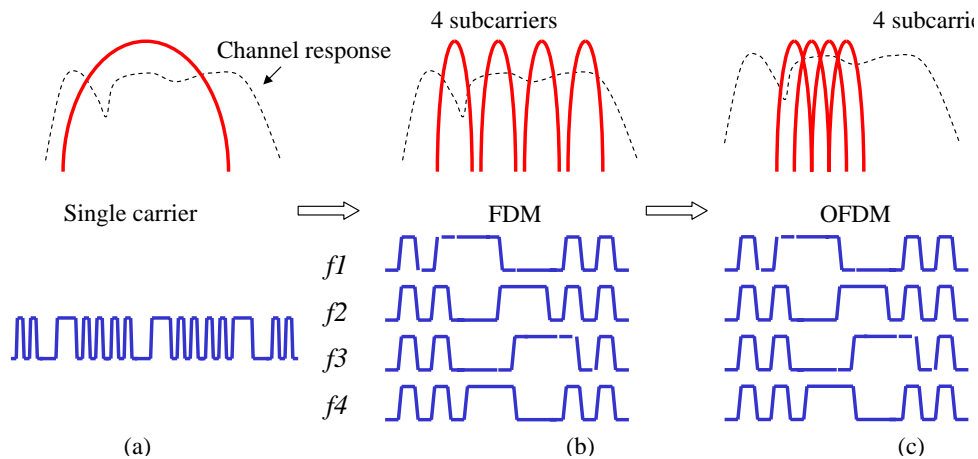
Figure 5.1: Comparison of (a) single carrier, (b) general frequency division multiplexing, (c) orthogonal frequency division multiplexing.

OFDM exhibits a number of advantages over the conventional multiplexing and modulation scheme. It is only natural that it also imposes a few disadvantages. For example, OFDM signals in the time domain are spiky, or high peak-to-average ratio [123], which makes OFDM signals susceptible to non-linearity, e.g., from RF amplifiers or fiber non-linearity in optical transmissions [126]. Because of the implementation difficulties, OFDM only reached sufficient maturity for employment in standard systems during 1990s after its concept was proposed in 1960s [123]. One significant invention is the employment of discrete Fourier transform (DFT) to replace conventional modulator and demodulator, which significantly reduces the implementation complexity of OFDM transmitter and receiver. We will show the application of DFT in OFDM in the following sections.

5.2.1 Mathematical Description of OFDM

This section present the mathematical description of OFDM, which is based on [21, 123] and is adopted for the context of this thesis. A subcarrier can be written as a complex wave:

$$s(t) = ae^{j(2\pi ft + \theta)} \tag{5.1}$$

where a and θ, the amplitude and phase of the carrier, can vary with time to carry information. For the sake of simplicity, the pulse shape term is dropped. OFDM consists of many carriers. We extend (5.1) by summation of multi-carrier:

$$s(t) = \frac{1}{N_{SC}} \sum_{k=1}^{N_{SC}} a_k e^{j(2\pi f_k t + \theta_k)} \tag{5.2}$$

$$f_k = f_0 + k\Delta f, \ \Delta f = \frac{1}{T} \tag{5.3}$$

The Δf is strictly defined to guarantee the orthogonality of all the subcarriers over T period of an OFDM symbol. Orthogonality is mathematically defined as:

$$\int_0^T e^{j2\pi f_i t} e^{j2\pi f_k t} dt = \begin{cases} T, \ i = k \\ 0, \ i \neq k \end{cases} \tag{5.4}$$

If we use x_k as the transmitted data information, or $x_k \triangleq a(k)e^{j2\pi\theta_k}$ and let $f_0 = 0$, the equivalent low-pass signal of (5.2) is:

$$s(t) = \sum_{k=1}^{N_{SC}} x_k e^{j2\pi k\Delta ft} \tag{5.5}$$

In reality, a number of OFDM symbols are grouped together as an OFDM frame, which might also include additional symbols for synchronization and channel estimation. For an OFDM frame with multiple OFDM symbols, the output is the summation of multiple (5.5). It is convenient to plot one OFDM frame structure in time and frequency dimension. Fig. 5.2 shows the two dimensional time/frequency structure for one OFDM frame, which includes N_f OFDM symbols in time and N_{SC} subcarriers in frequency. Each OFDM symbol consists of $x_k, \ k = 1, 2, \cdots N_{SC}$.

After modulation onto carrier, the OFDM symbol is in the form of (5.5).
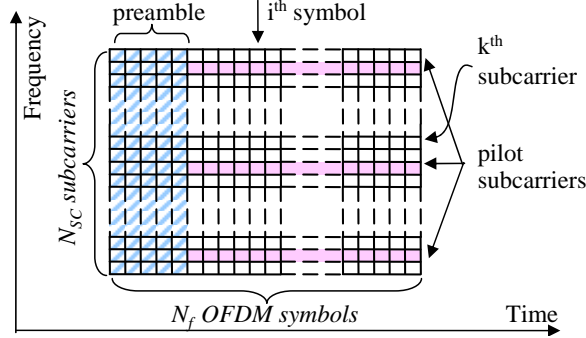
Figure 5.2: Two dimensional time/frequency structure of one OFDM frame.

For the purpose of digital signal processing (DSP), it is necessary to describe the OFDM symbol in digital sequence. For an OFDM symbol with T_s time duration, we sample $s(t)$ at an interval of $\frac{T_s}{N_{SC}}$:

$$s(\frac{n}{N_{SC}}T_s) = \sum_{k=1}^{N_{SC}} x_k e^{j2\pi k\Delta f \frac{nT}{N_{SC}}} \tag{5.6}$$

where $\Delta f T_s = 1$ for the orthogonality. We rewrite it as digital sequence:

$$s[n] \triangleq s(\frac{nT}{N_{SC}}), \ x[k] \triangleq x_k \tag{5.7}$$

$$s[n] = \sum_{k=1}^{N_{SC}} x[k] e^{j2\pi k \frac{n}{N_{SC}}} \tag{5.8}$$

If we note that the definition of the N-point discrete Fourier transform (DFT) is [127]:

$$X_p[k] = \sum_{n=0}^{N-1} x_p[n] e^{-j(2\pi/N)kn} \triangleq DFT\{x_P[n]\} \tag{5.9}$$

$$x_p[n] = \frac{1}{N} \sum_{k=0}^{N-1} X_p[k] e^{j(2\pi/N)kn} \triangleq IDFT\{X_p[k]\} \tag{5.10}$$

Therefore, the modulation of OFDM symbol can be obtained by IDFT:

$$s[n] = IDFT\{x[k]\} \tag{5.11}$$

$$x[k] = DFT\{s[n]\} \tag{5.12}$$

As a result, the modulation and demodulation for OFDM transmitter and receiver are simplified to IDFT and DFT operation, which can be computed efficiently by DSP.

5.2.2 Cyclic Prefix to Eliminate CD and PMD Distortions

When the signal described in (5.5) is transmitted in a dispersive channel, there are two impairments for the receiver to recover the data information. One impairment is that channel dispersion destroys the orthogonality between subcarriers and causes inter-carrier interference (ICI). Furthermore, a system may transmit multiple OFDM symbols in a series so that a dispersive channel causes inter-symbol interference (ISI) between successive OFDM symbols.
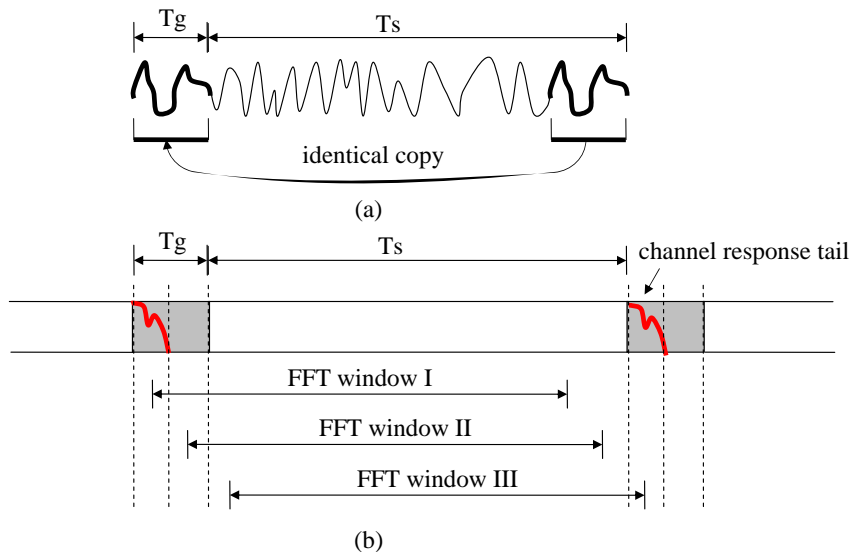
Figure 5.3: Cyclic prefix

One way to prevent ISI is to create a cyclically extended guard interval as shown in Fig. 5.3(a), where each OFDM symbol is preceded by a periodic extension of

the signal itself. This addition is done by copying the ending part of the OFDM symbol to the beginning of the OFDM symbol. This cyclic prefix (CP) preserves the orthogonality of the subcarriers and prevents the ISI between successive OFDM symbols [21]. The total symbol duration is $T_t = T_g + T_s$, where T_g is the guard interval and T_s is the useful symbol duration, or observation period.

At the receiver, the FFT window needs to be synchronized. As shown in Fig. 5.3(b), The region (I) and (III) are not appropriate because the FFT window in the region (I) contains the samples from the other OFDM symbols causing ISI and the FFT window in the region (III) loses the beginning of the OFDM symbol. In region (II) the data can be recovered but with a phase rotation after FFT. This can be seen from the circular time shift property of N-point DFT [127]:

$$c[k] = DFT\{s[n]\} \Leftrightarrow c[n-l] = DFT\{s[n]e^{-j2\pi kl/N}\} \tag{5.13}$$

It is apparent that the ISI can be eliminated when the guard interval is longer than the channel impulse response as shown in Fig. 5.3(b). In the context of optical transmissions, the delay spread due to the CD among the subcarriers should not exceed the guard time. Recall the pulse broadening caused by CD in (3.41) and (3.42), and the total bandwidth of the OFDM signals $B = N_{SC}\Delta f$, the fundamental condition for complete elimination of ISI of CD in optical fiber is thus given by [22]:

$$\Delta T = D_t \Delta \lambda = \frac{c}{f_c^2} D_t B \leq T_g$$
$$or \quad \frac{c}{f_c^2} D_t N_{SC} \Delta f \leq T_g \tag{5.14}$$

where f_c is the frequency of the optical carrier, c the speed of light, D_t the total accumulated CD in units of ps/nm, and N_{SC} the number of subcarriers.

When the pulse broadening is caused by PMD, the condition is [97]:

$$DGD_{max} \leq T_g \tag{5.15}$$

where DGD_{max} is the maximum budgeted DGD, which is about 3 times of the PMD

as we have discussed in Section 3.4.3.

5.3 Phase Estimation Theory

In conventional intensity modulation/direct detection (IM/DD) optical systems, the square-law photodiode discards the optical phase information and limits its performance and application for higher capacity and longer transmission distance. In general, the transfer function of optical channel includes the amplitude and phase information, therefore the optical phase needs to be recovered at the received side for the compensation of the optical channel response. Although there are a few methods which try to avoid the optical phase recovery for OFDM transmission, these methods generally sacrifice the spectral efficiency or transmission performance [95]. Recently, CO-OFDM has been proposed where coherent detection can be realized by digital phase estimation without conventional OPLL. This section is devoted to phase estimation theory for CO-OFDM.

5.3.1 Coherent Optical OFDM

Recall that the equivalent low-pass OFDM symbol is $s(t)$ in (5.5). After the up-conversion at the transmitter, the optical signal is:

$$E_s = e^{j2\pi(f_c t + \Phi_c)} \cdot s(t) \tag{5.16}$$

where f_c is the frequencies for transmitted optical carrier, Φ_c is the phase noise of the transmitter laser and is a function of time t. After transmitting through the optical fiber with total CD value D_t, the optical signal is:

$$E_s = e^{j2\pi(f_c t + \Phi_c)} \cdot s(t) \otimes F^{-1}\{\sum_{k=1}^{N_{SC}} h(k)\} \tag{5.17}$$

$$= e^{j2\pi(f_c t + \Phi_c)} \cdot \sum_{k=1}^{N_{SC}} x_k e^{j2\pi f_k t} e^{j\Phi_D(k)} \tag{5.18}$$

where $h(k)$ is the frequency response for kth subcarrier, and $\Phi_D(k)$ is the phase dispersive of each subcarrier owing to fiber CD discussed in Section 3.4.2. At the coherent receiver, the optical signal is down converted by beating with a local laser. The signal is written as:

$$r(t) \propto e^{j2\pi(f_c - f_l)t + j(\Phi_c - \Phi_l)} \cdot \sum_{k=1}^{N_{SC}} x_k e^{j2\pi f_k t} e^{j\Phi_D(k)} \tag{5.19}$$

As we discussed in Section 3.3.5, if $f_c = f_l$, the detection is homodyne, otherwise hyterodyne, which needs one more down-conversion step in the RF domain to baseband signals. The frequency drift is a slow process and can be easily compensated by a low speed electronic circuit or in DSP. The phase recovery is more difficult and therefore is the thrust of this work. After satisfying the coherent conditions, the received baseband signal is:

$$r(t) \propto \sum_{k=1}^{N_{SC}} x_k e^{j2\pi f_k t} e^{j\Phi_D(k)} \tag{5.20}$$

The advantage of the coherent detection becomes obvious in (5.20): the system is simply a linear channel with a constant phase shift $\Phi_D(k)$ as far as each individual subcarrier k is concerned. This constant phase will be automatically included in symbol decision on the individual subcarrier basis and cause no troubles for data recovery.

Before we proceed to the next section, it is helpful to summary the mathematical symbols as in Table 5.1.

5.3.2 Phase Noise

Similar to (5.16), if the initial optical phase is assumed to be 0, the OFDM signal after up-conversion to optical domain is $s(t)e^{j2\pi f_c t}$. The transmission channel impairments include CD and optical noise, which is treated as additive white Gaussian

i	index of OFDM symbol
k	index of OFDM subcarrier
$h(k)$	optical channel response at kth subcarrier
$s(t)$	one OFDM symbol in continuous time domain
$x(k), x_k$	transmitted OFDM data at kth subcarrier
$y(k), y_k$	received OFDM data at kth subcarrier
N_{SC}	number of subcarriers
N_f	number of OFDM symbols in one OFDM block
f_c	the optical carrier frequency
f_l	the local laser frequency for coherent detection
Φ_c	the phase of optical carrier
Φ_l	the phase of local laser
$\Phi_D(k)$	the CD phase delay of kth subcarrier
$n(t)$	complex white Gaussian noise

Table 5.1: List of mathematical symbols.

noise. The received optical signal before the receiver is:

$$r(t) = e^{j2\pi f_c t} \cdot \sum_{k=1}^{N_{SC}} x_k e^{j2\pi f_k t} e^{j\Phi_D(k)} + n(t) \qquad (5.21)$$

where $n(t)$ is the additive complex white Gaussian noise.

By using coherent detection, $r(t)$ is linearly converted to baseband. However, as described in Section 3.3.5, the frequency and phase of local oscillator must lock to $r(t)$. Frequency locking is comparatively simple task while phase locking needs more sophisticated methods. Assume the frequency locking is obtained and the phase is free running, the $r(t)$ is linearly down-converted to baseband with the introduction of local oscillator phase drift $\Phi(t)$. The $r(t)$ is written as:

$$r(t) = \{\sum_{k=1}^{N_{SC}} x_k e^{j2\pi f_k t} e^{j\Phi_D(k)} + n(t)\} e^{j\Phi(t)}. \qquad (5.22)$$

It is apparent that the $r(t)$ is corrupted by $\Phi(t)$, which is a function of t. It is possible to estimate the $\Phi(t)$ in time domain [123]. However, this approach loses the advantage of OFDM in frequency domain, i.e., each subcarrier has a much lower speed. Therefore, we continue to discuss the $\Phi(t)$ in frequency domain. After digital

sampling and FFT, the received signal in frequency domain is [128]:

$$y(k) = x(k)h(k)p_{CPE} + p_{ICI} + n(k) \tag{5.23}$$

$$p_{CPE} \triangleq \frac{1}{N_{sc}} \sum_{n=1}^{N} e^{j\Phi(n)} \tag{5.24}$$

$$p_{ICI} \triangleq \sum_{l=0,l\neq k}^{N_{sc}} x(k)h(k)\left[\frac{1}{N} \sum_{n=0}^{N} e^{j2\pi(l-k)\frac{n}{N}+j\Phi(n)}\right] \tag{5.25}$$

p_{CPE} is common phase error (CPE) and can be treated as the mean value of $\Phi(t)$ in one FFT window. Note p_{CPE} is independent of k and represents a common phase error adding to every sub-carrier that is a rotation of the constellation. Since it is constant for all sub-carriers, it can be corrected by appropriate phase rotation. p_{ICI} term corresponds to the summation of the interference from the other sub-carriers, multiplied by some complex number which comes from an average of phase noise with a spectral shift. The result is also a complex number and has an appearance of Gaussian noise. Because of its random nature, it is difficult to be corrected.
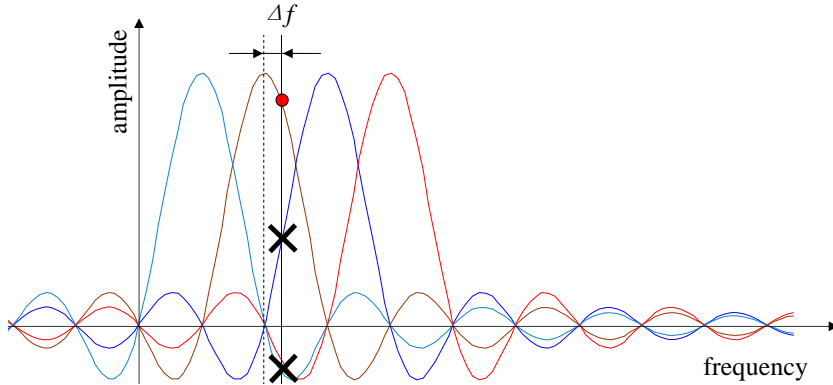
Figure 5.4: Loss of orthogonality.

Phase noise can be also treated as small frequency error. We can explain p_{ICI} as the results from the loss of orthogonality. Fig. 5.4 illustrates the loss of orthogonality. The dashed vertical line corresponds to no frequency error. The subcarrier at the dashed line has no interference from the rest subcarriers because of the orthogonality among the subcarriers. The solid line has a small frequency error resulting

from phase noise, or loss of orthogonality. The phase noise not only results in inter-subcarrier interference, but it also reduces the useful signal amplitude at the frequency domain, which directly reduce the signal-to-noise ratio (SNR) of that subcarrier. In general, it is possible but difficult to compensate ICI. However, (5.23) can be simplified in two ways: (i) the ICI contribution imposed on each subcarrier can be viewed as additional noise, which becomes near-Gaussian distributed as a consequence of the central limit theorem when the subcarriers count is large [123]; (ii) the phase drift $\Phi(t)$ is approximated as constant over the time of one OFDM symbol and therefore the FFT transform of (5.23) contains no ICI but only a constant phase shift. In either way, (5.23) can be simplified as:

$$y(k) = x(k)h(k)e^{i\Phi(i)} + n(k) \tag{5.26}$$

where $\Phi(i)$ is p_{CPE}, using index of OFDM symbol. Note the $\Phi(i)$ and $n(k)$ in (5.26) take slight different values to those in (5.23) due to approximation. Equation (5.26) is a much simpler expression of phase noise and it is the basis of phase estimation and compensation for CO-OFDM.

5.3.3   Phase Estimation and Compensation

Based on the description in the previous section, phase noise upon OFDM signal reception consists of two components: a random noise term that can be modeled as additive Gaussian noise, and a common deterministic term originated from laser phase drift that affects all the subcarriers uniformly. The thrust of phase estimation is to extract laser phase drift from noisy received signals for OFDM subcarrier phase estimation and symbol decision.

Because CO-OFDM utilizes linear RF-to-optical up conversion in the transmitter and linear optical-to-RF down conversion in the receiver [22], we model CO-OFDM transmission as parallel linear channels as shown in Fig. 5.5, where x_{ik} and y_{ik} are transmitted and received signal respectively, h_k is the transfer function for the kth subcarrier, Φ_i is the phase drift of the ith OFDM symbol and n_{ik} is the white Gaussian noise. The transfer functions of the subcarriers in optical fibers are treated
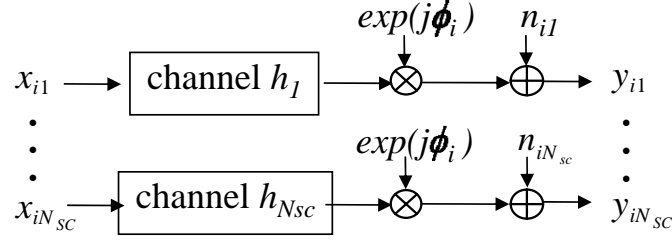
Figure 5.5: Parallel subcarrier model for OFDM transmission.

as static within one OFDM frame and obtained by using a training sequence in the preamble. Since the OFDM symbol used in our following experiments has a period of 36 ns and the laser sources both have about 20 kHz line width in our experiment, the phase drift within one OFDM symbol can be considered as constant and common to all the subcarriers.

Following the discussion in (5.26), the channel model is:

$$y_{ik} = x_{ik} \cdot h_k \cdot e^{j\Phi_i} + n_{ik}; \tag{5.27}$$

$$h_k = |h_k| \cdot e^{j(\Phi_0 + 2\pi\tau_0 f_k + \frac{c\pi}{f_{LD}^2} D_t f_k^2)}; \tag{5.28}$$

$$i = 1, \cdots, N_f; k = 1, \cdots, N_{SC}$$

where Φ_i is the common phase error, n_{ik} is complex white Gaussian noise with zero-mean, including the inter carrier interference p_{ICI}. The channel response h_k is essentially caused by group velocity delay, which shows a quadratic expression, including a zero-order dc term Φ_0, a linear term proportional to the time delay of the first subcarrier τ_0, and a quadrature term proportional to the fiber chromatic dispersion D_t in the units of ps/nm. f_k the frequency of kth subcarrier and f_{LD} is the frequency of local laser. c is the light speed.

The basic idea of pilot-aided phase estimation is to subtract the phase angles of the received pilot subcarriers by those of the transmitted pilot subcarriers and then average the outcomes across the pilot subcarriers in one OFDM symbol. Therefore,

the estimated phase drift of the ith OFDM symbol can be formally written as:

$$\Phi_i = E\left\{arg(y_{ik}) - arg(\widehat{x}_{ik})\right\};\; k = 1, \cdots, N_p \qquad (5.29)$$

where arg(.) is the phase angle of the information symbol, E(.) is the mean over index i, $\widehat{x}_{ik}$ is the corresponding transmitted pilot subcarrier, and N_p is the number of pilot subcarriers. After the h_k and Φ_i are acquired, the received signal y_{ik} can be phase compensated and channel compensated, i.e., from (5.27), the estimated $\bar{x}_{ik}$ for data decision can be expressed as:

$$\bar{x}_{ik} = y_{ik} \cdot e^{-j\Phi_i} \cdot h_k^* / |h_k|^2;$$
$$i = 1, \cdots, N_f; k = 1, \cdots, N_{SC} \qquad (5.30)$$

where h_k^* is the conjugate of the estimated transfer function of the kth subcarrier.

For data-aided phase estimation, the channel model is the same as (5.27). The phase estimation follows the Mth-power-law method for M-ary PSK to remove data modulation [99, 103]. As an example, we consider a QPSK signal in (5.31), the fourth power is $E^4 \propto e^{j2\pi x_n}$, which is always equal to unit because x_n is an integral number. Therefore, the residual phase divided by 4 can be considered as the optical carrier phase. Since the signal is corrupted by noise, it is necessary to average the phase estimation cross all the subcarriers, data-aided phase estimation can be written as [22]:

$$\Phi_i = E\left\{arg(y_{ik}^M)/M\right\};\; k = 1, \cdots, N_{SC} \qquad (5.31)$$

Similar to pilot-aided phase estimation, (5.30) is used to obtain the estimated signal $\bar{x}_{ik}$. Because of the phase ambiguity associated with the Mth-power-law method [99], the error of phase estimation can be significant when the phase noise is strong. Considering $\bar{x}_{ik}$ as processed y_{ik}, we can iterate the phase estimation (5.31) and compensation (5.30) for better performance by replacing y_{ik} with $\bar{x}_{ik}$ in (5.31).

The advantage of pilot-aided phase estimation is apparent from (5.29), namely, it does not suffer from phase ambiguity. Therefore it can achieve accurate phase

estimation even with a very noisy signal. On the other hand, conventional data-aided phase estimation suffers from phase ambiguity as a result of multiple levels of data signals. Differential encoders and decoders are generally added to resolve the phase ambiguity but the effects from random noise can not be completely avoided [99, 129]. Therefore, the performance of data-aided phase estimation is degraded while its implementation complexity is increased in both hardware and software.

5.3.4 Simulation Results

To verify the phase estimation theory and method, we program in Matlab and carry out a simulation using similar parameters in the following experiment in Table 5.2. The subcarriers are encoded as QPSK format. The ASE noise is simulated as additive complex white Gaussian noise. The laser phase noise is simulated by white Gaussian frequency noise as described in Section 3.3.1.
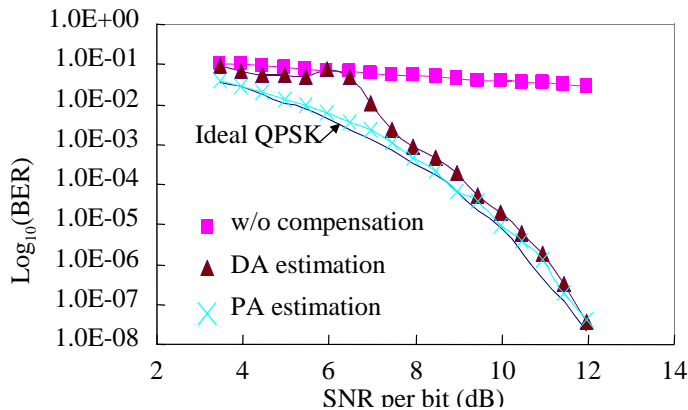
Figure 5.6: Simulation results of phase compensation of a 200 kHz laser. PA: pilot-aided. DA: data-aided.

In Fig. 5.6, the solid curves is from an ideal zero linewidth laser and is the lower bound for all the remaining curves. The ideal curve is almost identical to the theoretical curves in [99]. When we use a 200 kHz laser, the BER floor is as high as 2×10^{-2} if the laser phase noise is not compensated. On the other hand, after phase estimation and compensation, the BER curve is close to the ideal curve. The pilot-aided phase estimation is always slightly better than the data-aided phase

estimation. Note when the noise is strong, the data-aided phase estimation and compensation break down and no sensible improvement can be seen when the SNR per bit is lower than 7 dB. The reason is that the data-aided phase estimation suffers from the phase ambiguity of Mth-power-law methods, as we have discussed in Section 5.3.3. In contrast, the pilot-aided phase estimation is robust even when the BER is as low as 10^{-2}.

This simulation verifies that our theory and methods are successful in the simulation scenario. We then carry out two CO-OFDM transmission experiments to further prove it.

5.4   Experimental Demonstration at 8 Gb/s

At the time of this experiment, we only had a 4 GSa/s arbitrary waveform generator. As a result, it is difficult to generate an OFDM signal at 10 Gb/s. Therefore, this experiment is for proof-of-concept and verify feasibilities of CO-OFDM, including phase estimation. The signal processing was carried out after the sampled data were uploaded to a computer with MATLAB program, which is the so-called off-line signal processing. The real-time signal processing is challenging due to the speed and memory constraints, but feasible based on the complexity analysis in [130].

5.4.1   Experimental Setup

We apply pilot-aided and data-aided phase estimation to a 1000-km CO-OFDM transmission experiment. Fig. 5.7 shows the experimental setup for CO-OFDM transmissions. The OFDM signal is generated by using Tektronix arbitrary waveform generator (AWG710B) as an OFDM transmitter. The time domain waveform is first generated with a Matlab program including mapping 2^{15}-1 PRBS into corresponding 128 subcarriers with QPSK modulation. The preamble, pilot subcarriers and guard interval are subsequently inserted. One OFDM block has 400 OFDM symbol. The bit rate for each subcarrier is about 55.6 Mb/s. The digital waveform is uploaded into the AWG to generate real time analogue RF OFDM signal. An MZ modulator is used to up-convert the OFDM signal to optical carriers. The optical
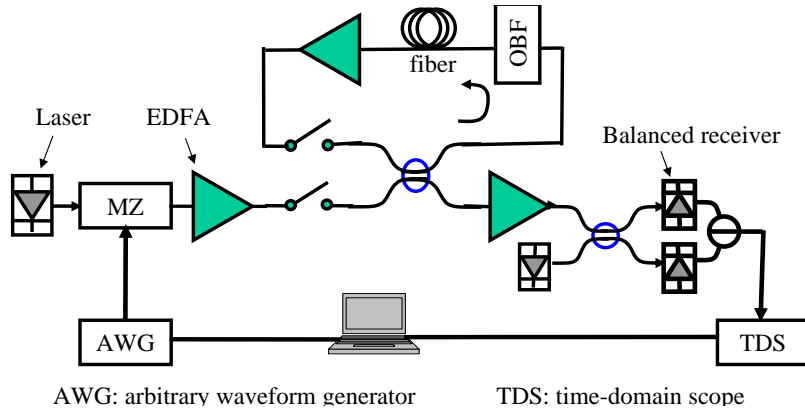
Figure 5.7: Experimental setup of CO-OFDM.

OFDM signal is then fed into a recirculation loop for 1000-km transmission that includes one span of 78 km SSMF fiber and an EDFA to compensate the fiber loss. The optical signal coupled out from the loop is down-converted into RF domain through a coherent detector as an OFDM optical-to-RF down converter that includes a balanced receiver and local laser without OPLL. The transmitter and receiver lasers both have about 20 kHz linewidth, which is achievable by the commercial available lasers for telecommunications [101]. There are three couplers to monitor the optical power at the transmitter, inside the re-circulating loop, and before the receiver, respectively. An optical attenuator is inserted before the receiver EDFA to facilitate the BER curve test. For the sake of simplicity, the couplers and optical attenuator are not illustrated in Fig. 5.7. The RF OFDM traces are acquired with a real time domain sampling scope (TDS) at 20 GSa/s. The acquired traces are processed with another Matlab program as an OFDM receiver. The OFDM receiver signal processing involves (1) software down-conversion of the OFDM RF signal to base-band by using either a residual main carrier tone, or a pilot subcarrier tone, (2) window synchronization using Schmidl format to identify the start of the OFDM symbol , (3) phase estimation for each OFDM symbol, and (4) constellation construction for each carrier and BER computation. Pilot-aided phase estimation and data-aided phase estimation are both realized according to the theory in Section 5.3.

In this experiment, the optical power per channel into optical fiber is limited to about -10 dBm to avoid any nonlinearity in transmission fiber, and the polarization

of the receiver laser is manually aligned to the incoming optical signal. The fiber non-linearity tolerance of CO-OFDM is beyond the scope of this thesis. The polarization alignment can be avoid by using polarization diversity receivers, which will be demonstrated in Section 5.5.

More parameters in the experiment are list in Table 5.2.

$N_{SC} = 128$	number of subcarriers
$N_f = 400$	number of OFDM symbols in one OFDM block
$CP = 16$	cyclic prefix length
$T_s = 32\ ns$	useful symbol duration
$T_g = 4\ ns$	guard interval time
$\Delta f = 31.25\ MHz$	frequency spacing of subcarriers
$f_c = 193.55\ THz$	optical carrier frequency
$D = 17\ ps/nm/km$	chromatic dispersion parameter
$NF \approx 4dB$	EDFA noise figure
$P_s < -10\ dBm$	optical power per channel

Table 5.2: List of 8 Gb/s experimental parameters.

The MZ modulator used in transmitter is of interest for further explanation. In theory, an optical I/Q modulator should be used for direct up-conversion to optical domain, with real/imaginary part of the OFDM signal feeding into real/imaginary arm of the optical modulator, which is described in Section 3.3.2. However, in our first OFDM experiment, the AWG only has one output, equivalent of only real part of the OFDM signal. As a result, a single MZ modulator biased at zero output is used for RF-to-optical OFDM up conversion. By using the small signal approximation $sin(x) \approx x$, we can express the amplitude output of the modulation as:

$$E_o = E_i sin[s(t)] \approx E_i s(t) \tag{5.32}$$

which is standard double side band amplitude modulation. It is well known the amplitude of such a signal is even symmetry and the phase is odd symmetry in frequency domain. Since the data are encoded in PSK in frequency domain, from Fig. 5.8, we can see such waveform generation produces 128 OFDM subcarriers, but with the constraint expressed as:

$$a_i + a_{128-i} = [00],\ a_i \in \{00, 11\}$$

$$a_i + a_{128-i} = [11], \ a_i \in \{01, 10\} \tag{5.33}$$

where $a_i \in \{00, 01, 10, 11\}, i = 1, 2, \cdots, 128$ is the two-bit QPSK symbol represented by each subcarrier symbol.
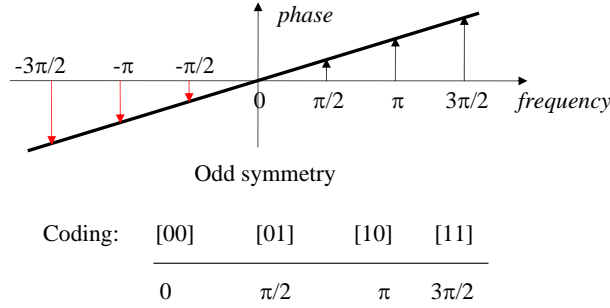
Figure 5.8: Phase function of double-sideband amplitude modulation.

The CP length is $\frac{1}{8}$ of the number OFDM subcarriers, corresponding a guard interval of 4 ns. We can use (5.14) to calculate the CD tolerance:

$$D_t = \frac{T_g f_c^2}{c N_{SC} \Delta f} \approx 1.25 \times 10^5 \ ps/nm \tag{5.34}$$

which is equivalent to the total CD of 7000 km SSMF fiber. Therefore the ISI of CD from less than 7000 km SSMF fiber can be totally eliminated.

5.4.2 Signal Processing Flowchart of Coherent Optical OFDM Receiver

By using digital signal processing, the OFDM receiver is simplified as optical front end, ADC and digital signal processor, where intensive signal processing is carried out. The digital signal processor replaces the conventional discrete circuits, such as the frequency down-converter and data slicer. Fig. 5.9 shows the flowchart of the signal processing and some visual results of some important intermediate steps. The main steps are the coarse and fine synchronization from Step 2 to Step 4. We explain the steps as follows:

1. Load the data sequence from the oscilloscope to the computer with Matlab program. The important parameters of the oscilloscope are also imported to

the program, such as sampling speed.

2. Locate the start of one OFDM frame. We elect to use the Schmidl format [21], which is to find a peak by auto-correlation as shown in the inset for the 2nd step in Fig. 5.9.

3. Determine the carrier frequency and down convert the signal to baseband. The frequency estimation is simply by looking at the frequency domain and peak frequency is used as the carrier frequency for IF down-conversion.

4. Phase estimation and compensation. After we obtain the baseband signal, the CP is deleted and the resultant sequence is converted to frequency domain by FFT for the transmitted data. Phase estimation and compensation are then carried out either by pilot-aided methods or data-aided methods.

5. Channel estimation and compensation. This step is achieved by using training sequence at the beginning of one OFDM frame. By channel estimation and compensation, the constellation is rotated to original position. The channel estimation and compensation may be skipped if we use data-aided phase estimation and differential coding.

6. BER calculation. The estimated data are compared with the transmitted sequence for BER calculation. For the better performance, the symbol mapping uses Gray code [99].

5.4.3 Analysis of Phase Noise

For QPSK format, the phase noise is one of the limiting factors of the transmission performance. Fig. 5.10 shows the overlapped phase noise distributions of all the subcarriers. The time interval of phase change is 36 ns, i.e., one OFDM symbol period. Fig. 5.10(a) is the result with back-to-back (B2B) transmission and the OSNR is 15.6 dB (0.1 nm resolution). There is no phase change bigger than the decision window, $\pi/2$ for QPSK, so there is no BER errors. As predicted in theory, the phase change histograms follow the Gaussian distribution illustrated by the thick Gaussian

1: Sampling trace from scope

⇩

2: Locate the OFDM frame header,
   trunk out the OFDM symbol.

⇩

3: Determine the carrier frequency, down
   convert to base-band.

⇩

4:FFT transform to frequency domain,
   phase estimation and compensation.

⇩

5: Channel estimation and compensation

⇩

6: BER calculation
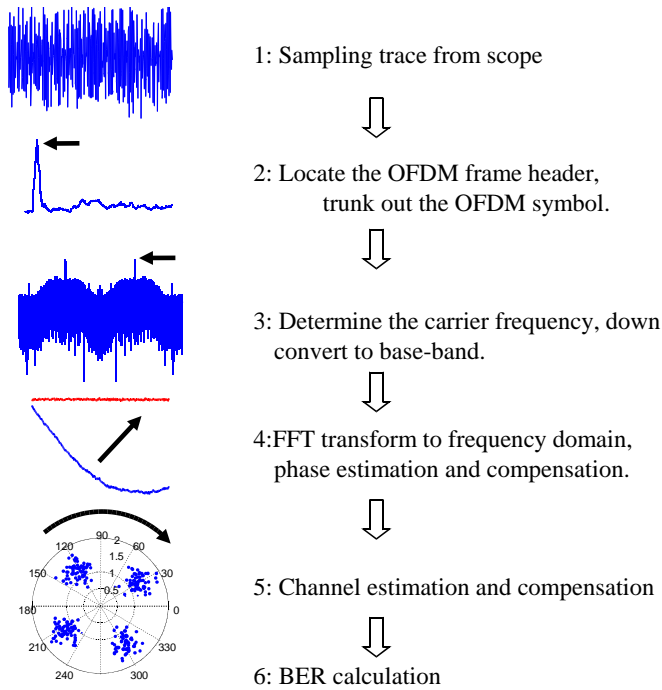
Figure 5.9: Flowchart of OFDM receiver functions

fit curves. The variance of the distribution is reduced to 0.025 after compensation. By using (3.12) in Section 3.3.1, we can estimate the combined laser linewidth of the transmitter laser and local laser is 101 kHz. This is close to specification of the laser source. Fig. 5.10(b) is the result for one OFDM frame after 1000-km transmission with 9.9 dB received OSNR (0.1 nm resolution). Compared with back-to-back transmission in Fig. 5.10(a), the variance of the phase noise increases, which is from the low OSNR and the fiber transmission. Without compensation, a non-zero mean value of the distribution indicates the laser frequency drift. After compensation, the mean value of the distribution is reduced close to 0. As expected, the variance of the distribution has barely changed. In Fig. 5.10(b), the phase change exceeding the decision window will result in the errors after data decision.

Fig. 5.11 shows the phase estimation results for one OFDM frame after 1000-km transmission with 9.9 dB received OSNR. It includes the comparison of the phase estimation and compensation between data-aided and pilot-aided estimation. It is interesting to note that the phase evolution could be very fast, i.e., about 1 MHz frequency drift within 10 μs between the transmitter and receiver lasers. This fast
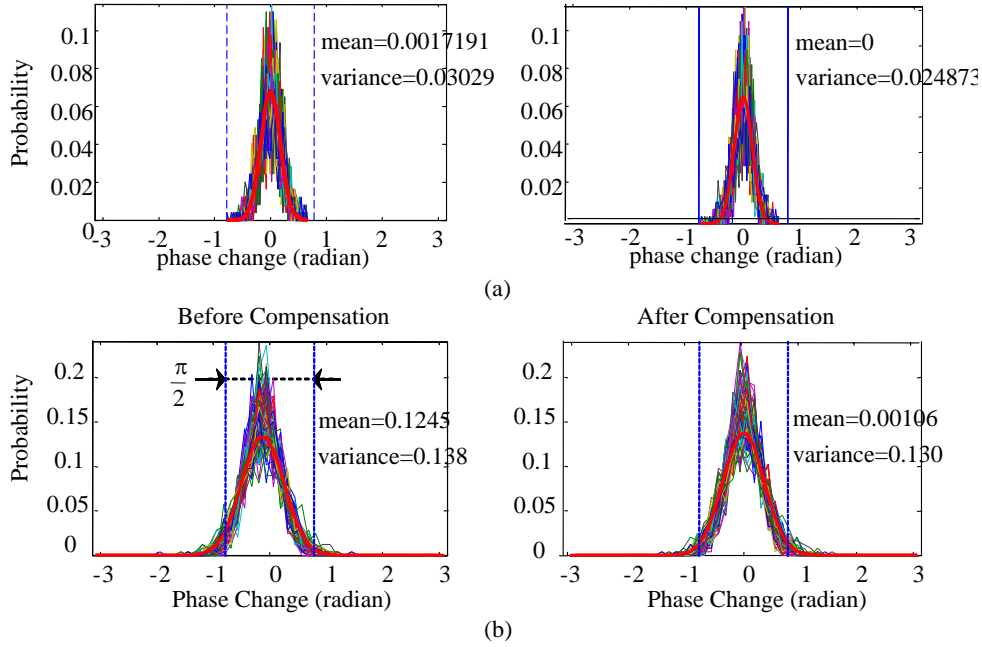
Figure 5.10: Phase noise distribution at a time interval of 36 ns (a) with back-to-back transmission, (b) after 1000 km SSMF transmission.

change poses a challenge for the phase estimation. This fast drift is unexpected based on the intrinsic line width of the laser sources used in this experiment. However, this is confirmed by a similar report of fast phase drift in [66]. One possible reason is the frequency jitter of the laser sources since we do not use any frequency locking circuit.

The bold curve (a) shows the result of pilot-aided phase estimation, namely, the symbol phase drift Φ in (5.29). After phase compensation by (5.30), we can calculate the individual subcarrier phase noise as $arg(\bar{x}_{ik}) - arg(x_{ik})$, illustrated by the bold curve (e). From the curve (a) and (e), the pilot-aided phase estimation only needs to be carried out once and the phase drift is fully compensated, which is demonstrated by the flat phase noise evolution curve (e) only showing random noise. On the other hand, the symbol phase drift Φ of data-aided phase estimation in (5.31), as shown by the thin curve (b), clearly deviates from pilot-aided phase estimation, which is caused by phase ambiguity, particularly manifested as the occasional phase kinks. Similarly, we can calculate the individual subcarrier phase noise as $arg(\bar{x}_{ik}) - arg(x_{ik})$ after phase compensation by (5.30). As a result of phase ambiguity, the phase noise evolution curve (c) shows residual phase drift and phase kinks. For data-aided
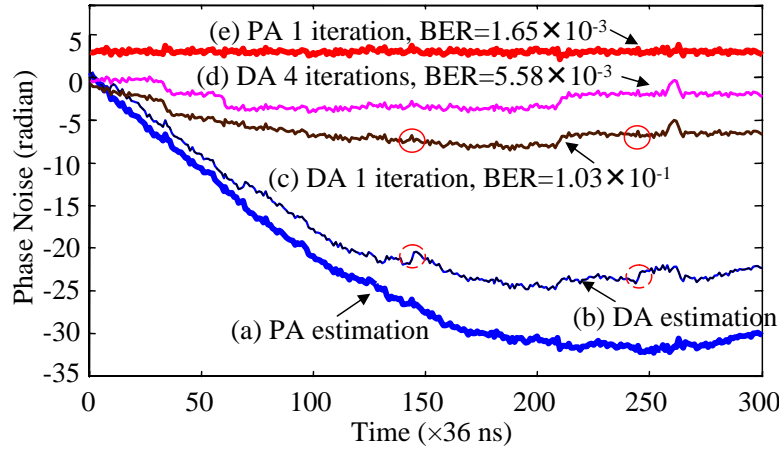
Figure 5.11: OFDM symbol phase noise evolution versus time by pilot-aided (PA) and data-aided (DA) phase estimation and compensation.

method, after one iteration of phase estimation and compensation, some phase kinks indicated by the small circles of the curve (c) are eliminated, which means less symbol decision errors. The residual phase drift can be further reduced for a better BER if we iterate phase estimation and compensation as shown by the curve (d). This is because the phase compensation of the last iteration reduces the BER and improves the phase estimation accuracy for the next iteration. We find 4 iterations are adequate to obtain the minimum BER since further iteration can not improve phase estimation accuracy. However, this is still more complex and requires more computation power in comparison with pilot-aided phase estimation.

Fig. 5.12 shows the back-to-back QPSK constellations before and after phase compensation. Before phase compensation, the constellation are smeared due to the phase spreading. After phase compensation, the constellation converges to the four phase levels. Note the amplitude noise is unchanged since we do not process the amplitude information.

5.4.4 BER Results

Although pilot subcarriers are effective for phase estimation, they have the disadvantage of consuming useful bandwidth. It is important to find the minimal number of pilot subcarriers to maintain sufficient performance. Fig. 5.13(a) shows the ex-
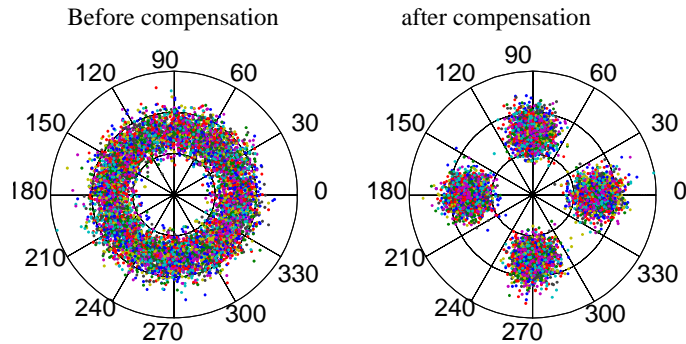
Figure 5.12: QPSK constellations before and after phase compensation.

perimental BER performance as a function of number of pilot subcarriers at three different OSNRs after 1000-km transmission. It can be seen that 5 pilot subcarriers are adequate for the phase estimation because the BER performance is barely improved beyond 5 pilot subcarriers. This result is similar to the report in [131], where 4 subcarriers out of 64 subcarriers are used as pilot subcarriers.
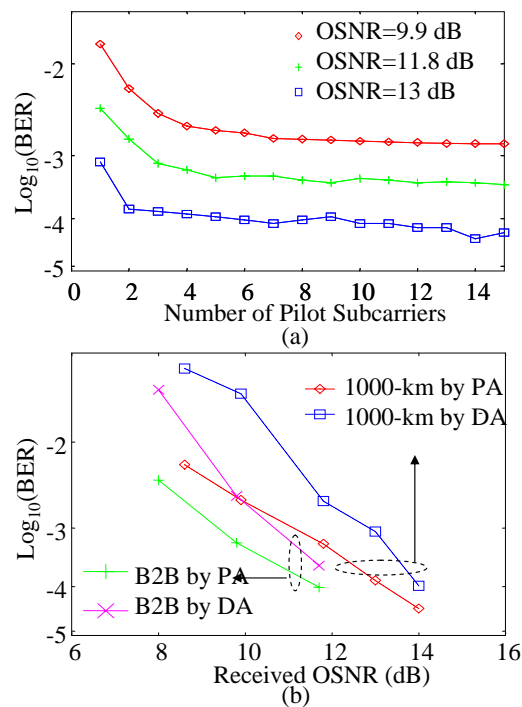
Figure 5.13: (a) BER performance versus number of pilot subcarriers; (b) BER performance of 1000-km transmission.

Based on the result in Fig. 5.13(a), we use 5 pilot subcarriers for CO-OFDM

system performance evaluations. Fig. 5.13(b) shows the BER results of 1000-km transmission after applying the phase estimation. With pilot-aided phase estimation, the BER performance after transmission shows about 1 dB OSNR penalty at BER of 10^{-3}. However, if data-aided phase estimation is employed, the BER performance degrades over 0.5 dB at BER of 10^{-3} either for the back-to-back or 1000-km measurements in comparison with the pilot-aided phase estimation. Our approach using a small number of pilot subcarriers enhances the performance of CO-OFDM systems compared with data-aided phase estimation. This advantage will be more significant if we employ 8-ary PSK and beyond. Furthermore, pilot-aided phase estimation can be easily applied to high-order (larger than 8) quadrature amplitude modulation (QAM), which has better performance than PSK [99]. In contrast, data-aided phase estimation depends on the constellation and coding method, and is difficult to be adopted to QAM signal [132].

5.5 PMD Tolerance Experiment at 10 Gb/s

This experiment is the extension of the previous one. Most parameters and configurations are similar. Therefore the description in this section emphasizes the difference. We use an arbitrary waveform generator (AWG) with two independent 10 GSa/s outputs for I/Q channels. Consequently, the AWG can generate 10 Gb/s OFDM signal. In the previous experiment described in Section 5.4, CD distortion shows little degradation of transmission performance. We further include a PMD emulator (PMDE) at the transmitter side to investigate PMD tolerance of CO-OFDM. Although the experiment and signal processing are complicated in several other aspects, the phase estimation theory and compensation methods discussed in Section 5.3.3 are still applicable to this experiment. Therefore we focus on the main experimental results which proves the effectiveness of the phase estimation theory and methods.

5.5.1 Experimental Setup

The experimental setup is shown in Fig. 5.14, which is similar to Fig. 5.7. The optical modulator in the transmitter is a dual-parallel MZ modulator for optical I/Q modulation, which has been introduced in Section 3.3.2. Inside the loop, the SSMF fiber is extended to 100 km with 21 dB insertion loss. A PMDE is added at the transmitter side. The PMDE is based on the description in Section 2.3 and 3.4.3. The input light of PMDE is polarization split into two paths and combined with the addition of a time delay, which is DGD. Due to the shortage of components, we only construct a fixed time delay: 340 ps DGD. As per the discussion in Section 3.4.3, the conventional IM/DD system has non-negligible power penalty even the DGD is only about 30% of one bit period, i.e., 30 ps at 10 Gb/s. Therefore, 340 ps DGD is a significant value for signals at 10 Gb/s and is an order-of-magnitude improvement over the IM/DD systems. Note this PMDE only introduces the first order PMD. In the experiment, we adjust the state of input polarization for an even polarization split, which maximizes the PMD effects.
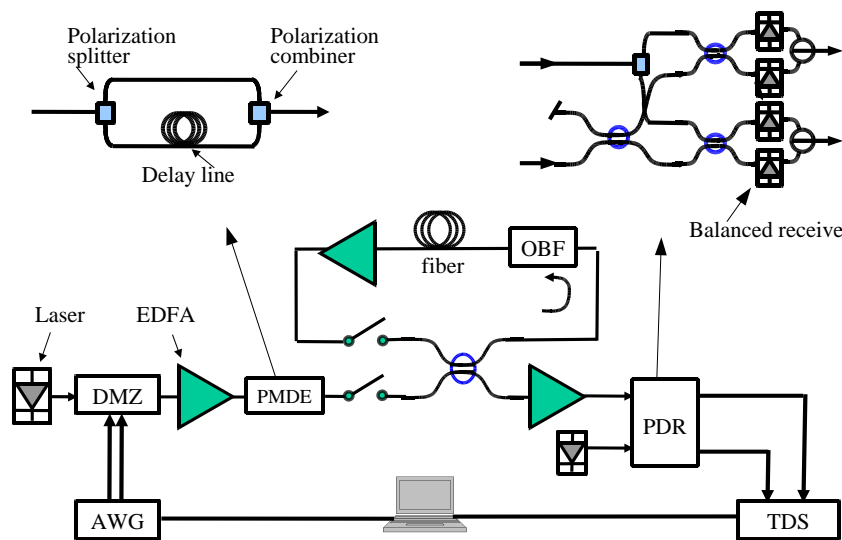

Figure 5.14: Experimental setup for 10 Gb/s. PMDE: PMD emulator, PDR: polarization diversity receiver, DMZ: dual-parallel MZ modulator

A polarization diversity receiver is used at the receiver side. The principle of polarization diversity is well discussed in [4, 67]. As shown by the right inset in Fig.

5.14, the incoming signal and the local laser are both split according to two orthogonal polarization states, which are mixed by coupler and detected by photodiode (balanced receiver in our case). The outputs of two balanced receiver capture the two orthogonal polarization states of incoming signals and therefore contain all the polarization information in theory. Note in this experimental setup, the local laser is divided by a normal 3 dB coupler instead of polarization splitter. In another words, we use two polarization controllers to emulate the two orthogonal polarization states of polarization splitter. In principle, the signal processing of the polarization diversity receiver should be based on the electrical field vector, similar to (3.1) and (3.46). However, we can independently process the two polarization signals and add them right before the decision circuit. This strategy is effective since we only try to avoid the power fluctuation caused by the polarization change [67].

More parameters in the experiment are listed in Table 5.3. Note the number of subcarriers is the FFT length. 64 subcarriers is actually used for data transmission. The rest subcarriers are filled with 0 as frequency guard band for anti-aliasing purpose. Each subcarrier has a bit rate of about 139 MHz and total useful data rate is about 8.9 Gb/s.

$N_{SC} = 128$	number of subcarriers
$N_f = 400$	number of OFDM symbols in one OFDM block
$T_s = 12.8\ ns$	useful symbol duration
$T_g = 1.6\ ns$	guard interval time
$\Delta f = 78.15\ MHz$	frequency spacing of subcarriers
$f_c = 193.55\ THz$	optical carrier frequency
$D = 17\ ps/nm/km$	chromatic dispersion parameter
$NF \approx 4dB$	EDFA noise figure
$P_s \approx -7\ dBm$	optical power per channel
$L = 21\ dB$	insertion loss of 100 km SSMF

Table 5.3: List of 10 Gb/s experimental parameters.

5.5.2 Measurement Results

In the experiment, we measure the performance degradation versus transmission distance. We elect to monitor OSNR and electrical SNR (ESNR). The OSNR is measured by an optical spectrum analyzer (OSA) synchronized to the re-circulating

loop. The ESNR of CO-OFDM can be found in [133] and is essentially the spreading of the constellation. Fig. 5.15 shows the OSNR and ESNR versus transmission distance, or the number of loops. The thin solid OSNR line is the theoretical calculation from (3.33) in Section 3.4.1. The measured OSNR agrees with the theoretical curves with a small deviation. For the ESNR curve, the maximum value is limited by transmitter and receiver for the short distance transmission. The ESNR is bigger than 12 dB after 1000 km transmission. For an indication, the 8.2 dB ESNR corresponds to about 10^{-3} BER in our back-to-back measurement.
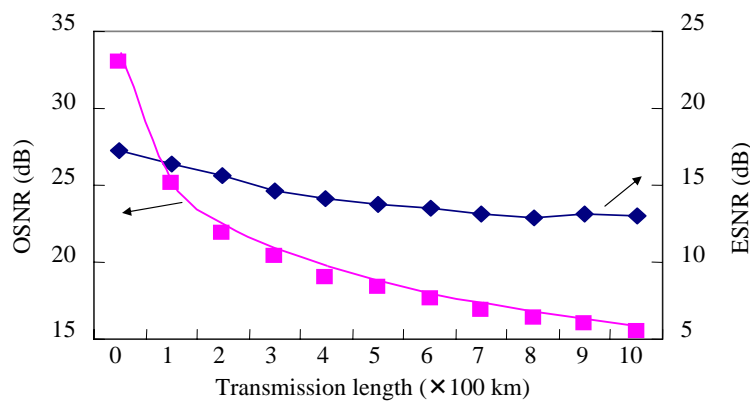
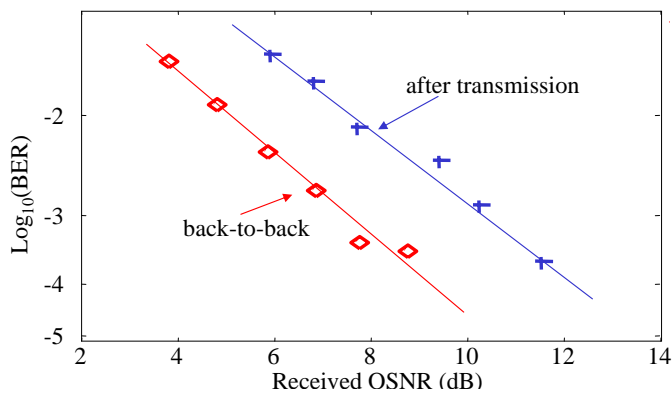Figure 5.15: OSNR and ESNR versus transmission distance.

Figure 5.16: BER performance after transmission over the 340 ps PMD emulator and 1000 km SSMF fiber.

Fig. 5.16 shows the system performance after transmission over the 340 ps PMD emulator and 1000 km SSMF fiber. The OSNR penalty is about 2 dB at 10^{-3}

BER by pilot-aided phase estimation. This result is an order-of-magnitude improvement compared with the IM/DD system, which only has around 30 ps tolerance as described in Section 3.4.3.

5.6 Conclusions

Combined with coherent detection, OFDM is an effective way to eliminate the CD and PMD distortion. In this chapter, we have presented the phase estimation theory and method for CO-OFDM, which enables coherent detection of optical OFDM without conventional OPLL. For QPSK OFDM signal, the phase estimation can be realized by pilot-aided or data-aided phase estimation. Pilot-aided phase estimation takes advantage of multiple parallel subcarrier structure of OFDM and is more robust for noisy received signals.

We have applied the phase estimation in two experiments to combat CD and PMD distortion. For the first time, we have experimentally demonstrated the pilot-aided phase estimation in long-haul optical fiber transmissions. In the first experiment at a nominal bit rate of 8 Gb/s, we have successfully reconstructed the QPSK constellations for a CO-OFDM transmission experiment after 1000-km transmission over SSMF without optical dispersion compensation. The OSNR penalty has been found to be about 1 dB at BER of 10^{-3} after 1000-km transmission. By using pilot-aided phase estimation, the system performance can be improved over 0.5 dB in comparison with that using data-aided phase estimation. We have also shown that as few as 5 pilot subcarriers are sufficient for pilot-aided phase estimation. In the second experiment at a nominal bit rate of 10 Gb/s, we have demonstrated the PMD tolerance of CO-OFDM at 10 Gb/s. The phase estimation theory and method is applicable with almost no change in the presence of strong PMD. The OSNR penalty is about 2 dB for the transmission after a 340 ps PMD emulator and 1000 km SSMF without any optical CD and PMD compensation.

Chapter 6

Optical Performance Monitoring for Optical Fiber Networks

6.1 Introduction

As per the discussions in Section 2.1, two primary tasks in optical fiber networks are data transmission and data routing. We have presented two techniques for such tasks in the previous two chapters. Furthermore, optical performance monitoring is of importance for practical network operation and maintenance. Optical performance monitoring will be helpful for carriers to provide guaranteed quality of service (QoS) to their users. To determine the health of optical signals in optical networks, it is necessary to monitor many parameters in the physical layer such as optical power [69, 70], optical signal-to-noise ratio (OSNR) [71, 72], chromatic dispersion (CD) [73, 74, 75], Q-factor [76, 77], polarization mode dispersion (PMD) [78, 79].

In this chapter, we present two optical performance monitoring techniques in the context of the two research areas we have discussed: optical packet switched networks and electronic dispersion compensation of optical distortions. In Section 6.2, we propose an OSNR monitor suitable for OPSN. In Section 6.3, we propose a CD monitoring technique for electronic dispersion compensation receivers.

6.2 OSNR Monitoring for OPSN

Many functions of current and future optical networks rely on optical performance monitoring of various optical parameters. Consequently, optical performance monitoring has drawn tremendous research interest in recent years [23]. On the other hand, OPSN have been proposed as an effective way to support data-centric inter-

net networks [5]. However, the concept of OPSN creates a host of new challenges in terms of efficient network monitoring and maintenance. Optical performance monitoring for OPSN adds a new dimension to the research topics of performance monitoring. Unlike conventional optical communication networks or optical circuit switched networks, optical channels in OPSN may consist of different optical packets. They could originate from diverse sources and traverse different optical links, which therefore results in vast wide dynamic range of optical parameters in a short time span of one packet. The use of optical amplifiers in an OPSN is necessary to compensate the loss incurred by the packet in all the nodes and fiber segments, but the optical amplifies introduce unwanted ASE noise into the optical packets, which degrades the OSNR of the optical packets and is one of the fundamental limiting factors. Hence, OSNR is one of the critical parameters to monitor.

Various approaches have been proposed to monitor OSNR. Polarization-nulling method using the polarization properties of signal and amplified spontaneous emission (ASE) noise includes the optimization of a polarization controller [71], and therefore cannot be applied to performance monitoring for a packet varying at a rate in the order of *nanosecond.* Another approach using uncorrelated signal-to-ASE beat noise requires precise matching of the receiver pair and may need more calibration procedures [72]. Indirect OSNR monitoring by measuring bit errors for the purpose of determining Time-to-Live is only sensitive around the threshold OSNR and may not provide enough dynamic range for general purpose network maintenance [134]. In this section, we propose and demonstrate a novel OSNR monitor capable of direct OSNR monitoring based on radio frequency (RF) noise measurement. This OSNR monitor can measure the OSNR values of the consecutive optical packets with varying OSNR.

6.2.1 Principle of OSNR Monitor for Packets

Fig. 6.1 shows the schematic diagram of the OSNR monitor for packets. The packet capable of performance monitoring (PM) contains an additional performance monitoring segment (PM segment). In this paper, the PM segment consists of $\sim$10 ns of consecutive $'1'$ bits at 10 Gb/s. At the packet switching node, a part of

the input optical signal power is tapped and fed into the OSNR monitor. Inside the OSNR monitor, the PM segment is extracted from the entire packet by using a Mach-Zenhder (MZ) modulator. The pulse after the PM extractor is fed into a photodiode. The optical signal power is tested after the photodiode. There will be RF spectral components at least in a range of $0 \sim 10$ GHz for the entire packet contributed by the payload. In contrast, the RF spectral components are absent at high frequency for the extracted PM segment, which can be treated as a CW signal. Fig. 6.2(a) and (b) show the measured spectra for the whole packet and extracted PM segment, respectively. The resolution bandwidth is set to 2 MHz. As expected, the RF spectral components are compressed and there are no signal components at frequency beyond 4 GHz for the extracted PM segment. Therefore, we can apply an electrical filter to filter out the RF noise of the interested frequency range for OSNR monitoring as shown in Fig. 6.2(b). The RF noise level is then detected by an RF power detector. The OSNR can be calculated by analyzing the optical signal power and RF noise level at the high frequency range.

In practice, the optical label processing unit should recover the clock on the label, and in return provides the timing information to the OSNR monitor to locate the PM segment. It is not the intention of this work to demonstrate the location of the PM segment. In addition, the accuracy of the pulse curving timing is quite forgiving in the order of 1 ns and the PM segment is only a continuous wave (CW) signal.
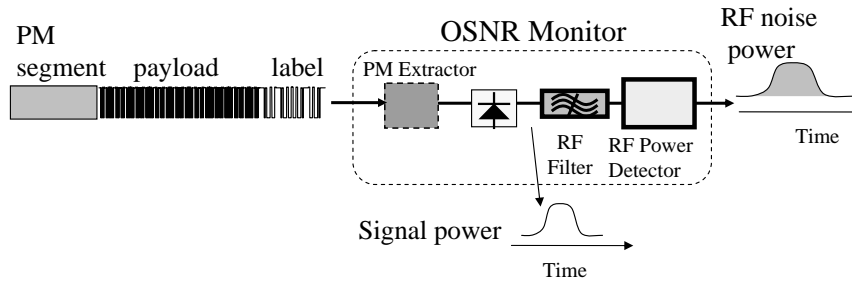
Figure 6.1: Conceptual diagram of proposed OSNR monitor

The OSNR is formally defined as:

$$OSNR = \frac{P_S}{P_{ase}} \tag{6.1}$$
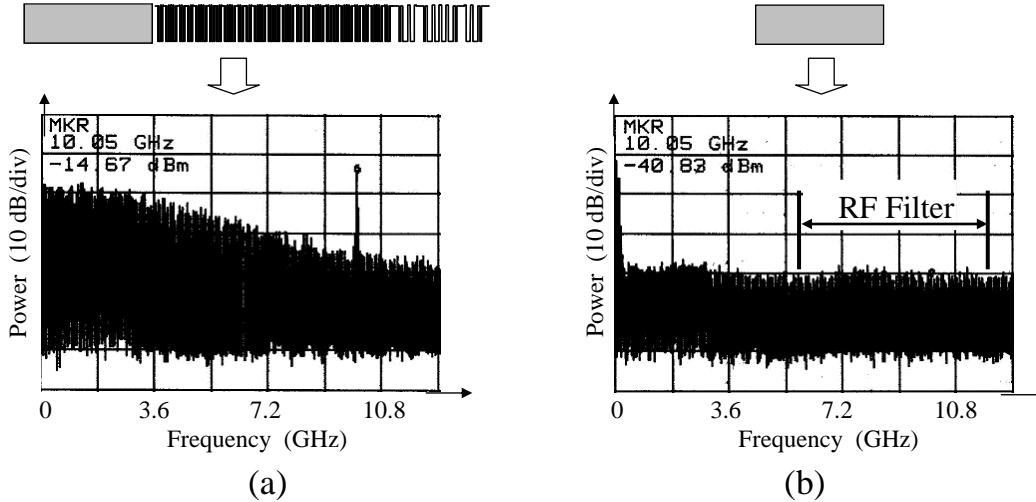
Figure 6.2: RF spectra for (a) the whole optical packet, (b)the PM segment only.

where P_S is the optical signal power and P_{ase} is the ASE noise power measured in 0.1 nm optical bandwidth. The RF power density consists of signal-ASE beat noise, the ASE-ASE beat noise, and the RIN noise [135]. Using the OSNR definition in (6.1), we write the RF power density as:

$$p(f) = A_1 \cdot P_S \cdot P_{ase} + B_1 \cdot P_{ase}^2 + C_1 \cdot P_S^2 \tag{6.2}$$

$$= A_1 \frac{P_S^2}{OSNR} + B_1 \frac{P_S^2}{OSNR^2} + C_1 P_S^2 \tag{6.3}$$

where $p(f)$ is the RF power density, P_S is the input optical signal power, $OSNR$ is the optical signal-to-noise ratio defined in (6.1), and A_1, B_1, and C_1 are related to various detection parameters and weekly dependent on frequency in theory. Therefore, with a reasonable approximation, we can move A_1, B_1, and C_1 coefficients out of the integral in (6.3). Hence, the RF power P integrated in a bandwidth of B_e can be expressed as:

$$P = \int_{B_e} p(f) \cdot df = A \frac{P_s^2}{OSNR} + B \frac{P_s^2}{OSNR^2} + C P_s^2 \tag{6.4}$$

where A, B, and C coefficients are constants and can be obtained empirically. There are no frequency dependent parameters in (6.4), therefore the RF power in bandwidth B_e can be used to estimate the total RF power in the full signal frequency

range. Equation (6.4) shows that the detected RF noise power P is a function of both signal power P_S and $OSNR$. Consequently the OSNR can be evaluated by measuring the optical signal power P_S and RF power P using an RF power detector for the extracted PM segment. Our proposed technique has three advantages:

- Good immunity to the interference from the payload/label modulation. Because the PM segment is serial with the regular packet and is void of the high frequency data modulation components in the time slot of the PM segment;

- High sensitivity. Because a large chunk of noise spectrum about a few GHz can be integrated to provide reliable and repeatable measurements;

- In-band ASE noise measurement. It eliminates the extrapolation uncertainty using out-band approach, since the measured RF noise is right within the signal bandwidth.

6.2.2 Experimental Setup

Fig. 6.3 shows the experimental setup. The arrangement of payload/label is not important for this work. The optical packet is generated by a pattern generator and has a length of 1024 bits at 10 Gb/s with the 100 bits at the end set to all "1" as the PM segment. The transmitter starts from a 1545-nm laser source and an MZ modulator (MZ1). A second modulator (MZ2) is added to generate two dissimilar packets with different power levels. An EDFA follows the MZ2 and boosts the optical signal. The output signal from the transmitter is coupled with a second EDFA to emulate the link noise. The added ASE noise level is varied by adjusting the bias currents of the EDFA pump lasers. The optical signal contaminated with the noise passes through a 1-nm bandwidth optical filter and split into two branches for the OSNR measurements. One branch uses an optical spectrum analyzer (OSA) as reference and the other branch has the proposed OSNR monitor. Inside the OSNR monitor, the PM segment is firstly extracted out by using a modulator MZ3. It is then received by a 10-GHz bandwidth photodiode, and amplified with a 6~12-GHz bandpass RF amplifier. The output from the RF amplifier is then fed into a crystal

detector (CD, Agilent 8473C) for RF power detection. The CD will output negative voltages proportional to the input RF power level. A high speed oscilloscope is used to record the traces of the packets. An Anritsu 10-Gb/s pattern generator is used to drive the MZ1 while two signal generators are used to drive the MZ2 and MZ3. The oscilloscope and the two signal generators are synchronized to the pattern generator.
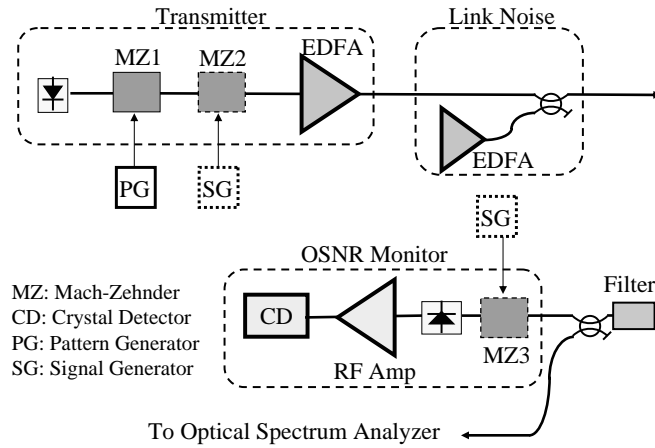
Figure 6.3: Experimental Setup.

6.2.3   Results and Discussions

To use (6.4) for OSNR monitoring, our first step is to calibrate A, B, C coefficients. We disable the driving signal to MZ2 for one uniform packet to provide a baseline for the calibration. The responsivity versus input optical power of the photodiode and the non-linear response of the CD are calibrated separately in the experiment. The RF amplifier operates in the linear range because of the relatively low output from the photodiode. The optical power into the photodiode is around -15 dBm and the output voltage of CD changes from -80 mV to -623 mV when OSNR varies. Fig. 6.4(a) shows the oscilloscope trace for the transmitted packets. Fig. 6.4(b) shows the extracted pulse after the MZ3, and Fig. 6.4(c) shows the output pulse of the CD. The pulse is relatively noisy due to the leakage of the high frequency components from its input. However, after we use a 100-MHz filter, the output is smoothed as shown in Fig. 6.4(d), which improves the noise measurement accuracy. We also note the oscilloscope traces in Fig. 6.4 are trace measurement without averaging. The

repeatable values of the CD voltages for consecutive packets in Fig. 6.4(d) show the reliability of the OSNR monitor.
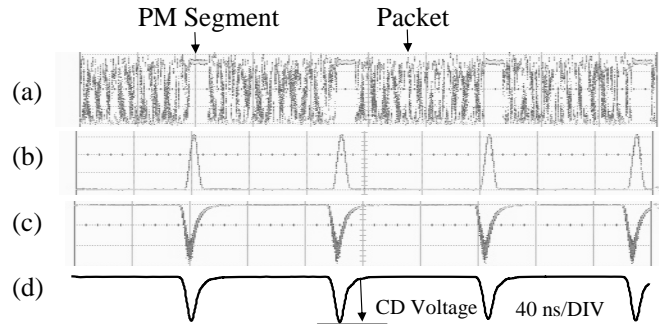
Figure 6.4: Oscilloscope traces for (a) the original packets, (b) the extracted performance monitoring pulse, (c) the output from the crystal detector, (d) the smoothed output of the crystal detector with a 100-MHz filter.
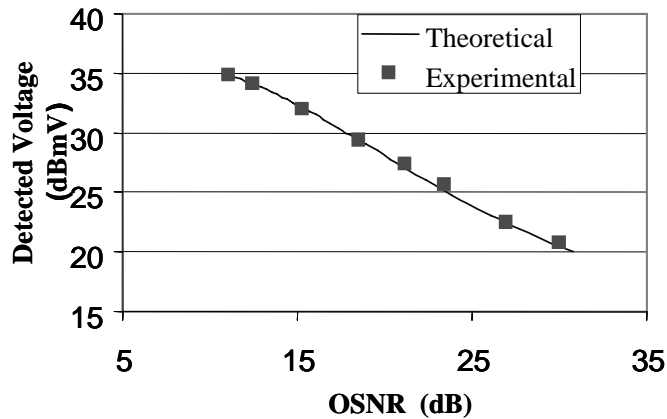
Figure 6.5: The voltage output of the crystal detector as a function of the OSNR. The OSNR is measured by an OSA.

Equation (6.4) shows that the measured RF power P is a second-order function of the reciprocal of OSNR. We perform a second-order fit of the CD voltage as a function of the reciprocal of OSNR. The theoretical curve fit is also shown in Fig. 6.5. The A, B, and C coefficients in (6.4) are calculated through a second-order curve fit. The maximum error of the measurement data points of 10 dB to 30 dB OSNR from the curve fit is 0.6 dB.

Finally we use the OSNR monitor for consecutive optical packets with varying

OSNR. MZ2 in Fig. 6.3 is driven to generate two optical signal levels. Two dissimilar packets with different OSNR are then obtained after the EDFA. The power level P_S and noise level P at the output of the crystal detector are recorded for both packets, and (6.4) is used to calculate the OSNR. To obtain the reference OSNR from OSA, we measure both the optical signal powers and ASE noise levels of the two dissimilar packets from OSA. Fig. 6.6 shows the OSNR monitoring errors as we vary the OSNR for both packets. The plot includes the data points for both packets. The inset of Fig. 6.6 shows the oscilloscope trace for two consecutive packets with different OSNR and crystal detector output. The crystal detector output pulses clearly demonstrate the real time noise measurement. The maximum OSNR measurement error is found to be 0.6 dB. The error may come from the imperfect non-linearity calibration for the crystal detector.
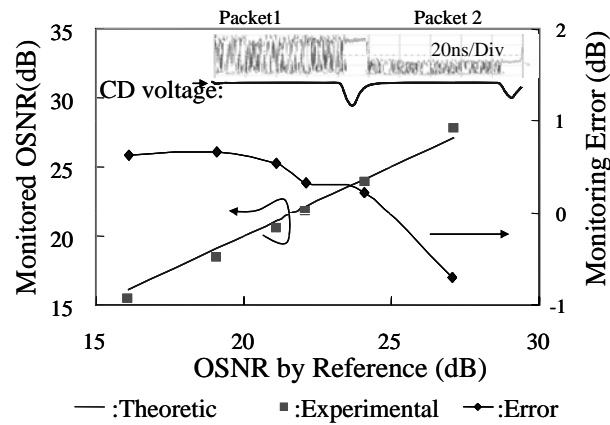
Figure 6.6: OSNR monitoring for packets with different OSNR.

The ∼10 ns of time duration of the PM segment in this experiment may be a large overhead for high speed transmission and therefore, may not be feasible for every packet. However, there may be a need to monitor the OSNR on the time scale of one packet duration, such as 10 ns for 100 bit length at 10 Gb/s. Intuitively, the PM packet may be best used when an optical packet path is being set up for the incoming packets originated from diverse sources. The computation complexity after detection is moderate to solve the quadratic equation derived from (6.4). Therefore the ∼10 ns time duration is dependent on the response time of the Agilent crystal

detector in our experiment. However, it is possible to choose an RF power detector with faster response. This will shorten the time duration further.

The OSNR monitor can be further simplified by replacing the MZ3 and crystal detector in Fig. 6.3 with ADC and DSP. In this case, the PM segment can be located and extracted out by the DSP. Subsequently, the RF noise power can be calculated. It is expected that the bandwidth/speed of ADC and DSP will determine the minimum duration of the PM segment for a sufficient accurate OSNR measurement. This simplification using electronic components holds the potential to be more cost effective.

6.3   Chromatic Dispersion Monitoring in Electronic Dispersion Compensation Receivers

Recently, advances of microelectronics have enabled electronic compensation of optical distortions. Electronic dispersion compensation (EDC) has drawn considerable research interests to mitigate optical CD distortions [58, 62, 56]. There are various approaches in the literature, from simple to sophisticated. The performance is generally dependent on the cost and complexity. Among the approaches, the most promising receiver based equalizers include feed-forward equalizers (FFE) and decision feedback equalizers (DFE) because of their relatively simple structures. In fact, FFE/DFE based products have been tested for emerging telecommunication standards [55]. We anticipate electronic equalizers will be prevalent in optical fiber networks. On the other hand, there is a strong need for optical performance monitoring in terms of efficient network monitoring and maintenance. CD is one of the important parameters to monitor. Among the existing CD monitoring techniques [73, 74, 75], most of them need additional hardware to realize CD monitoring. An inherent nature of electronic compensation is that optical distortions are down-converted to the electrical domain. When the electronic compensation receiver compensates the optical distortion, it also reflects the strength of optical distortion. Therefore, we propose a CD monitoring technique by analyzing the tap coefficients

of tapped delay lines, which are generally used in FFE and DFE. This technique does not require additional hardware in EDC receivers using tapped delay lines.

6.3.1   Principle of the Proposed CD Monitoring

Fig. 6.7(a) shows the principle for CD monitoring in EDC receivers. The optical data signal is distorted by CD in transmission fiber. The distortion spreads the power of one bit to adjacent bits, resulting in the ISI between neighboring bits. After O/E conversion, an electronic equalizer, in particular FFE, recovers the distorted signal. In such an equalizer, the current value, pre- and post-cursors of the received signal are linearly weighted by the tap coefficients and summed to produce the output. As a result, the tap coefficients are strongly determined by ISI effects. Hence, the information of ISI effects or CD can be extracted by analyzing the tap coefficients and CD monitoring is realized without additional hardware, or additional cost. This monitoring scheme can achieve a fast response through adaptive algorithms, which can be in the order of microsecond [11]. The proposed technique can also be extended to other equalizers using tapped delay lines, such as DFE and FFE+DFE.
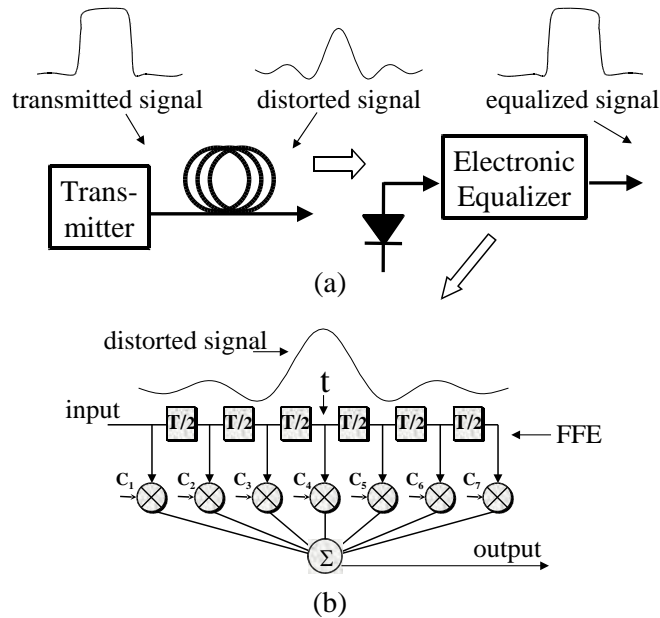

Figure 6.7: (a) Principle of CD monitoring in EDC receivers; (b) Definition of ISI factor in this work.

In this work, the FFE has 7 taps with half-bit delay (half-spaced) as shown in Fig.

6.7(b). The tap coefficients are $C_1, C_2, \ldots, C_7$. The C_4 corresponds to the current bit at t moment. We align the C_4 to the center of eye diagram or optimal sampling phase. We can plot $C_1, C_2, \ldots, C_7$ in order, called tap shape. In this arrangement, the tap shape is symmetrical around C_4 in theory. From the equalization principle, C_n represents the ISI component from the bit at $t - nT/2$. If we consider CD distortion producing ISI within a delay of one bit period, which corresponds to C_2 and C_6 in Fig. 6.7(b), we can define an ISI factor f_{ISI} as:

$$f_{ISI} = k(C_2 + C_6)/C_4 \tag{6.5}$$

where k is calibration parameter decided by the difference between simulation and experiment. Equation (6.5) includes the one-bit ISI components from pre- and post-bit. It is possible to use only pre (C_2) or post-bit (C_6) for ISI factor calculation. However, the inclusion of pre- and post-cursors together increases the tolerance of the sampling phase shift. By normalized to C_4, the ISI factor is independent of the input signal and noise powers, which also correspond to different OSNR values.

6.3.2 Simulation and Experimental Setup

In this work, we construct linear CD transmission systems to verify the monitoring scheme in simulation and experiment, respectively. Fig. 6.8(a) shows the simulation setup. The transmitter consists of 10 Gb/s NRZ-ASK modulation with 2^7 pseudo-random binary sequence (PRBS). Using short PRBS sequence can accelerate the simulation speed and 2^7 is enough to cover all the patter effects from CD since the maximum CD value in this work is below 3000 ps/nm. A CD emulator generates variable CD. The distorted signal is combined with ASE noise and passes a 40-GHz bandwidth optical filter. The ASE noise is simulated by white complex Gaussian noise. The O/E conversion is simulated by square-law detection. The following electrical filter is a 5th order Bessel low pass filter (LPF) with 7 GHz bandwidth. The signal is then fed to the FFE, which adopts the least mean-square (LMS) algorithm to minimize the mean-square-error (MSE) [14, 136]. After the convergence of the LMS algorithm, the resultant tap coefficients are used to calculate the ISI factor by

(6.5). The ISI factor as a function of the CD is then investigated by changing the CD value.
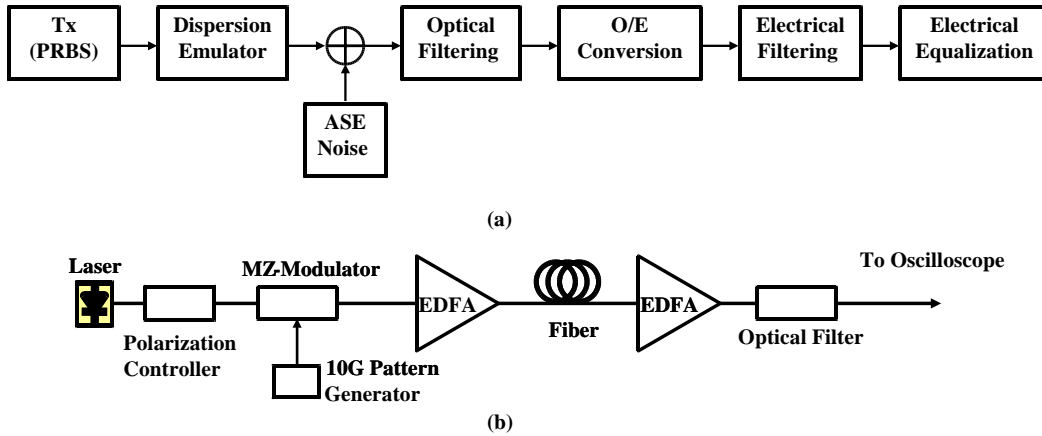
Figure 6.8: (a) Simulation setup; (b) Experimental setup.

Fig. 6.8(b) shows the experimental setup, which is similar to the simulation setup. The 10-Gb/s transmitter includes the laser source and external optical modulator. Standard single-mode fibers (SSMF) (D=17 ps/nm/km @ 1550 nm) of different length are used to achieve variable CD. The input power into the fibers is kept below 0 dBm to avoid any nonlinear effects. An EDFA is used to boost the optical power after the SSMF fibers. A high-speed oscilloscope is used to record the pattern traces, which are saved and loaded into a computer for signal processing. The traces are normalized to the average power of 1 level, which corresponds to the limiting amplification. The traces are then filtered by a 5th order Bessel low pass filter with 5 GHz bandwidth to match the signal format in simulation. The filtered traces are equalized by the FFE and the resultant tap coefficients are used to calculate the ISI factor by (6.5).

6.3.3   Results and Discussions

Fig. 6.9(a) and (b) shows some examples of tap shapes with different CD and OSNR. The tap coefficients are discrete values and the solid curves in Fig. 6.9(a) and (b) enable a clear comparison. As expected by the theory, the tap shapes change systematically with the CD. The OSNR also changes the tap shapes. For example,

C_4 at 2000 ps/nm changes from 1.3 to 1.7 when OSNR increases from 15 dB to 30 dB. However, Fig. 6.9(c) shows that the ISI factors change about 10% when OSNR varies from 10 dB to 30 dB, which is a small sensitivity to ASE noise.
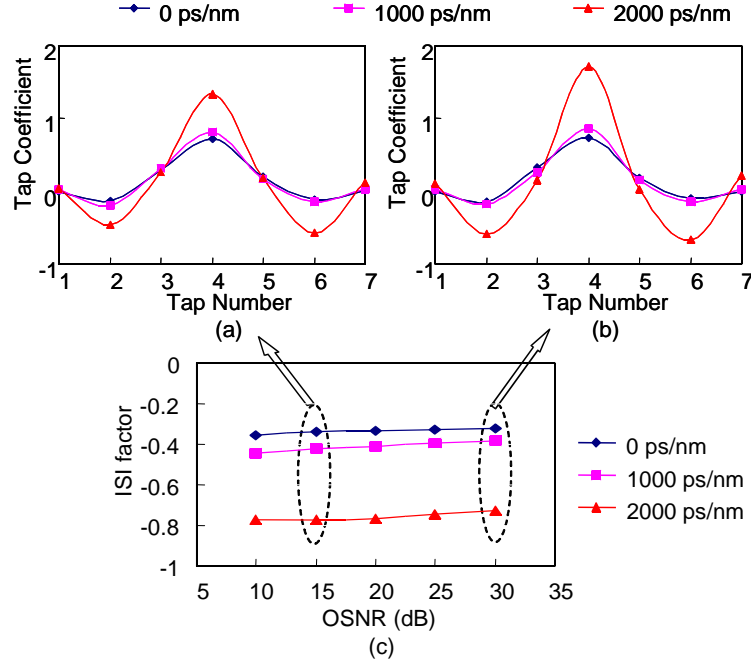
Figure 6.9: (a) The tap shapes when the OSNR is 15 dB, (b) when the OSNR is 30 dB, and (c) the ISI factors with different OSNR and CD.

The solid curve in Fig. 6.10 shows the ISI factor as a function of the CD, which is calculated in a CD range of $0 \sim 2400$ ps/nm with 200 ps/nm spacing. As the CD increases, the ISI factor decreases which means the ISI effects increasing. The ISI factor within 500 ps/nm CD remains almost unchanged because the ISI effects are week in such a dispersion range. However, the ISI factor shows a strong correlation to CD in the range of $500 \sim 2000$ ps/nm. After the 2200 ps/nm CD, the ISI factor increases again, which causes ambiguity for CD monitoring. The main reason is that the strong CD spreads the power of the bits far away to adjacent bits. This phenomenon is not included in (6.5). In addition, it is possible to use a more complicated expression in (6.5) to cover a wider CD range.

Finally, we verify the monitoring scheme by the experiment. We record the data sequence from the high-speed scope for different CD values by changing the length of SSMF fiber. The traces are loaded into a computer and equalized by the FFE with
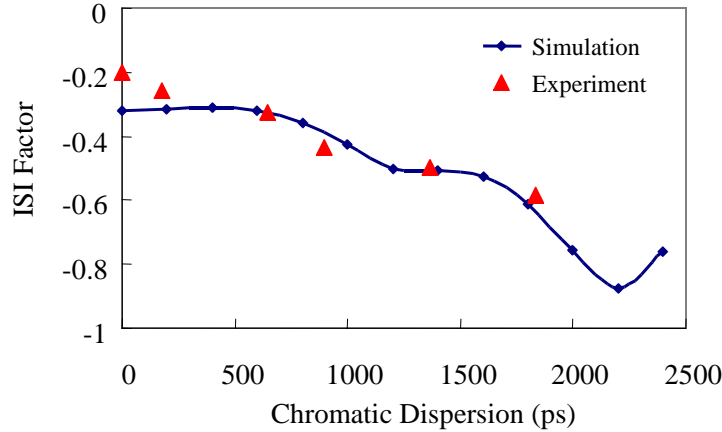
Figure 6.10: Simulation and experimental results of CD monitoring.

LMS algorithm. The resultant tap coefficients are used to calculate the ISI factor by (6.5). The calibration parameter k in (6.5) is set to be 0.7. The ISI factor is then used to predict the CD according to the functional relationship acquired from simulation. As shown in Fig. 6.10, the experimental monitoring results generally agree with the simulation in the range of $500 \sim 2000$ ps/nm, which is most interesting in the applications of the proposed new telecommunication standards [55]. The maximal monitoring error occurs at 900 ps/nm CD with a difference of about 150 ps/nm.

The ISI factor is determined not only by the CD distortion but also the signal format, OSNR, electrical bandwidth, polarization mode dispersion (PMD) and non-linearity. Hence, further improvement of CD monitoring to the proposed technique may include more calibrations, as well as a more comprehensive expression to replace (6.5), or multiple receiver ISI factors for multi-parameter monitoring. However, the relative CD monitoring we have proposed is simpler and more practical.

6.4 Conclusions

Optical performance monitoring is increasingly important for any practical deployment of optical fiber networks. In this chapter, we have presented two optical performance monitoring techniques for optical fiber networks.

In Section 6.2, we have propose an OSNR monitor suitable for OPSN. By measuring the RF noise from optical packets with a special performance monitoring

segment, the OSNR monitoring error is found to be less than 0.6 dB for consecutive packets with varying OSNR of 16 dB to 27 dB. The response time of the OSNR monitor can be around 10 ns.

In Section 6.3, we have proposed a CD monitoring technique for EDC receivers, which requires no additional hardware. By analyzing the tap coefficients in electronic dispersion equalizers using tapped delay lines, we have defined an ISI factor to monitor the CD. This technique has been verified by simulation and experiment.

Chapter 7

Conclusions

7.1 Summary of the Work

In the thesis, we have made contributions in three areas in optical fiber networks. We have shown the advantages of signal processing of optical phase. We summarize our work as follows.

7.1.1 All-Optical Label Swapping Using Synchronous Phase Modulation

All-optical label swapping (AOLS) is one of the most important techniques in optical packet switched networks (OPSN). By exploiting the unique symmetry of DPSK coding, we have proposed an AOLS technique using synchronous phase modulation. We have then investigated this technique in detail, and found the following results.

- For the first time, optical label erasure and insertion are performed in a single step by a phase modulator without wavelength conversion. The power penalty of label swapping is found to be as small as 0.2 dB.

- We investigate the polarization sensitivity of all-optical label swapping for the first time. The polarization insensitivity of power penalty for the label swapping is found to be less than 0.3 dB and 0.5 dB for the packet label and payload, respectively.

- We emulate cascaded all-optical label swapping in a re-circulating loop to investigate the power penalties from the accumulated phase errors and the timing mismatch between the incoming label and the new label. The power

penalty is less than 1 dB at 10^{-7} BER after 5 hops. The experimental power penalty is below 1 dB for a timing mismatch within 20% of one bit period.

7.1.2 Phase Estimation for Coherent Optical OFDM

Phase estimation is one of the enabling functionalities in coherent optical orthogonal frequency division multiplexing (CO-OFDM) systems. Phase estimation realizes coherent detection without conventional phase-locked loop. We have presented phase estimation theories for CO-OFDM and applied phase estimation to two long-haul CO-OFDM transmission experiments. The main results are below:

- For the first time, we discuss and apply experimentally pilot-aided phase estimation theory of OFDM to optical fiber transmissions. We find that the system performance can be improved over 0.5 dB in comparison with data-aided phase estimation.

- We study the optimum number of pilot subcarriers and find as few as 5 subcarriers are sufficient for digital phase estimation to realize coherent detection.

- We report the first experimental demonstration of coherent optical OFDM transmission at a bit rate of 8 Gb/s. The power penalty is less than 1 dB at 10^{-3} BER after 1000 km transmission. Our work serves to substantiate the suitability of coherent optical OFDM for optical transmission without a need for optical compensation of CD and polarization mode dispersion.

- We demonstrate the PMD tolerance of CO-OFDM at 10 Gb/s. The OSNR penalty is about 2 dB for the transmission after a 340 ps PMD emulator and 1000 km SSMF without any optical CD and PMD compensation.

7.1.3 Optical Performance Monitoring in Optical Fiber Networks

Optical performance monitoring has become not only beneficial but also essential for optical fiber networks. Hence, we have proposed an OSNR monitor for OPSN,

which is capable of measuring the varying OSNR of consecutive optical packets. We have also proposed a CD monitoring technique in electronic dispersion receiver. The main results are below:

- We have proposed an OSNR monitor capable of direct OSNR monitoring based on radio RF noise measurement. By measuring the RF noise from optical packets with a special performance monitoring segment, the OSNR monitoring error is found to be less than 0.6 dB for consecutive packets with varying OSNR of 16 dB to 27 dB. The response time of the OSNR monitor can be about 10 ns.

- We have proposed a CD monitoring technique for electronic dispersion compensation (EDC) receivers, which requires no additional hardware. By analyzing the tap coefficients in electronic dispersion equalizers using tapped delay lines, we have defined an ISI factor to monitor the CD. This technique has been verified by simulation and experiment.

7.2   Future Work

In the proposed AOLS scheme in the first part work, we have used phase modulators for phase modulation. However, it has been shown that an intensity modulator biased at null point is better for DPSK coding [89]. Therefore it is of interest to use the intensity modulator for the AOLS scheme and find which modulator is better in multi-hop transmissions.

In the second part work, the performance of phase estimation and compensation is strongly determined by the phase noise characteristics of the transmitter and receiver laser. A close equation may be formed. In addition, there are several different coherent receiver structure, such as homodyne detection. A comparison study is needed to find their pros and cons with respect to phase estimation and compensation. In addition, a more efficient algorithm is important due to the high-speed context of optical fiber networks, where memory space and operation time are demanding.

In the third part work, the OSNR monitor might be expensive due to the per-

formance monitoring segment extractor. Therefore, it will be cost-effective if the extractor can be saved. The concept of chromatic dispersion monitoring in EDC receiver can be extended to various EDC techniques. This extension may lead to more interesting results and applications.

Bibliography

[1] G. P. Agrawal, *Fiber-Optic Communication Systems*, 3rd ed. New York: John Wiley & Sons, 2002.

[2] A. Sano, H. Masuda, Y. Kisaka, S. Aisawa, E. Yoshida, Y. Miyamoto, M. Koga, K. Hagimoto, T. Yamada, T. Furuta, and H. Fukuyama, "14-Tb/s (140 x 111-Gb/s PDM/WDM) CSRZ-DQPSK transmission over 160 km using 7-THz bandwidth extended L-band EDFAs," in *Europ. Conf. Optical Commun. (ECOC)*, vol. 6, Sept. 2006, Th4.1.1, pp. 1–2.

[3] P. J. Winzer, G. Raybon, C. R. Doerr, L. L. Buhl, T. Kawanishi, T. Sakamoto, M. Izutsu, and K. Higuma, "2000-km WDM transmission of 10 x 107-Gb/s RZ-DQPSK," in *Europ. Conf. Optical Commun. (ECOC)*, vol. 6, Sept. 2006, Th4.1.3, pp. 5–6.

[4] T. Okoshi and K. Kikuchi, *Coherent Optical Fiber Communications*. Boston: Kluwer Academic Publishers, 1988.

[5] D. J. Blumenthal, B. E. Olsson, G. Rossi, T. E. Dimmick, L. Rau, M. Masanovic, O. Lavrova, R. Doshi, O. Jerphagnon, J. E. Bowers, V. Kaman, L. A. Coldren, and J. Barton, "All-optical label swapping networks and technologies," *J. Lightwave Technol.*, vol. 18, no. 12, pp. 2058–2075, Dec. 2000.

[6] C. Qiao, "Labeled optical burst switching for IP-over-WDM integration," *IEEE Trans. Commun.*, vol. 38, no. 9, pp. 104–114, Sept. 2000.

[7] E. N. Lallas, N. Skarmoutsos, and D. Syvridis, "An optical FSK-based label coding technique for the realization of the all-optical label swapping," *IEEE Photon. Technol. Lett.*, vol. 14, no. 10, pp. 1472–1474, Oct. 2002.

[8] D. J. Blumenthal, "Photonic packet and all-optical label switching technologies and techniques," in *Conf. Optical Fiber Communication (OFC)*, Mar. 2002, pp. 282–284.

[9] T. Koonen, G. Morthier, J. Jennen, H. de Waardt, and P. Demeester, "Optical packet routing in IP-over-WDM networks deploying two-level optical labeling," in *Europ. Conf. Optical Commun. (ECOC)*, vol. 4, Sept. 2001, pp. 608–609.

[10] H. Bülow, W. Baumert, F. Buchali, and W. Kuebart, "Adaption of an electronic PMD mitigator by maximization of the eye opening," in *Europ. Conf. Optical Commun. (ECOC)*, Sept. 2000, P3.10.

[11] F. Buchali and H. Bülow, "Adaptive PMD compensation by electrical and optical techniques," *J. Lightwave Technol.*, vol. 22, no. 4, pp. 1116–1126, April 2004.

[12] J. H. Winters, "Equalization in coherent lightwave systems using a fractionally spaced equalizer," *J. Lightwave Technol.*, vol. 8, no. 10, pp. 1487–1491, Oct. 1990.

[13] M. Sieben, J. Conradi, and D. E. Dodds, "Optical single sideband transmission at 10 Gb/s using only electrical dispersion compensation," *J. Lightwave Technol.*, vol. 17, no. 10, pp. 1742–1749, Oct. 1999.

[14] T. S. Rappaport, *Wireless Communications: Principles and Practice*, 2nd ed. N. J.: Prentice Hall, 2002.

[15] V. Eramo and M. Listanti, "Packet loss in a bufferless optical WDM switch employing shared tunable wavelength converters," *J. Lightwave Technol.*, vol. 18, no. 12, pp. 1818–1833, 2000.

[16] A. G. Fayoumi, F. A. Al-Zahrani, A. A. Habiballa, and A. P. Jayasumana, "Performance analysis of multi-fiber synchronous photonic share-per-link packet switches," in *IEEE Conf. Local Computer Networks*, Nov. 2005, pp. 182–189.

[17] R. Ramaswami and K. N. Sivarajan, *Optical Networks: A Practical Perspective*, 2nd ed. San Francisco: Morgan Kaufmann Publishers, 2002.

[18] H. Rosenfeldt, "Deploying optical PMD compensators," in *Conf. Optical Fiber Communication (OFC)*, vol. 3, Mar. 2005, OWO1.

[19] A. Hidayat, A. F. Abas, D. Sandel, S. Bhandare, H. Zhang, F. Wust, B. Milivojevic, R. Noe, M. Lapointe, Y. Painchaud, and M. Guy, "5.94 Tb/s capacity of a multichannel tunable -700 to -1200 ps/nm dispersion compensator," in *Europ. Conf. Optical Commun. (ECOC)*, vol. 3, Sept. 2005, pp. 329–330.

[20] C. Francia, F. Bruyère, J.-P. Tliékry, and D. Penninckx, "Simple dynamic polarisation mode dispersion compensator," *Electron. Lett.*, vol. 35, no. 5, pp. 414–415, Mar. 1999.

[21] S. Hara and R. Prasad, *Multicarrier Techniques for 4G Mobile Communications.* Boston: Artech House, 2003, Chapter 5.

[22] W. Shieh and C. Athaudage, "Coherent optical orthogonal frequency division multiplexing," *Electron. Lett.*, vol. 42, no. 10, pp. 587–589, May 2006.

[23] D. C. Kilper, R. Bach, D. J. Blumenthal, D. Einstein, T. Landolsi, L. Ostar, M. Preiss, and A. E. Willner, "Optical performance monitoring," *J. Lightwave Technol.*, vol. 22, no. 1, pp. 294–304, Jan. 2004.

[24] N. Ghani, S. Dlxit, and T. S. Wang, "On IP-over-WDM integration," *IEEE Communication Magazine*, vol. 38, no. 3, pp. 72–84, Mar. 2000.

[25] D. K. Hunter and I. Andonovic, "Approaches to optical internet packet switching," *IEEE Communication Magazine*, vol. 38, no. 9, pp. 116–122, Sept. 2000.

[26] L. Xu, H. G. Perros, and G. Rouskas, "Techniques for optical packet switching and optical burst switching," *IEEE Communication Magazine*, vol. 39, no. 1, pp. 131–142, Jan. 2001.

[27] A. Pattavina, "Architectures and performance of optical packet switching nodes for IP networks," *J. Lightwave Technol.*, vol. 22, no. 3, pp. 1023–1032, Mar. 2005.

[28] S. J. B. Yoo, "Optical packet and burst switching technologies for the future photonic internet," *J. Lightwave Technol.*, vol. 24, no. 12, pp. 4468–4492, Dec. 2006.

[29] S. Keshav and R. Sharma, "Issues and trends in router design," *IEEE Communication Magazine*, vol. 36, no. 5, pp. 144–151, May 1998.

[30] D. J. Blumenthal, J. E. Bowers, L. Rau, C. Hsu-Feng, S. Rangarajan, W. Wei, and K. N. Poulsen, "Optical signal processing for optical packet switching networks," *IEEE Communication Magazine*, vol. 41, no. 2, pp. s23–s29, Feb. 2003.

[31] W. Hung, C. K. Chan, L. K. Chen, and F. Tong, "A bit-serial optical packet label-swapping scheme using DPSK encoded labels," *IEEE Photon. Technol. Lett.*, vol. 15, no. 11, pp. 1630–1632, 2003.

[32] T. Fjelde, A. Kloch, D. Wolfson, B. Dagens, A. Coquelin, I. Guillemot, F. Gaborit, F. Poingt, and M. Renaud, "Novel scheme for simple label-swapping employing XOR logic in an integrated interferometric wavelength converter," *IEEE Photon. Technol. Lett.*, vol. 13, no. 7, pp. 750–752, July 2001.

[33] N. Chi, J. Zhang, P. V. Holm-Nielsen, C. Peucheret, and P. Jeppesen, "Transmission and transparent wavelength conversion of an optically labeled signal using ASK/DPSK orthogonal modulation," *IEEE Photon. Technol. Lett.*, vol. 15, no. 5, pp. 760–762, May 2003.

[34] C. W. Chow and H. K. Tsang, "Orthogonal label switching using polarization-shift-keying payload and amplitude-shift-keying label," *IEEE Photon. Technol. Lett.*, vol. 17, no. 11, pp. 2475–2477, Nov. 2005.

[35] A. Carena, M. D. Vaughn, R. Gaudino, M. Shell, and D. J. Blumenthal, "OPERA: an optical packet experimental routing architecture with label swap-

ping capability," *J. Lightwave Technol.*, vol. 16, no. 12, pp. 2135–2145, Dec. 1998.

[36] K. V. Shrikhande, I. M. White, M. S. Rogge, F.-T. An, A. Srivatsa, E. S. Hu, S. S.-H. Yam, and L. G. Kazovsky, "Performance demonstration of a fast-tunable transmitter and burst-mode packet receiver for HORNET," in *Conf. Optical Fiber Communication (OFC)*, vol. 4, Feb. 2001, ThG2.

[37] H. Sotobayashi, W. Chujo, and K. Kitayama, "Photonic gateway: Multiplexing format conversions of OCDM-to-WDM and WDM-to-OCDM at 40 Gbit/s (4 x10 Gbit/s)," *J. Lightwave Technol.*, vol. 20, no. 12, pp. 2022–2028, Dec. 2002.

[38] Y. G. Wen, Y. Zhang, and L. K. Chen, "On architecture and limitations of optical multiprotocol label switching (MPLS) networks using optical-orthogonal-code (OCC)/wavelength label," *Optical Fiber Technology*, vol. 8, no. 1, pp. 43–70, Jan. 2002.

[39] A. Chowdhury, J. Yu, and G. K. Chang, "Cascaded operation of optical label swapping using optical carrier suppression, separation and without regular wavelength converter in a multi-hop label switched optical network," in *Europ. Conf. Optical Commun. (ECOC)*, vol. 4, Sept. 2005, pp. 961–962.

[40] N. Deng, Y. Yang, C. K. Chan, W. Hung, and L. K. Chen, "Intensity-modulated labeling and all-optical label swapping on angle-modulated optical packets," *IEEE Photon. Technol. Lett.*, vol. 16, no. 4, pp. 1218–1220, April 2004.

[41] R. Gaudino and D. J. Blumenthal, "A novel transmitter architecture for combined baseband data and subcarrier-multiplexed control links using differential Mach-Zehnder external modulators," *IEEE Photon. Technol. Lett.*, vol. 9, no. 10, pp. 1397–1399, Oct. 1997.

[42] B. Meagher, G. K. Chang, G. Ellinas, Y. M. Lin, W. Xin, T. F. Chen, X. Yang, A. Chowdhury, J. Young, S. J. Yoo, C. Lee, M. Z. Iqbal, T. Robe, H. Dai,

Y. Chen, and W. I. Way, "Design and implementation of ultra-low latency optical label switching for packet-switched WDM networks," *J. Lightwave Technol.*, vol. 18, no. 12, pp. 1978–1987, Dec. 2000.

[43] H. Lee, V. Hernandez, V. K. Tsui, and S. J. B. Yoo, "Simple, polarization independent, and dispersion-insensitive SCM signal extraction technique for optical switching systems applications," *Electron. Lett.*, vol. 37, no. 20, pp. 1240–1241, Sept. 2001.

[44] Y. M. Lin, M. C. Yuang, S. L. Lee, and W. I. Way, "A superimposed ASK label in a 10 Gbps multi-hop all-optical label swapping system," in *Conf. Optical Fiber Communication (OFC)*, vol. 1, Feb. 2004, pp. 23–27.

[45] H. C. Ji, J. H. Lee, and Y. C. Chung, "Evaluation on system outage probability due to temperature variation and statistically distributed chromatic dispersion of optical fiber," *J. Lightwave Technol.*, vol. 22, no. 8, pp. 1893–1898, Aug. 2004.

[46] H. Bülow, W. Baumert, H. Schmuck, F. Mohr, T. Schulz, F. Kuppers, and M. Weiershausen, "Measurement of the maximum speed of PMD fluctuation in installed field fiber," in *Conf. Optical Fiber Communication (OFC)*, vol. 2, Feb. 1999, P3.10, pp. 83–85.

[47] R. Lachance, S. Lelievre, and Y. Painchaud, "50 and 100 GHz multichannel tunable chromatic dispersion slope compensator," in *Conf. Optical Fiber Communication (OFC)*, vol. 1, Mar. 2003, pp. 164–165.

[48] D. Stahl, P. J. Winzer, C. R. Doerr, and S. Chandrasekhar, "Extending the chromatic dispersion tolerance by optical equalization at 43 Gb/s," in *Conf. Optical Fiber Communication (OFC)*, vol. 2, Feb. 2004, ThU5, pp. 3–5.

[49] C. R. Doerr, "Optical compensation of system impairments," in *Conf. Optical Fiber Communication (OFC)*, Mar. 2006, OThL1.

[50] C. R. Doerr, S. Chandrasekhar, P. J. Winzer, A. R. Chraplyvy, A. H. Gnauck, L. W. Stulz, R. Pafchek, and E. Burrows, "Simple multichannel optical equal-

izer mitigating intersymbol interference for 40-Gb/s nonreturn-to-zero signals," *J. Lightwave Technol.*, vol. 22, no. 1, pp. 249–256, Jan. 2004.

[51] J. H. Winters and R. D. Gitlin, "Electrical signal processing techniques in long-haul fiber-optic systems," *IEEE Trans. Commun.*, vol. 38, no. 9, pp. 1439–1453, Sept. 1990.

[52] C. K. Madsen, G. Lenz, A. J. Bruce, M. A. Cappuzzo, L. T. Gomez, and R. E. Scotti, "Integrated all-pass filters for tunable dispersion and dispersion slope compensation," *IEEE Photon. Technol. Lett.*, vol. 11, no. 12, pp. 1623–1625, Dec. 1999.

[53] H. Tsuda, H. T. A. Hirano, T. Kurokawa, and K. Okamoto, "Performance analysis of a dispersion compensator using arrayed-waveguide gratings," *J. Lightwave Technol.*, vol. 18, no. 8, pp. 1139–1147, Aug. 2000.

[54] H. Bülow, "Electronic equalization of transmission impairments," in *Conf. Optical Fiber Communication (OFC)*, Mar. 2002, TuE4.

[55] A. Ghiasi, A. Momtaz, A. Dastur, F. Chang, G. Noh, B. Gomatam, E. Ibragimov, A. Shanbhag, O. Schreiber, E. Su, K. Conroy, R. Jambunathan, and J. Wood, "Experimental results of EDC based receivers for 2400 ps/nm at 10.7 Gb/s for emerging telecom standards," in *Conf. Optical Fiber Communication (OFC)*, Mar. 2006, OTuE3.

[56] A. Faerbert, "Application of digital equalization in optical transmission systems," in *Conf. Optical Fiber Communication (OFC)*, Mar. 2006, OTuE5.

[57] D. McGhan, C. Laperle, A. Savchenko, C. Li, and G. M. A. M. O'Sullivan, "5120-km RZ-DPSK transmission over G.652 fiber at 10 Gb/s without optical dispersion compensation," *IEEE Photon. Technol. Lett.*, vol. 18, no. 2, pp. 400–402, Jan. 2006.

[58] N. Kikuchi, K. Mandai, S. Sasaki, and K. Sekine, "Proposal and first experimental demonstration of digital incoherent optical field detector for chromatic

dispersion compensation," in *Europ. Conf. Optical Commun. (ECOC)*, vol. 6, Sept. 2006, Th4.4.4, pp. 47–48.

[59] X. Yi, W. Chen, and W. Shieh, "Optical signal-to-noise ratio monitoring for optical packet switched networks," in *Europ. Conf. Optical Commun. (ECOC)*, vol. 3, Sept. 2005, pp. 731–732.

[60] X. Yi, F. Buchali, W. Chen, and W. Shieh, "Chromatic dispersion monitoring in electronic dispersion equalizers using tapped delay lines," *Optics Express*, vol. 15, no. 2, pp. 312–315, Jan. 2007.

[61] W. Shieh, R. S. Tucker, W. Chen, and X. Yi, "Optical performance monitoring through channel estimation by receiver signal processing," in *Europ. Conf. Optical Commun. (ECOC)*, Sept. 2006, We3.P.104.

[62] U. V. Koc, K.-Y. Tu, and N. Kaneda, "Adaptive electronic equalization using higher-order statistics for PMD compensation in long-haul fiber-optic system," in *Europ. Conf. Optical Commun. (ECOC)*, vol. 3, Sept. 2002, pp. 1–2.

[63] K. Roberts, C. Li, L. Strawczynski, M. O'Sullivan, and I. Hardcastle, "Electronic precompensation of optical nonlinearity," *IEEE Photon. Technol. Lett.*, vol. 18, no. 2, pp. 403–405, Jan. 2006.

[64] M. G. Taylor, "Accurate digital phase estimation process for coherent detection using a parallel digital processor," in *Europ. Conf. Optical Commun. (ECOC)*, vol. 2, Sept. 2005, pp. 263–264.

[65] D. S. Ly-Gagnon, K. Katoh, and K. Kikuchi, "Unrepeated 210-km transmission with coherent detection and digital signal processing of 20-Gb/s QPSK signal," in *Conf. Optical Fiber Communication (OFC)*, vol. 2, Mar. 2005, pp. 3–5.

[66] S. J. Savory, A. D. Stewart, S. Wood, G. Gavioli, M. G. Taylor, R. I. Killey, and P. Bayvel, "Digital equalisation of 40 Gbit/s per wavelength transmission over 2480km of standard fibre without optical dispersion compensation," in *Europ. Conf. Optical Commun. (ECOC)*, Sept. 2006, Th2.5.5.

[67] S. Ryu, *Coherent Lightwave Communication Systems.* Boston: Artech House, 1995.

[68] B. Spinnler, P. M. Krummrich, and E.-D. Schmidt, "Chromatic dispersion tolerance of coherent optical communications systems with electrical equalization," in *Conf. Optical Fiber Communication (OFC)*, Mar. 2006, OWB2.

[69] T. Sasaki, T. Komiya, Y. Fujimura, M. Saito, S. Semura, and M. Nishimura, "Multi-channel power level monitor with upward-reflector and sensor-array integrated in planar lightwave circuit," in *Conf. Optical Fiber Communication (OFC)*, vol. 3, Mar. 2001, pp. WB–1–WB6–3.

[70] Y. Liu, C. W. Chow, W. Y. Cheung, and H. K. Tsang, "In-line channel power monitor based on helium ion implantation in silicon-on-insulator waveguides," *IEEE Photon. Technol. Lett.*, vol. 18, no. 17, pp. 1882–184, Mar. 2006.

[71] J. H. Lee and Y. C. Chung, "Improved OSNR monitoring technique based on polarization-nulling method," *Electron. Lett.*, vol. 37, no. 15, pp. 972–973, July 2001.

[72] W. Chen, R. S. Tucker, X. Yi, W. Shieh, and J. S. Evans, "Optical signal-to-noise ratio monitoring using uncorrelated beat noise," *IEEE Photon. Technol. Lett.*, vol. 17, no. 11, pp. 2484–2486, Nov. 2005.

[73] L. Meflah, B. Thomsen, J. Mitchell, and P. Bayvel, "Chromatic dispersion monitoring of a multi-channel 40 Gbit/s system for dynamically reconfigurable networks," in *Europ. Conf. Optical Commun. (ECOC)*, vol. 4, Sept. 2005, pp. 935–936.

[74] A. Liu, G. J. Pendock, and R. S. Tucker, "Chromatic dispersion monitoring using time-multiplexed in-band RF tones," in *Conf. Optical Fiber Communication (OFC)*, Mar. 2005, paper OThH6.

[75] Q. Yu, Z. Pan, L. S. Yan, and A. E. Willner, "Chromatic dispersion monitoring technique using sideband optical filtering and clock phase-shift detection," *J. Lightwave Technol.*, vol. 20, no. 12, pp. 2267–2271, Dec. 2002.

[76] I. Shake, H. Takara, and S. Kawanishi, "Simple Q factor monitoring for BER estimation using opened eye diagrams captured by high-speed asynchronous electrooptical sampling," *IEEE Photon. Technol. Lett.*, vol. 15, no. 4, pp. 620–622, April 2003.

[77] D. C. Kilper, A. Azarov, W. Weingartner, and P. Vorreau, "Q-factor monitoring for fault management applications," in *Conf. Optical Fiber Communication (OFC)*, vol. 2, Feb. 2004.

[78] Z. Li and G. Li, "Chromatic dispersion and polarization-mode dispersion monitoring for RZ-DPSK signals based on asynchronous amplitudehistogram evaluation," *J. Lightwave Technol.*, vol. 24, no. 7, pp. 2589–2866, July 2004.

[79] S. M. R. M. Nezam, Y.-W. Song, C. Yu, J. E. McGeehan, A. B. Sahin, and A. E. Willner, "First-order PMD monitoring for NRZ data using RF clock regeneration techniques," *J. Lightwave Technol.*, vol. 22, no. 4, pp. 1086–1093, April 2004.

[80] D. Derickson, Ed., *Fiber Optic Test and Measurement.* New Jersey: Prentice Hall PTR, Upper Saddle River, 1998.

[81] K. Asahi, M. Yamashita, T. Hosoi, K. Nakaya, C. Konishi, and S. Fujita, "Optical performance monitor built into EDFA repeaters for WDM networks," in *Conf. Optical Fiber Communication (OFC)*, Feb. 1998, pp. 318–319.

[82] H. Suzuki and N. Takachio, "Optical signal quality monitor built into WDM linear repeaters using semiconductor arrayed waveguide grating filter monolithically integrated with eight photodiodes," *Electron. Lett.*, vol. 35, no. 10, pp. 836–837, May 1999.

[83] M. Rasztovits, M. Danner, and W. R. J. Leeb, "Optical signal-to-noise ratio measurement in WDM networks using polarization extinction," in *Europ. Conf. Optical Commun. (ECOC)*, vol. 1, Spet. 1998, pp. 549–550.

[84] D. K. Jung, C. H. Kim, and Y. C. Chung, "OSNR monitoring technique using polarization-nulling method," in *Conf. Optical Fiber Communication (OFC)*, vol. 2, Mar. 2000, pp. 176–178.

[85] M. H. Cheung, L. K. Chen, and C. K. Chan, "A PMD-insensitive OSNR monitoring scheme based on polarization-nulling with off-center narrowband filtering," in *Conf. Optical Fiber Communication (OFC)*, Feb. 2004, paper FF2.

[86] G. Rossi, T. E. Dimmick, and D. J. Blumenthal, "Optical performance monitoring in reconfigurable WDM optical networks using subcarrier multiplexing," *J. Lightwave Technol.*, vol. 18, no. 12, pp. 1639–1648, Dec. 2000.

[87] B. Fu and R. Hui, "Fiber chromatic dispersion and polarization-mode dispersion monitoring using coherent detection," *IEEE Photon. Technol. Lett.*, vol. 17, no. 7, pp. 1561–1563, July 2005.

[88] W. I. Way, Y. M. Lin, and G. K. Chang, "A novel optical label swapping technique using erasable optical single-sideband subcarrier label," in *Conf. Optical Fiber Communication (OFC)*, vol. 2, Mar. 2000, pp. 59–61.

[89] A. H. Gnauck and P. J. Winzer, "Optical phase-shift-keyed transmission," *J. Lightwave Technol.*, vol. 23, no. 1, pp. 115–130, Jan. 2005.

[90] X. Liu, C. Xu, and X. Wei, "Nonlinear phase noise in pulse-overlapped transmission based on return-to-zero differential-phase-shift-keying," in *Europ. Conf. Optical Commun. (ECOC)*, vol. 4, Sept. 2002, pp. 1–2.

[91] A. H. Gnauck, G. Raybon, S. Chandrasekhar, J. Leuthold, C. Doerr, L. Stulz, A. Agarwal, S. Banerjee, D. Grosz, S. Hunsche, A. Kung, A. Marhelyuk, D. Maywar, M. Movassaghi, X. Liu, C. Xu, X. Wei, and D. M. Gill, "2.5 Tb/s (64×42.7 Gb/s) transmission over 4×100 km NZDSF using RZ-DPSK format and all-Raman-amplified spans," in *Conf. Optical Fiber Communication (OFC)*, Mar. 2002, FC2-1.

[92] J.-X. Cai, D. G. Foursa, C. R. Davidson, Y. Cai, G. Domagala, H. Li, L. Liu, W. W. Patterson, A. N. Pilipetskii, M. Nissov, and N. S. Bergano, "A DWDM demonstration of 3.73 Tb/s over 11,000 km using 373 RZ-DPSK channels at 10 Gb/s," in *Conf. Optical Fiber Communication (OFC)*, vol. 3, Mar. 2003, PD22.

[93] C. Rasmussen, T. Fjelde, J. Bennike, F. Liu, S. Dey, B. Mikkelsen, P. Mamyshev, P. Serbe, P. van der Wagt, Y. Akasaka, D. Harris, D. Gapontsev, V. Ivshin, and P. Reeves-Hall, "DWDM 40 G transmission over trans-pacific distance (10,000 km) using CSRZ-DPSK, enhanced FEC and all-Raman amplified 100 km ultrawave fiber spans," in *Conf. Optical Fiber Communication (OFC)*, vol. 3, Mar. 2003, PD18.

[94] W. Shieh, X. Yi, and A. V. Tran, "Label swapping for DPSK encoded labels without wavelength conversion," in *Conf. Optical Fiber Communication (OFC)*, vol. 2, Mar. 2005, pp. 43–45.

[95] N. E. Jolley, H. Kee, P. Pickard, J. Tang, and K. Cordina, "Generation and propagation of a 1550 nm 10 Gbit/s optical orthogonal frequency division multiplexed signal over 1000m of multimode fibre using a directly modulated DFB," in *Conf. Optical Fiber Communication (OFC)*, vol. 6, 2005, OFP3.

[96] A. J. Lowery, L. Du, and J. Armstrong, "Orthogonal frequency division multiplexing for adaptive dispersion compensation in long haul WDM systems," in *Conf. Optical Fiber Communication (OFC)*, Mar. 2006, PDP39.

[97] W. Shieh, W. Chen, and R. S. Tucker, "Polarization mode dispersion mitigation in coherent optical orthogonal frequency division multiplexed systems," *Electron. Lett.*, vol. 42, no. 17, pp. 996–997, Aug. 2006.

[98] E. Ciaramella, A. D'Errico, R. Proietti, and G. Contestabile, "WDM-POLSK transmission systems by using semiconductor optical amplifiers," *J. Lightwave Technol.*, vol. 24, no. 11, pp. 4039–4046, Nov. 2006.

[99] J. G. Proakis, *Digital Communications*, 4th ed. Boston: McGraw-Hill, 2000.

[100] K. Kikuchi, "Effect of 1/f-type FM noise on semiconductor-laser linewidth residual in high-power limit," *IEEE J. Quantum Electron.*, vol. 25, no. 4, pp. 684–688, April 1989.

[101] E. Ip, J. M. Kahn, D. Anthon, and J. Hutchins, "Linewidth measurements of MEMS-based tunable lasers for phase-locking applications," *IEEE Photon. Technol. Lett.*, vol. 17, no. 10, pp. 2029–2031, Oct. 2005.

[102] D. McGhan, "Electronic dispersion compensation," in *Conf. Optical Fiber Communication (OFC)*, Mar. 2006, OWK1.

[103] D. S. Ly-Gagnon, S. Tsukamoto, K. Katoh, and K. Kikuchi, "Coherent detection of optical quadrature phase-shift keying signals with carrier phase estimation," *J. Lightwave Technol.*, vol. 24, no. 1, pp. 12–21, Jan. 2006.

[104] E. Desurvire, *Erbium-Doped Fiber Amplifiers, Principles and Applications.* New York: John Wiley & Sons, Inc., 1994.

[105] C. D. Poole, R. W. Tkach, A. R. Chraplyvy, and D. A. Fishman, "Fading in lightwave systems due to polarization-mode dispersion," *IEEE Photon. Technol. Lett.*, vol. 3, no. 1, pp. 68–70, Jan. 1991.

[106] ITU, *ITU Recommendation G.691 (2003),p.12.*

[107] C. D. Poole and R. E. Wagner, "Phenomenological approach to polarisation dispersion in long single-mode fibres," *Electron. Lett.*, vol. 22, no. 19, pp. 1029–1030, Sept. 1986.

[108] N. S. Bergano and C. R. Davidson, "Circulating loop transmission experiments for the study of long-haul transmission systems using erbium-doped fiber amplifiers," *J. Lightwave Technol.*, vol. 13, no. 5, pp. 879–888, May 1995.

[109] N. Chi, J. Zhang, P. V. Holm-Nielsen, L. Xu, I. T. Monroy, C. Peucheret, K. Yvind, L. J. Christiansen, and P. Jeppesen, "Experimental demonstration of cascaded transmission and all-optical label swapping of orthogonal IM/FSK labelled signal," *Electron. Lett.*, vol. 39, no. 8, pp. 676–678, April 2003.

[110] X. Yi and W. Shieh, "Demonstration of polarization insensitivity for all-optical label swapping," in *The Fourth International Conference on Optical Internet (COIN)*, May 2005, pp. 175–177.

[111] M. Y. Jeon, Z. Pan, J. Cao, Y. Bansal, J. Taylor, Z. Wang, V. Akella, K. Okamoto, S. Kamei, J. Pan, and S. J. B. Yoo, "Demonstration of all-optical packet switching routers with optical label swapping and 2R regeneration for scalable optical label switching network applications," *J. Lightwave Technol.*, vol. 21, no. 11, pp. 2723–2733, Nov. 2003.

[112] X. Yi, W. Shieh, and A. V. Tran, "Multi-hop optical label swapping using synchronous phase modulation," in *Conf. Optical Fiber Communication (OFC)*, May 2006, JThB53.

[113] F. Halsall, *Data Communications, Computer Networks and Open Systems.* Addison-Wesley Publishing Company, (Chapter 3), 1995.

[114] G. T. Kanellos, L. Stampoulidis, N. Pleros, T. Houbavlis, D. Tsiokos, E. Kehayas, H. Avramopoulos, and G. Guekos, "Clock and data recovery circuit for 10-Gb/s asynchronous optical packets," *IEEE Photon. Technol. Lett.*, vol. 15, no. 11, pp. 1666–1668, Nov. 2003.

[115] C. Xu, L. Mollenauer, and L. Xiang, "Compensation of nonlinear self-phase modulation with phase modulators," *Electron. Lett.*, vol. 38, no. 24, pp. 1578–1579, Nov. 2002.

[116] K. Inoue, T. Hasegawa, K. Oda, and H. Toba, "Multichannel frequency conversion experiment using fibre four-wave mixing," *Electron. Lett.*, vol. 29, no. 19, pp. 1708–1710, Sept. 1993.

[117] L. H. Spiekman, M. R. Amersfoort, A. H. D. Vreede, F. P. G. M. V. Ham, A. Kuntze, J. W. Pedersen, P. Demeester, and M. K. Smit, "Design and realization of polarization independent phased array wavelength demultiplexers using different array orders for TE and TM," *J. Lightwave Technol.*, vol. 14, no. 6, pp. 991–995, June 1996.

[118] K. H. Chung and J. I. Shim, "A new polarization-insensitive 1.55-μm In-GaAs(P)InGaAsP multiquantum-well electroabsorption modulator using a strain-compensating layer," *IEEE J. Quantum Electron.*, vol. 35, no. 5, pp. 730–736, May 1999.

[119] X. Yi and W. Shieh, "On polarization sensitivity of all-optical label swapping using synchronous phase modulation," *IEEE Photon. Technol. Lett.*, vol. 18, no. 11, pp. 1210–1212, June 2006.

[120] X. Yi, W. Shieh, and A. V. Tran, "Cascadability study for optical label swapping using synchronous phase modulation," *IEEE Photon. Technol. Lett.*, vol. 18, no. 13, pp. 1445–1447, July 2006.

[121] A. J. McDonald, R. S. Fyath, and J. J. O'Reilly, "Influence of extinction ratio on performance of optical receivers incorporating laser preamplifiers," *Electron. Lett.*, vol. 25, no. 4, pp. 249–250, Feb. 1989.

[122] J. D. Downie, F. Annunziata, and J. Hurley, "Relative contributions to filter-induced Q penalty from eye closure and OSNR degradation," in *Conf. Optical Fiber Communication (OFC)*, Mar. 2003, ThT4.

[123] L. Hanzo and T. Keller, *OFDM and MC-CDMA: A Primer.* New York: John Wiley & Sons, 2006.

[124] X. Yi, W. Shieh, and Y. Tang, "Phase estimation for coherent optical OFDM," *IEEE Photon. Technol. Lett.*, vol. 19, no. 12, pp. 919–921, June 2007.

[125] W. Shieh, X. Yi, and Y. Tang, "Experimental demonstration of transmission of coherent optical OFDM systems," in *Conf. Optical Fiber Communication (OFC)*, Mar. 2007, paper OMP2.

[126] W. Shieh, X. Yi, Y. Ma, and Y. Tang, "Theoretical and experimental study on PMD-supported transmission using polarization diversity in coherent optical OFDM systems," *Optics Express*, vol. 15, no. 16, pp. 9936–9947, Aug. 2007.

[127] J. G. Proakis and D. G. Manolakis, *Digital Signal Processing*, 4th ed. Prentice Hall, 2006.

[128] S. Wu and Y. Bar-Ness, "OFDM systems in the presence of phase noise: Consequences and solutions," *IEEE Trans. Commun.*, vol. 52, no. 5, pp. 1988–1996, May 2004.

[129] W. Lindsey and M. Simon, "On the detection of differentially encoded polyphase signals," *IEEE Trans. Commun.*, vol. 20, no. 6, pp. 1121–1128, Dec. 1972.

[130] H. Bülow, "Tutorial electronic dispersion compensation," in *Conf. Optical Fiber Communication (OFC)*, March 2007, OMG5.

[131] I. B. Djordjevic and B. Vasic, "Orthogonal frequency division multiplexing for high-speed optical transmission," *Optics Express*, vol. 14, no. 9, pp. 3767–3775, May 2006.

[132] F. Xiong, *Digital Modulation Techniques*, 2nd ed. Boston: Artech House, 2006.

[133] W. Shieh, R. S. Tucker, W. Chen, X. Yi, and G. Pendock, "Optical performance monitoring in coherent optical OFDM systems," *Optics Express*, vol. 15, no. 2, pp. 350–356, Jan. 2007.

[134] J. Yang, Z. Zhu, H. Yang, Z. Pan, and S. J. B. Yoo, "All-optical time-to-live using error-checking labels in optical label switching networks," in *Europ. Conf. Optical Commun. (ECOC)*, Sept. 2004, Th3.6.5.

[135] N. A. Olsson, "Lightwave systems with optical amplifiers," *J. Lightwave Technol.*, vol. 7, no. 7, pp. 1071–1082, July 1989.

[136] X. Yi, F. Buchali, W. Chen, and W. Shieh, "Adaptation algorithms for receiver based electronic dispersion equalization," in *Australian Conference on Optical Fiber Technology (ACOFT)*, July 2006, paper 140Mon.

Appendix A

Acronyms

ADC Analogue-to-Digital Converter

AOLS All-Optical Label Swapping

APD Avalanche Photodiode

ASE Amplified Spontaneous Emission

ASK Amplitude-Shift Keying

ATM Asynchronous Transfer Mode

AWG Arbitrary Waveform Generator

B2B Back to Back

BER Bit Error Rate

BERT Bit Error Rate Tester

BPF Bandpass Filter

BPSK Binary Phase-Shift Keying

CD Chromatic Dispersion

CDR Clock and Data Recovery

CO-OFDM Coherent Optical Orthogonal Frequency Division Multiplexing

CP Cyclic Prefix

CPE Common Phase Error

CW Continuous Wave

DAC Digital-to-Analogue Converter

DC Direct Current

DCF Dispersion Compensation Fiber

DCM Dispersion Compensation Module

DFE Decision Feedback Equalizer

DFB Distributed Feedback

DFT Discrete Fourier Transform

DGD Differential Group Delay

DPSK Differential Phase-Shift Keying

DQPSK Differential Quadrature Phase-Shift Keying

DSP Digital Signal Processing

DWDM Dense Wavelength Division Multiplexing

EDC Electronic Dispersion Compensation

EDFA Erbium-Doped Fiber Amplifier

FDL Fiber Delay Line

FDM Frequency Division Multiplexing

FEC Forward Error Correction

FFE Feed Forward Equalizer

FFT Fast Fourier Transform

FSK Frequency-Shift keying

GI Guard Interval

GVD Group Velocity Dispersion

LAN Local area networks

ICI Inter-Carrier Interference

IDFT Inverse Discrete Fourier Transform

IF Intermediate Frequency

IFFT Inverse Fast Fourier Transform

IM/DD Intensity Modulation/Direct Detection

IP Internet Protocol

IQ In-phase and Quadrature

ISI Inter-symbol Interference

ITU International Telecommunication Union

LMS Lease Mean Square

LPF Low Pass Filter

MLSE Maximum Likelihood Sequence Estimation

MZ Mach-Zehnder

NF Noise Figure

NRZ Non-Return-to-Zero

OADM Optical Add-Drop Multiplexer

OCDM Optical Code Division Multiplexing

OE Optical-Electrical

OEO Optical-Electrical-Optical

OFDM Orthogonal Frequency Division Multiplexing

OOK On-Off Keying

OPLL Optical Phase Locked Loop

OPM Optical Performance Monitoring

OPSN Optical Packet Switched Networks

OSA Optical Spectrum Analyzer

OSCM Optical Subcarrier Multiplexing

OSNR Optical Signal-to-Noise Ratio

OSSB Optical Single Sideband

OXC Optical Cross-Connect

QoS Quality of Service

PD Photodiode

PDL Polarization Dependent Loss

PG Pattern Generator

PIPM Polarization Insensitive Phase Modulator

PM Phase Modulator

PMD Polarization-Mode Dispersion

PMDE PMD Emulator

PMF Polarization Maintaining Fiber

PolSK Polarization-Shift Keying

PRBS Pseudo-Random Binary Sequence

PSK Phase-Shift Keying

PSP Principle State Polarization

QAM Quadrature Amplitude Modulation

QPSK Quadrature Phase-Shift Keying

RF Radio Frequency

RIN Relative Intensity Noise

RX Receiver

SNR Signal-to-Noise Ratio

SPM Synchronous Phase Modulation

SSMF Standard Single-Mode Fiber

TCP/IP Transmission Control Protocol/Internet Protocol

TDM Time Division Multiplexing

TX Transmitter

WDM Wavelength-Division Multiplexing

XOR Exclusive OR

XPM Cross Phase Modulation

Author/s:
Yi, Xingwen

Title:
Signal processing techniques for optical fiber networks

Date:
2007

Citation:
Yi, X. (2007). Signal processing techniques for optical fiber networks. PhD Thesis, Faculty of Engineering, Electrical and Electronic Engineering, University of Melbourne.

Publication Status:
Published

Persistent Link:
http://hdl.handle.net/11343/39427

File Description:
Signal processing techniques for optical fiber networks